2001

Experimental investigation of flow patterns in meandering channels of moderate sinuosity.

William Donald. Tape
University of Windsor

INFORMATION TO USERS

This manuscript has been reproduced from the microfilm master. UMI films the text directly from the original or copy submitted. Thus, some thesis and dissertation copies are in typewriter face, while others may be from any type of computer printer.

The quality of this reproduction is dependent upon the quality of the copy submitted. Broken or indistinct print, colored or poor quality illustrations and photographs, print bleedthrough, substandard margins, and improper alignment can adversely affect reproduction.

In the unlikely event that the author did not send UMI a complete manuscript and there are missing pages, these will be noted. Also, if unauthorized copyright material had to be removed, a note will indicate the deletion.

Oversize materials (e.g., maps, drawings, charts) are reproduced by sectioning the original, beginning at the upper left-hand corner and continuing from left to right in equal sections with small overlaps.

Photographs included in the original manuscript have been reproduced xerographically in this copy. Higher quality 6" x 9" black and white photographic prints are available for any photographs or illustrations appearing in this copy for an additional charge. Contact UMI directly to order.

ProQuest Information and Learning
300 North Zeeb Road, Ann Arbor, MI 48106-1346 USA
800-521-0600

Experimental Investigation of Flow Patterns in Meandering Channels of Moderate Sinuosity

by
William Tape

A Thesis submitted to the Faculty of Graduate Studies and Research through the department of Civil and Environmental Engineering in partial fulfillment of the requirements for the degree of Master of Applied Science at the University of Windsor

Windsor, Ontario, Canada

ABSTRACT

This thesis is an extension of the works by Whiting and Dietrich 1993, Silva 1995 and Termini 1995. These authors have found that the initial flow patterns in sine-generated meandering channels are mainly a function of the channels deflection angle θ_0. (Initial flow is the flow present in the channel prior to any bed deformation). However, the aforementioned works are restricted to cases of "small" and "large" θ_0; the flow pattern in the small θ_0-channels have been termed ingoing and in the large θ_0- channels, outgoing. In this thesis the flow patterns in channels having intermediate values of θ_0 were investigated experimentally.

The main objectives are: 1) to determine the relationship between flow patterns and plan shape, for the purpose of determining the transition region between ingoing and outgoing flow patterns, 2) to develop a database for use by other researchers in the calibration of numerical models. The experiments were carried out in three different channels defined by θ_0=90°, 70°, and 50°. The experimental facility was designed to allow for the same recirculating flow system to be used for all channels. The channels themselves were 40cm wide, with a rectangular cross-section. All three channels conveyed a 3-3.2cm deep flow, with flow rates in the range of 1.5 to 2.8 l/s for the purpose of measuring the vertically-averaged longitudinal flow velocity $\overline{u}$, deviation angle $\overline{\omega}_c$ and flow depth h.

It was found that the flow in the 90°-channel was outgoing, while the flow in the 50°-channel was ingoing. These findings were supported by both the deviation angle and velocity measurements. The initial flow in the 70°-channel was found to be neither ingoing nor outgoing, but rather a transitional flow between ingoing and outgoing. A discussion of a possible correlation between the velocity of expansion of a meandering channel and the maximum vertically-averaged deviation angle has also been presented.

ACKNOWLEDGEMENTS

I would like to extend my most heart felt thanks and gratitude to my advisor Dr. Ana da Silva and co-advisor Dr. Stan Reitsma for their invaluable guidance and support throughout my work on this thesis.

I would also like to offer my thanks to my graduate committee, Dr. Paul Henshaw, and Dr. Robert Gaspar for their support and assistance.

Thanks to Mr. Patrick Seguin for his assistance in preparing for the testing phase of this project, and Mr. Ee Yeong Lim and Mr. Paul Ankrett for their assistance during channel preparation. Special thanks to Mr. Colin Novak for his assistance during this work. As well, special thanks to Mr. Tarek El-Tahawy for his assistance during this work, including the furnishing of figures 5.3, 5.6 and 5.11.

Finally, to Mr. Richard Clark, I am indebted to him for his guidance, friendship and overwhelming assistance and support during all phases of this work.

Financial support from the University of Windsor, the Government of Ontario and the Natural Sciences and Engineering Research Council was also greatly appreciated.

TABLE OF CONTENTS

LIST OF TABLES

LIST OF FIGURES

LIST OF SYMBOLS

(a) General

a	apex section
B	channel width
C	centre of curvature
D	diameter of granular material
D_{50}	diameter of granular material, corresponding to 50% passing a given sieve
D_i	diameter of granular material, corresponding to i % passing a given sieve
E_o	coefficient of bank erosion
F_c	centrifugal force ($=\rho u^2/R$)
F_p	transverse pressure gradient ($=-\gamma\, dh/dr$)
g	gravitational constant (=9.81m/s^2)
h	flow depth
h_w	head of water over the weir
$J_0(\theta_0)$	Bessel function of the first kind and zero-th order of θ_0
k_s	effective roughness of the bed
L	length of a meandering channel over one meandering period
l	longitudinal coordinate along the channel; l=0 at the crossover
n	radial coordinate measured from the channel centreline
n_u	normal coordinate of the locus of high velocity
O	crossover, also denoted by O', O''
Q	flow rate
q_s	specific volumetric sediment transport rate
R	radius of curvature
r	radial coordinate measured from the centre on curvature
S	standard deviation
S_{bc}	slope of channel bed measured at the centreline
S_h	highest standard deviation
S_l	lowest standard deviation
S_m	average standard deviation

t	time
T_b	time taken by a channel to reach its equilibrium bed topography
u	(time-averaged) flow velocity
$\overline{U}$	Averaged value of flow velocity for the purpose of determining a standard deviation
u_{inst}	instantaneous flow velocity
v_*	shear velocity ($=\sqrt{gsh}$)
z	vertical coordinate, measured normal to the bed
χ	dimensionless centreline velocity
Δ	meander amplitude
Δh	super-elevation of the free surface
γ	specific weight of the fluid
Γ	cross-circulation
Λ	meander wave length
Λ_i	Loop number (i = 1,2,3)
ν	kinematic viscosity
θ	deflection angle between l_c and the x-axis at any flow section l_c
θ_0	value of θ at l_c=0
ρ	fluid density
ω	deviation angle
ω_c	deviation angle at the centreline
ζ	distance measured for the centreline to the new position of the channel bank (for Parker and Edmund Equation, Chapter 2)

(b) Dimensionless combinations

c_m channel averaged resistance factor

Fr Froude Number ($=u_m^2/gh_m$)

Re Reynolds number ($=u_m h_m/\nu$)

Re_* Reynolds number at the bed ($=v_* k_s/\nu$)

η dimensionless counterpart of n (=n/B)

ζ dimensionless counterpart of z ($=z/h_m$)

ξ_c dimensionless counterpart of l_c ($=l_c/L$)

σ channel sinuosity ($=L/\Lambda$)

ϕ_h dimensionless counterpart of h ($=h/h_m$)

ϕ_u dimensionless counterpart of u ($=u/u_m$)

(c) Superscripts and Subscripts

a	apex
av	cross-sectional average
c	value along the centreline
m	channel-averaged value

"bar" over a quantity signifies it is a vertically-averaged value

1.0 INTRODUCTION

1.1General

Rivers have fascinated engineers and scientists for many years, while providing water supply for domestic and industrial consumption, for irrigation, etc., as well as a means of transportation and recreation. However, the design and effective management of these systems requires a full understanding of the mechanics of the flow and sediment transport in rivers. A better understanding of river mechanics is also relevant for river management projects (involving e.g. shoreline protection, river restoration, land reclamation and transportation issues) to be handled in a more integrated fashion taking into consideration ever-increasing environmental concerns. In this search for a better understanding, meandering rivers have gained a great deal of attention, as meandering is the most common form taken by natural channels. Indeed, as stated by Leopold and Langbein 1966, "the striking geometric regularity of a winding river is no accident. Meanders appear to be the form in which a river does the least work in turning; hence they are the most probable form a river can take".

Meandering was defined by Yalin 1992 as "a self induced plan deformation of a stream which, under ideal conditions, is periodic and anti-symmetrical with respect to an axis x, say". As pointed out by this author, "an alluvial stream which deforms its initially straight channel into one of the periodic and anti-symmetrical plan forms, such as those shown in Fig. 1.1, is meandering; where as a stream flowing in a tortuous rocky terrain is not meandering". The meandering in Fig. 1.1a is defined as regular, that in Fig. 1.1b, as irregular or skewed.

Langbein and Leopold 1966 established that the path of the centreline of regular meanders, irrespective of their sinuosity, is best described by a "sine-generated" curve (see Sections 2.1 and 2.2 for a detailed discussion of sine-generated curves and their geometric properties). Fig. 1.2 shows two examples of meandering channels, where the

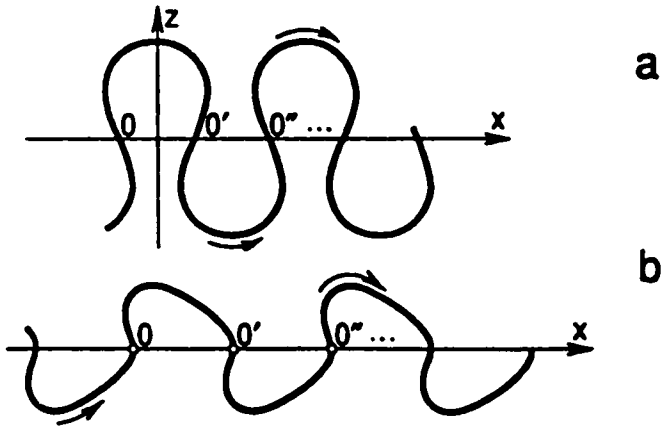

Figure 1.1: Regular and skewed paths of meandering channels (from Yalin 1992)

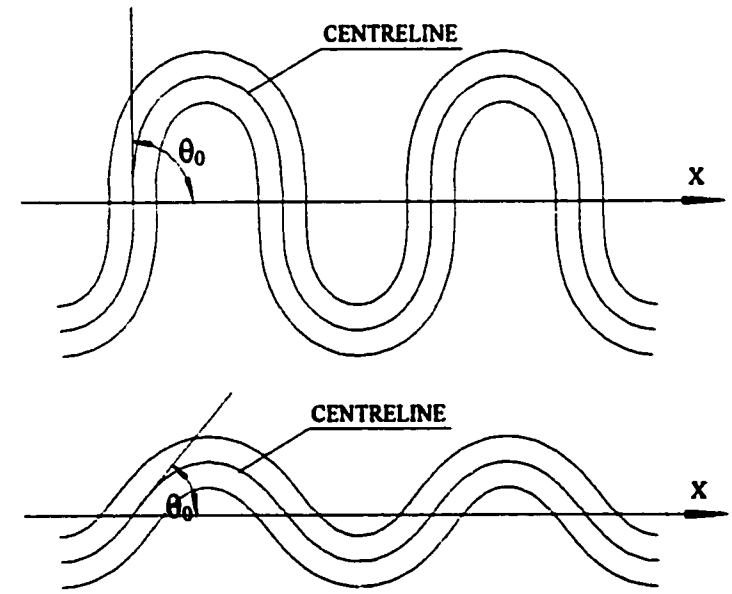

Figure 1.2: Meandering channels defined by sine-generated curves

centreline is defined as a "sine-generated" curve. The sine-generated curves are defined by the deflection angle θ_0, where θ_0 is the angle between the channel centreline and the horizontal axis, measured at the crossover *O* of a meander wave. It is important to note that θ_0 in the case of sine-generated curves uniquely defines the channel sinuosity.

Consider now the bed topography of meandering rivers. With the aid of both field and laboratory measurements, it has been established that if θ_0 is "small" ($\theta_0 \lesssim 30°$, say), then the largest erosion/deposition occurs around the crossovers (see Fig. 1.3a); whereas if θ_0 is "large" ($\theta_0 \gtrsim 90°$, say), then the erosion/deposition occurs in the vicinity of the apex (see Fig. 1.3b).

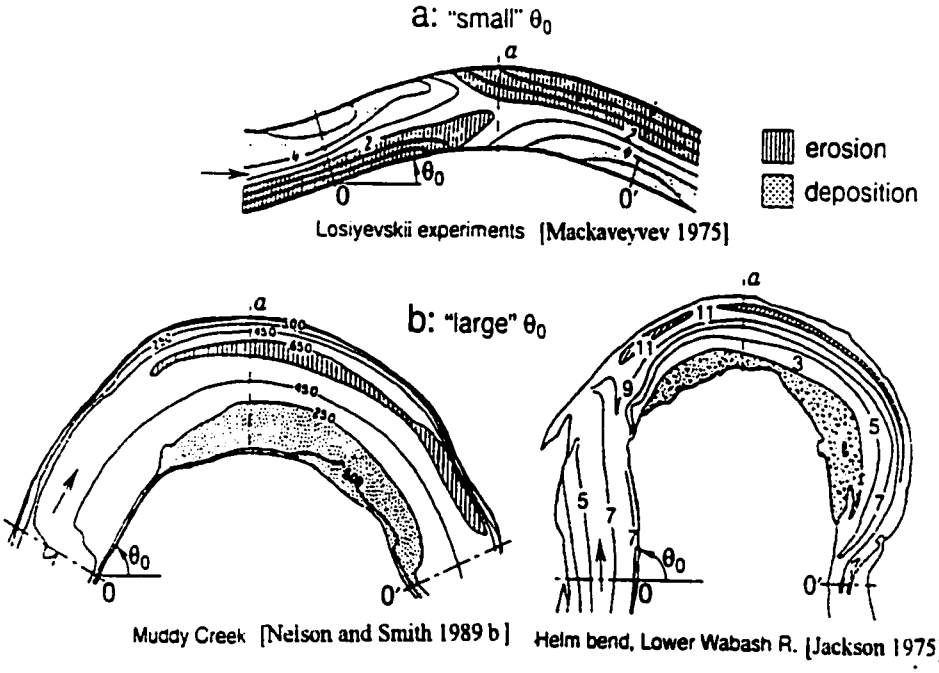

Figure 1.3: Variation in the location of erosion/deposition zones in naturally meandering streams with the deflection angle (from Yalin 1992)

In order to explain the bed formation caused by the flow in meandering streams, consider the typical laboratory experiment where the meandering channel has rigid banks and a movable bed. The bed is initially flat. Starting at the time t=0, allow a constant flow rate Q to flow in the channel. At t=0 the flow will pass over an initially flat bed, following Silva 1995 this flow will henceforward be termed initial flow. The initial flow is not in equilibrium with the flat bed, therefore, it will begin to erode sediment within certain regions of the channel, and deposit that sediment in other regions. These regions of erosion and deposition, which are termed deeps and shoals respectively, alter the flow through the channel for the flow tends to avoid the shoals, while being conveyed to the

deeps (Yalin 1992 and Dietrich and Whiting 1989). Therefore, as the bed topography continues to grow in magnitude over time, the flow continues to change, until at a time $t=T_b$ the bed reaches a state of dynamic equilibrium. At this point, the bed topography ceases to change; here the bed is said to have reached the "equilibrium bed topography". From the laboratory experiments carried out by a number of authors, it follows that the shoals and deeps do not shift in the flow plan during $0 \leq t \leq T_b$. Taking this into account, Silva 1995 has suggested that the bed topography is "locked" in the mechanical structure of the initial flow. As is well known, erosion is associated with the convective acceleration of the flow, and deposition with its convective deceleration. Taking this into account, as well as the fact that the erosion-deposition patterns in "small" and "large" sinuosity channels are very different, Silva 1995 further hypothesized that the initial flow pattern of "small" and "large" sinuosity channel should also be rather different.

The recent experiments of Whiting and Dietrich 1993, Silva 1995, Termini 1996 have confirmed this hypothesis, by showing that indeed the initial flow pattern in a small sinuosity channel (shown in Fig. 1.4a) is different from that in a large sinuosity channel (show in Fig. 1.4b).

For the initial flow in a channel of small sinuosity (Fig. 1.4a), the streamlines diverge from the outer bank and converge on the inner bank throughout the region between the crossover and apex sections (i.e. the flow is convectively decelerating at the outer bank and accelerating at the inner bank). As the flow passes the apex the streamlines begin to converge on the outer bank and diverge from the inner bank. The converging flow in the region of the outer bank results in the flow convectively accelerating leading to a zone of erosion in the neighbourhood of the crossover O', in the region of the inner bank the divergence results in a convective deceleration of the flow leading to a zone of deposition in this region. This initial flow pattern is in agreement with the bed topography reported in Fig. 1.3a. Silva 1995 termed this flow pattern "ingoing", a term that will often be used throughout this thesis.

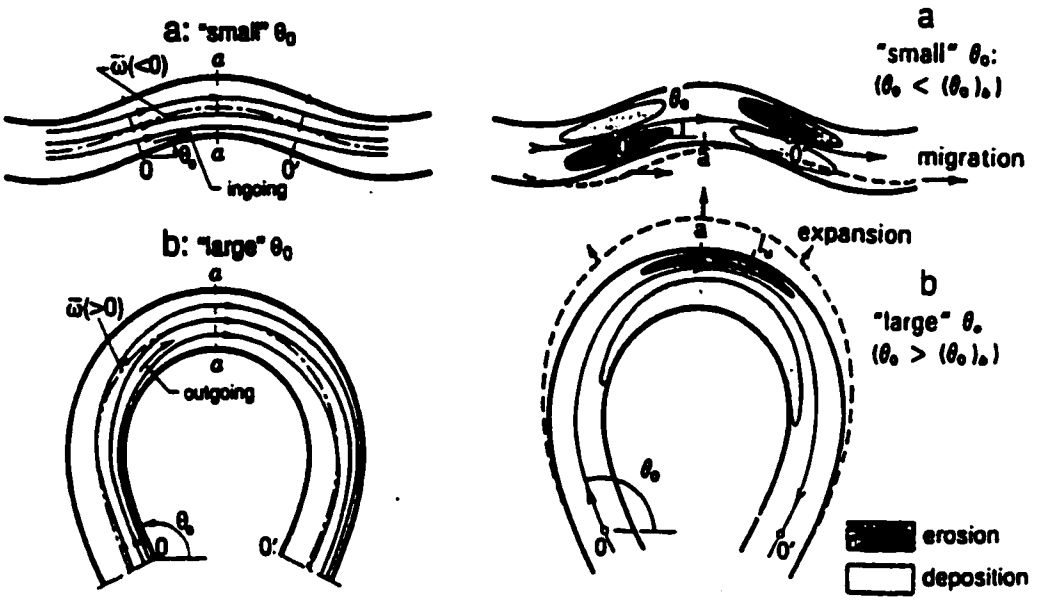

Figure 1.4: Convergence-divergence zones of meandering streams and the corresponding erosion/deposition zones (from Silva 1997)

For an initial flow in a channel of large sinuosity (Fig. 1.4b), the streamlines diverge from the inner bank throughout the entire region *OaO'*. This divergence of the streamlines implies that there is a convective deceleration of the flow in the region of the inner bank throughout the entire loop *OaO'*, and a convective acceleration of the flow in the region of the outer bank. This initial flow pattern is in agreement with the bed topography reported in Fig. 1.3b. Silva 1995 termed this flow pattern "outgoing".

Silva 1995 used the vertically-averaged deviation angle along the channel centreline $\overline{\omega}_c$ to distinguish between ingoing and outgoing flows. Consider the case of the small sinuosity channel conveying an ingoing flow in Fig. 1.4a. The vertically-averaged deviation angle $\overline{\omega}_c$ maintains a negative value throughout a region approximately between the crossover *O* and the apex *a*. After the apex section *a*, where the streamlines are diverging from each other at the inner bank, the deviation angle $\overline{\omega}$ changes to a positive value.

Consider now the case of a large sinuosity channel conveying an outgoing flow (Fig. 1.4b). As should be clear from this figure, the vertically-averaged deviation angle $\bar{\omega}_c$ maintains a constant sign approximately throughout the entire meander (i.e. throughout the region OaO'). In fact the deviation angle increases approximately between O and a, and decreases approximately between section a and O'.

In summary from previous experiments conducted in channels with "small" and "large" values of θ_0, it follows that the flow pattern is a strong function of θ_0; however, these experiments were confined to the limiting cases of "small" and "large" θ_0. Thus, where the initial flow patterns in channels of intermediate θ_0 are concerned no information is available which makes it impossible to formulate mathematically the flow patterns and associated bed topographies. Taking this into account, this thesis is intended as a contribution to the determination of the flow patterns in channels of intermediate values of sinuosity.

1.2 Objectives and Methodology

The primary objectives of this thesis are:

1. To investigate the initial flow patterns in sine-generated channels having intermediate values of θ_0;

2. To determine the relationship between flow patterns and plan shape, for the purpose of determining the transition region between ingoing and outgoing flow patterns;

3. To produce a database to be used by other researchers in the development and calibration of numerical models.

For the above purposes, measurements were carried out in three distinct sine-generated channels having θ_0= 90°, 70°,and 50°. The experimental conditions used for these experiments closely resembled those used by Silva 1995 in her θ_0=110° and θ_0=30° channels. The measurements included velocity profiling and the determination of the vertically averaged deviation angle ($\overline{\omega}_c$) of the streamlines from the centreline of the channel. In addition to these measurements the free surface profiles were also recorded.

1.3Layout of Thesis

Chapter 2 contains a review of literature relevant to the topic of this thesis. This chapter describes the geometry and mechanics of meandering flows; past experimental research is reviewed.

Chapter 3 describes the experimental setup. Information concerning the experimental facility that was used in this research, as well as a description of the flow systems designed for the experiments is given. Attention is also paid to bed roughness.

Chapter 4 describes in detail the experimental tests, which were carried out in order to obtain the required data. A description of the location for all measurements is given. The experimental procedures adopted, including the method used to establish the channel-averaged flow depth, are also provided. The equipment used to take measurements, and the methods used to calibrate the equipment will also be discussed.

Chapter 5 lists the results of the experimental tests. The discussion of the results is also a part of this chapter. All the test results will be provided in graphical form in this section.

Chapter 6 presents the conclusions obtained from the work. Recommendations for future research are included.

1.4 Pertinent Notation

An overview of the terms used to define a meander is in order. Figure 1.5 shows a complete meander, which contains two meander loops. Clearly defined in this diagram at positions *a* are the apexes located at the extremes of the loops relative to the *y*-axis, and the three crossovers marked as *O*,*O'*,*O''*. The *x*-axis of the channel runs through the crossover-sections along the valley slope in the average direction of flow. The symbol Λ defines the meander wavelength. As seen in Fig. 1.5 the meander wavelength is the distance between *O* and *O''* measured along the average direction of flow *x*. The distance between *O* and *O''* measured along the channel centreline is the meander length L. The symbol Δ denotes the amplitude of the meander. The sinuosity σ is defined as

$$\sigma = \frac{L}{\Lambda}. \tag{1.1}$$

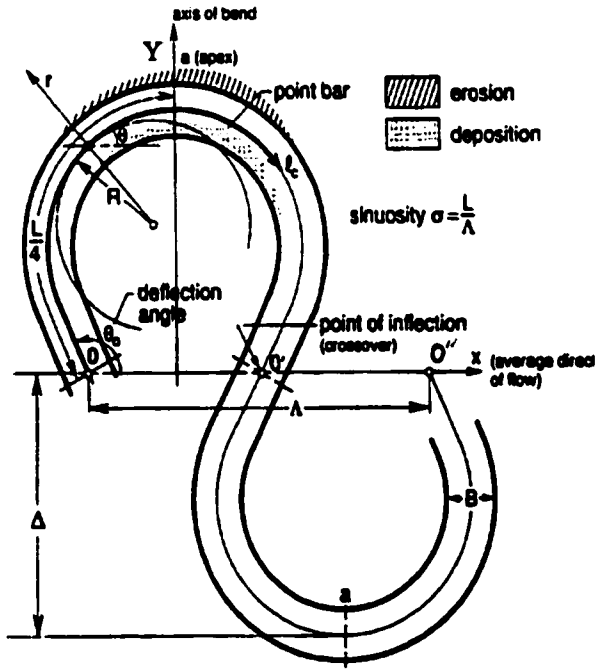

Figure 1.5: Geometric characteristics of a meandering channel (from Silva 1995)

The "channel fitted" system of cylindrical coordinates, l, r, z will be used throughout this thesis (see Fig. 1.6). The origin of the longitudinal coordinate l is at the crossover O (i.e. l=0 at O). The radial coordinate r is measured from the centre (C) of the channel curvature at that section. Instead of l and r, it is possible and, in fact, more common to use l_c ,which is l along the centreline, and n ,which is measured from the centreline. In the present thesis preference will be given to the latter, and thus the position of a point P will be defined by the coordinates

$$l_c, n, z . \tag{1.2}$$

The coordinate pairs (l_c, n) and (l, r) can be shown to be related to each other by

$$\frac{dl_c}{R} = \frac{dl}{r} \text{ where } r = n+R \tag{1.3}$$

(see e.g. Silva 1995 and Yalin 1992).

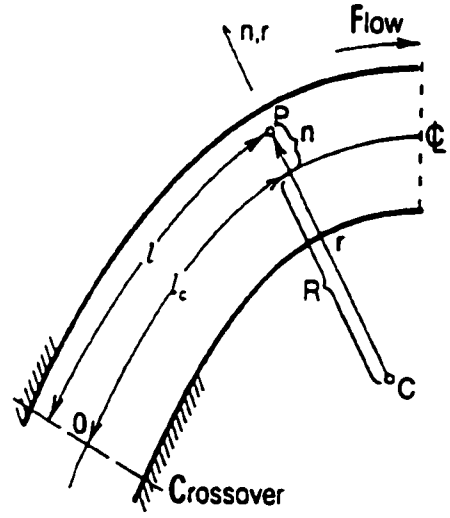

Figure 1.6: Channel-fitted cylindrical coordinates (from Silva and Yalin 1997)

Throughout this thesis the dimensionless counterparts of the coordinates will be used. These dimensionless coordinates are obtained by dividing l_c, n and z by their corresponding channel length scale (L, B, h_m, where L is meander length, B is flow width, and h_m is the channel-averaged flow depth) as follows

$$\xi_c = \frac{l_c}{L}\ ;\quad \eta = \frac{n}{B}\ ;\quad \zeta = \frac{z}{h_m}. \tag{1.4}$$

Consider now a meandering flow property which is a function of position $A=A(l_c,n,z)$. The following convention is used in this thesis:

1. Vertically-averaged value of $A=A(l_c,n,z)$ will be denoted by $\overline{A}$:

$$\overline{A} = \overline{A}(l_c,n) = \frac{1}{h}\int_0^h A(l_c,n,z)dz \qquad \text{where } h=h(l_c,n). \tag{1.5}$$

2. Cross-sectional average value of $A=A(l_c,n,z)$ will be denoted by A_{av}

$$A_{av} = A_{av}(l_c) = \frac{1}{B}\int_{-B/2}^{+B/2}\left[\int_0^h \frac{1}{h}A(l_c,n,z)dz\right]dn = \frac{1}{B}\int_{-B/2}^{+B/2}\overline{A}(l_c,n)dn. \tag{1.6}$$

3. Channel average value of $A=A(l_c,n,z)$ (taken over a given (integer) number of channel cycles) will be denoted by A_m:

$$A_m = (const) = \frac{1}{L}\int_0^L\left[\frac{1}{B}\int_{-B/2}^{+B/2}\left[\frac{1}{h}\int_0^h A(l_c,n,z)dz\right]dn\right]dl_c = \frac{1}{L}\int_0^L A_{av}(l_c)dl_c. \tag{1.7}$$

2.0 LITERATURE REVIEW

In this chapter, past and present research relating to meandering channels is reviewed. Here the focus is on sine-generated channels.

2.1 Meander Path: Sine-generated Curve

The path of an ideal alluvial meandering channel was first predicted by Von Schelling 1951, 1964. His theory can be explained in terms of a fluid element *m* moving between two points *A* and *B*. Von Schelling stated that the element *m* travels between *A* and *B* within a set number of steps and *m* changes its angle after each step. With this assumption Von Schelling predicted that the path having the highest probability of occurrence conforms to that represented by

$$l_c = \frac{1}{\varepsilon}\int_{\theta_0}^{\theta} \frac{d\theta}{[2(\cos\theta_0 - \cos\theta)]^{1/2}}. \tag{2.1}$$

He further demonstrated that the above expression implies

$$\frac{1}{L}\int_0^L (1/R^2)\,dl_c \rightarrow \min. \tag{2.2}$$

Eq. (2.2) means that the most probable path of the plan curve of a river is that for which the square of the curvature 1/R is a minimum over the entire length of the channel L.

Leopold and Langbein 1966 showed that Eq. (2.1) is equivalent to

$$\theta = \theta_0 \cos\left(2\pi l_c / L\right), \tag{2.3}$$

where θ represents the deflection angle between the *x*-axis and the channel centreline at a given location (l_c) and θ_0 is the value of θ at l_c=0 (see Fig. 1.5). The authors termed the curve defined by Eq. (2.3) a "sine-generated" curve. They further considered the sum of

the squares of the changes in direction over equal spacings for a parabolic curve, a sine curve, a circular curve and a sine generated curve and concluded that this sum was the lowest for the sine-generated curve. Leopold and Langbein applied Eq. (2.3) to natural meandering channels as seen in Figs. 2.1a and b. It can be seen that Eq. (2.3) which is represented by the solid lines in the θ versus l_c plot in Figs. 2.1a and b, closely follows the centreline of the channels examined. This led Leopold and Langbein 1966 to the conclusion that "The sine-generated curve closely approximates the shape of real river meanders". In terms of erosion, as it relates to the plan shape of the channel, Leopold and Langbein 1966 also stated:

The overall geometry of a meandering river is an important factor in determining the rate at which its banks will be eroded. In general the banks are eroded at a rate that is proportional to the degree with which the river channel is bent. Any curve other than a sine-generated curve would tend to concentrate bank erosion. Thus the sine-generated curve assumed by most meandering rivers tends to minimize total erosion.

Yalin 1992 considered the forces acting on the flow in successive circular bends, connected to each other with or without a straight reach, and noted the sudden changes in curvature (1/R) (see Fig. 2.2). Since the centrifugal force $F_c \sim u^2/R$, the sudden changes in curvature are accompanied by sudden changes in centrifugal force. Accordingly, Yalin 1992 stated that "nature would never create a channel where moving fluid elements experience jolts...".

Yalin 1992 used a different approach to derive Eq. (2.3). His work rests on the conviction that the flow turning within a meandering channel, having an average curvature

$$\frac{1}{R_{av}^2} = \frac{1}{L}\int_0^L (1/R)^2 dl, \tag{2.4}$$

tends to minimize the average rate of change of its curvature:

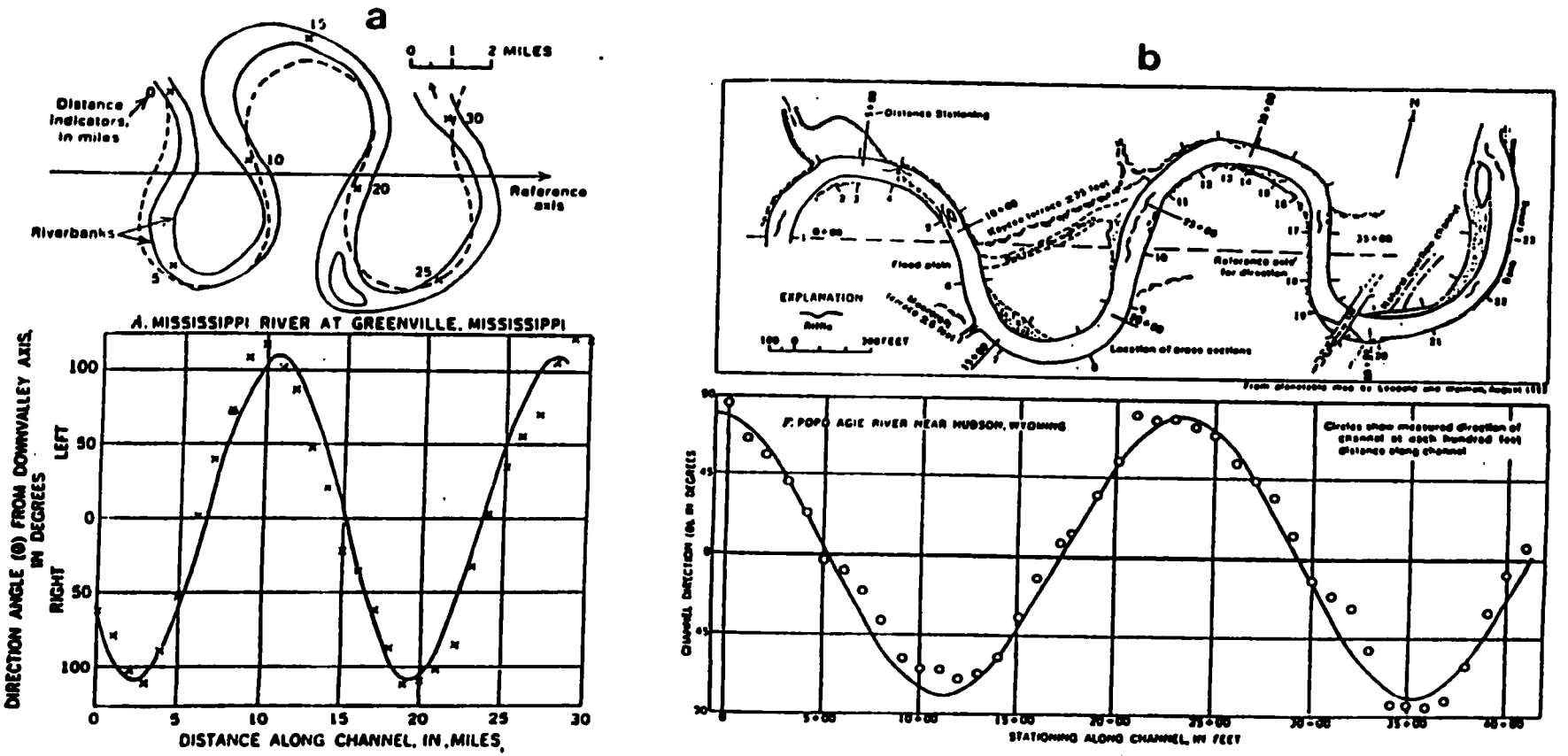

Figure 2.1: Comparison of sine-generated curves with plan-shapes of natural meanders (from Langbein and Leopold 1966)

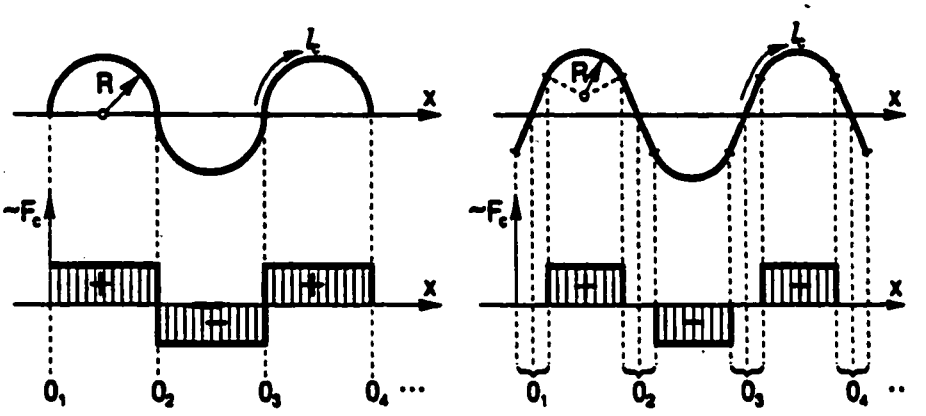

Figure 2.2: Variation of curvature of circular and composite channels as relates to flow direction (from Silva 1995)

$$\frac{1}{L} = \int_0^L (1/R)^2 dl \rightarrow \min . \qquad (2.5)$$

With the above considerations, Yalin derived Eq. (2.3) with the aid of variational calculus.

Yalin 1992 stated that "it appears to be generally accepted that the plan shape of a regular ideal river can be best reflected by the sine-generated curve". Yet some authors still prefer to use circular channels in their studies and formulations of meandering flows (Ghanmi 1999, Shiono et al. 1999, Ye and McCorquodale 1998, Guymer 1998, Julien and Kawai 1996, Struiksma et al. 1995). In fact, in their more recent work, Zhi-Qiang and Singh 1999 suggested that a semi-circular channel is more representative of a naturally occurring channel. Further, they added that the semi-circular shape should have a sinuosity of approximately 1.57, with the flow entropy being at a minimum for this value of sinuosity.

As mentioned in the Introduction, natural channels are not always regular, and following a sine-generated curve they can be irregular, and exhibit a "skewness" as shown in Fig. 1.1. The "skewing" leading to the deviation of a natural channel from the sine-generated path was explained by Parker and Edmund 1986, who associated channel

shifts with the bank erosion rate and the locus of high velocity at any given cross section. Parker and Edmund described the channel shift in terms of its displacement measured from the centreline of the channel by the following equation,

$$\zeta = 3\chi E_o n_u, \tag{2.6}$$

where ζ is the distance measured from the centreline to the new position of the channel's bank, χ is the dimensionless centreline velocity, E_o is the coefficient of bank erosion and n_u is the normal coordinate of a locus of high velocity.

2.2 Geometric Characteristics of Alluvial Sine-generated Channels

In this section the geometric characteristics pertinent to the current work will be discussed.

Silva 1991 showed that the sinuosity σ of a sine-generated channel is uniquely defined by the deflection angle θ_0 as

$$\sigma = \frac{L}{\Lambda} = \frac{1}{J_0(\theta_0)}, \tag{2.7}$$

where $J_0(\theta_0)$ is the Bessel function of the first kind and zero-th order of θ_0. In this thesis $J_0(\theta_0)$ will be approximated by the same polynomial expression employed by Silva 1995, namely

$$\begin{aligned} J_0(\theta_0) = 1 &- 2.2499997(\theta_0/3)^2 + 1.2656208(\theta_0/3)^4 - 0.3163866(\theta_0/3)^6 \\ &+ 0.0444479(\theta_0/3)^8 - 0.0039444(\theta_0/3)^{10} + 0.0002100(\theta_0/3)^{12} \\ &+ \varepsilon \text{ (with } \varepsilon < 5 \times 10^{-8}\text{)}. \end{aligned} \tag{2.8}$$

Using data collected from a number of Russian Rivers Yalin 1992 compared the inverse of their sinuosities with the predicted values given by this function. The results of this comparison are shown in Fig. 2.3. From this graph it appears that the function used to predict $J_0(\theta_0)$ and thus the theoretical value of the inverse of sinuosity appears to agree favourably with the field measurements.

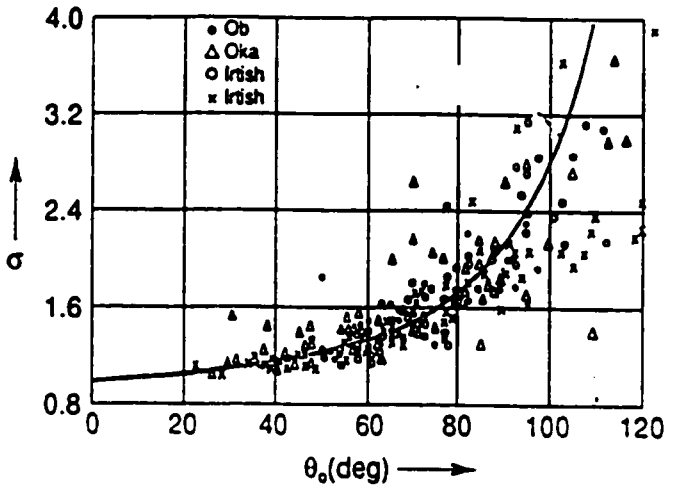

Figure 2.3: Comparison of sinuosity 1/σ of Russian rivers with predicted values (from Yalin 1992)

The meander wavelength Λ is another important geometric characteristic of sine-generated channels. It was Yalin 1992 who predicted that for streams in alluvium this distance is proportional to the flow width B. He later concluded that the wavelength can best be expressed by the expression:

$$\Lambda \approx 2\pi B, \tag{2.9}$$

To support his finding he compared this expression with a variety of field and laboratory measurements: see Fig.2.4. The regression line of $\Lambda=2\pi B$ appears to be in agreement with the data, as the line passes approximately through the centre of the data.

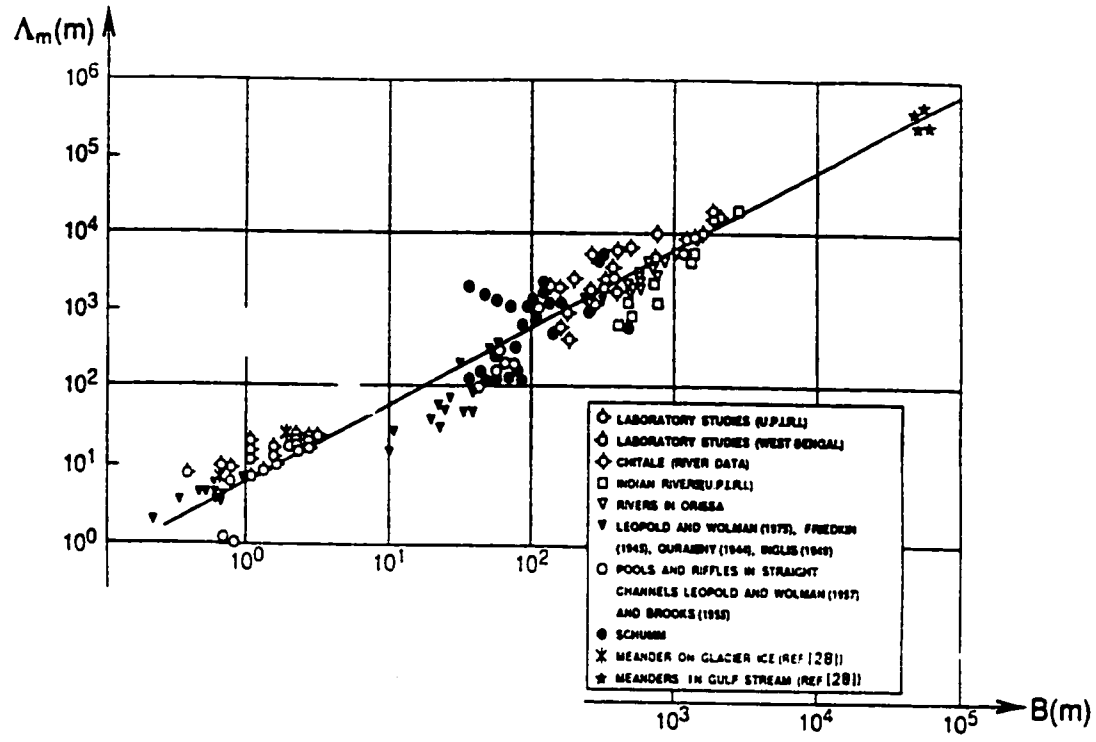

Figure 2.4: Relation between meander wavelength Λ and flow width B in alluvial meandering streams (from Yalin 1992)

Consider now Eq. (2.3) which provides the expression for the channel centreline as given by Langbein and Leopold. The local channel curvature 1/R can be obtained by taking the first derivative of this expression with respect to l_c (Silva 1991, 1995, Yalin 1992)

$$\frac{1}{R}=\frac{d\theta}{dl_c}=\theta_0\frac{2\pi}{L}\sin\left(2\pi\frac{l_c}{L}\right), \tag{2.10}$$

where R is the channel radius for a given value of l_c.

The dimensionless quantity B/R, which will often be used in this thesis, is thus

$$\frac{B}{R}=\theta_0 J_0(\theta_0)\sin\left(2\pi\frac{l_c}{L}\right). \tag{2.11}$$

At the apex section (where $l_c/L=0.25$)

$$\frac{B}{R_a} = \theta_0 J_0(\theta_0). \tag{2.12}$$

This expression, as relates to the value of B/R_a (at the apex), is shown graphically in Fig. 2.5a along with the curve representing the function $J_0(\theta_0)$. From this graph it can be seen that B/R_a reaches its maximum in a channel having θ_0 =70°. It is also shown that when $\theta_0 \approx 138°$ $J_0(\theta_0)$= 0 which results in $\sigma = \infty$. However, as stated by Yalin 1992 $\theta_0 \approx 138°$, "can never be realized, for the loops begin to touch each other already when θ_0 has grown to $\theta_0 \approx 126°$". The path of the 126°-channel can be seen in Fig. 2.5b.

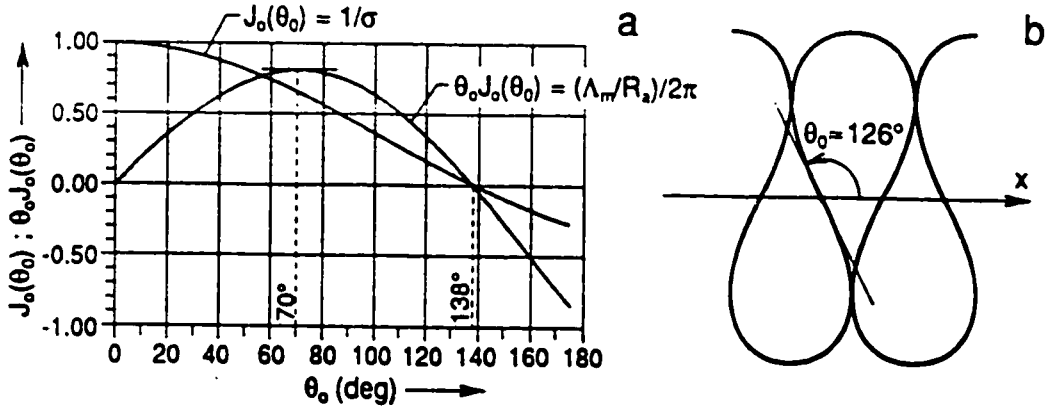

Figure 2.5: Variation of channel sinuosity $1/\sigma$ and relative channel curvature at the apex B/R_a with the deflection angle θ_0 (from Yalin 1992)

2.3 Experimental Research on Meandering Flows

Several aspects of meandering flows (flow patterns, shear stress distribution, erosion/deposition patterns, etc.) have been the object of intensive experimental research in the past. Yet, in most of the works, the meandering channels were represented as a single circular bend, as a series of interconnected circular sections, or as series of circular

sections connected by straight sections. Among the aforementioned works, the following appear most prominent: Einstein and Harder 1954, Ippen and Drinker 1962, Yen and Yen 1971, Francis and Asfari 1971, Varshney and Garde 1975, Kikkawa, Ikeda and Kitagawa 1976, Choudhary and Narasimhan 1977, De Vriend and Koch 1978, Odgaard 1984, Steffler 1984, Almquist and Holley 1985 and Odgaard and Bergs 1988. By contrast, very few experimental measurements, attempting to address the flow in natural meandering channels, were carried out in sine-generated channels (Hooke 1974, Hasegawa 1983, Ikeda and Nishimura 1986, Whiting and Dietrich 1993 a, b, c, Silva 1995 and Termini 1996). Table 2.1 gives a summary of the experimental conditions used by these Researchers.

Table 2.1: Summary of experimental conditions used by some previous researchers

Author	θ_o (°)	B (m)	Q (l/s)	S_{bc}	B/h_m
Hooke 1974	55	1	10-50	1/500	8-20
Hasegawa 1983	20	0.22	0.53	1/160	24
	30	0.3	0.75;1.87	1/300;1/70.9	12;34
	90	0.22	0.87	1/720	16
Ikeda & Nishimura 1986	40	0.3	2.6	1/720	6
Whiting & Dietrich 1993c	10	0.25	0.97-1.67	1/240-1/210	12-18
	20	0.25	1.04-1.08	1/230-1/150	14-17
Whiting & Dietrich 1993b	100	0.25	1.18	1/250	13
Whiting & Dietrich 1993a	100	0.25	0.94-1.18	1/250-1/167	15-17
	115	0.125-0.520	0.42-1.26	1/250-1/150	5-64
Silva 1995	30	0.4	2	1/1000	13
	110	0.4	2	1/1120	13
Termini 1996	110	0.5	6.5	1/270	17

Hooke 1974 conducted research in a sine-generated channel having θ_0=55°. The tests conducted in this channel involved various flow rates (10, 20, 35 and 50 l/s). In his experiments, Hooke allowed an initially flat bed to deform until it reached equilibrium. The measurements carried out in this channel included bed topography (see Fig. 2.6), bed shear stress distribution and helix strength. However, the bed shear stress and helix strength were measured only in the channel conveying 35 l/s. In order to take these two measurements, the bed was replaced with a concrete replica of the equilibrium bed (formed by means of a mold).

Hasegawa 1983 conducted tests in sine-generated channels having θ_0=20°, 30°, and 90°. Only the equilibrium bed topography was investigated. The contour map of the 30°-channel is shown in Fig. 2.7. In the 20° and 30°-channels the velocity distributions over the equilibrium bed were also recorded.

Ikeda and Nishimura 1986 conducted research in a sine-generated channel having θ_0=40°. Only one run was conducted in this channel with the purpose of this run being the measurement of the bed topography at equilibrium. The results of these measurements are shown in Fig. 2.8.

Whiting and Dietrich 1993 conducted an investigation into time development of bed topography in channels having $0° \leq \theta_0 \leq 20°$. In most of these channels, only observations were reported. However, for θ_0 = 10° and 20°, the equilibrium bed topography was also measured, the bed topography for the 20°-channel being shown in Fig. 2.9. They continued their work by conducting a similar investigation in channels of θ_0 = 110° and 115°. The results of the bed topography measurements in the 110°-channel are shown in Fig. 2.10. As part of their study, they also conducted a single experiment over a flat bed in the 110°-channel, for this experiment the value of B/h_m being equal to 13. Only the flow depths were measured; the free surface velocities were roughly estimated with the aid of the measurements of flow depth throughout the loop. This estimation of velocity was made by equating the centrifugal force to the radial pressure force. The measured free surface topography and the computed velocities are shown in

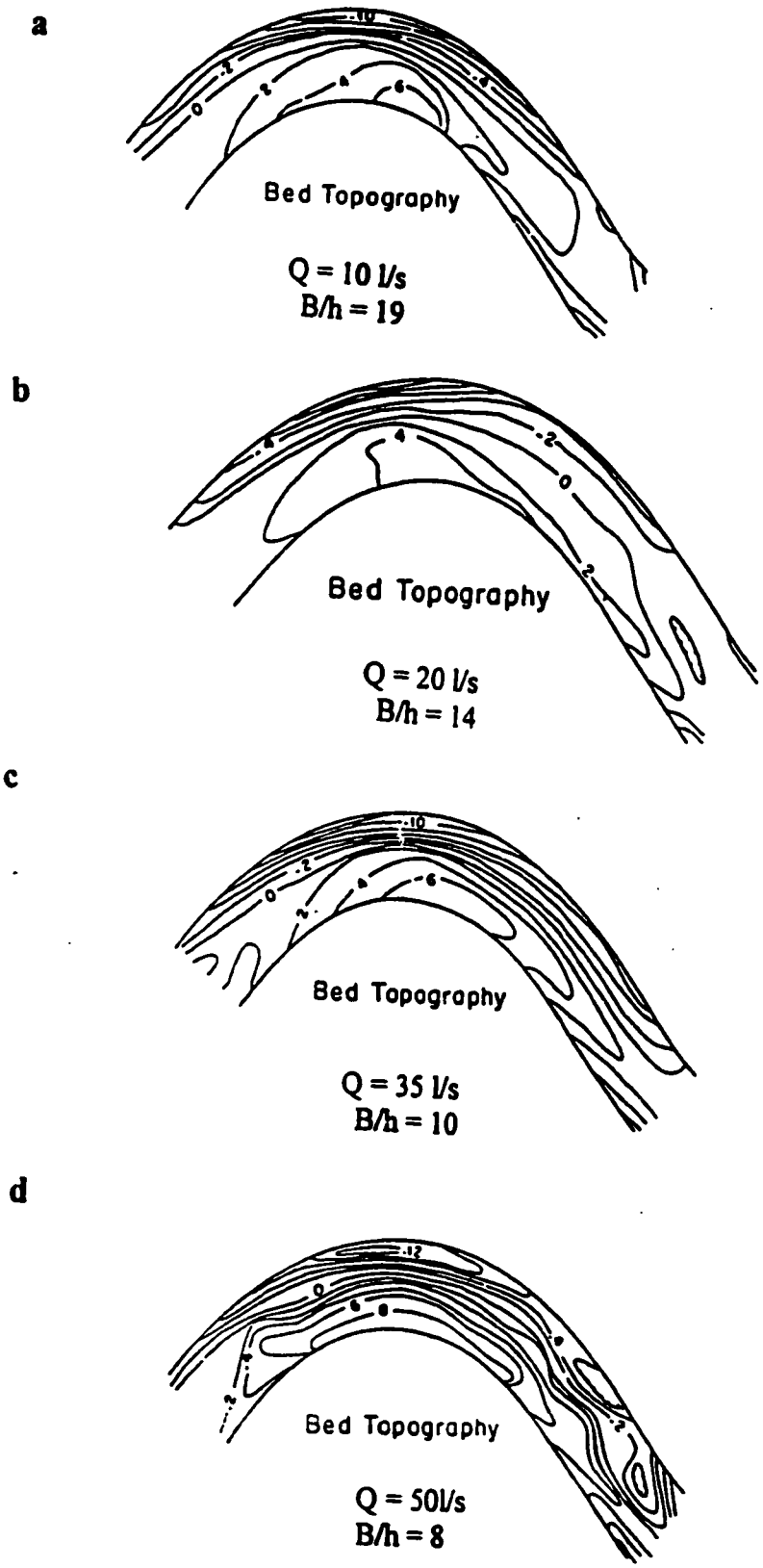

Figure 2.6: Bed topography as measured by Hooke 1974 from runs associated with flow rates of 10, 20, 35, 50 l/s (from Hooke 1974)

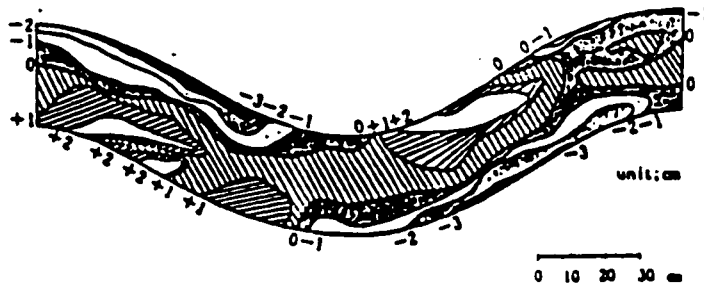

Figure 2.7: Bed topography for the 30°-channel as measured by Hasegawa 1983 (from Shimizu and Itakura 1989)

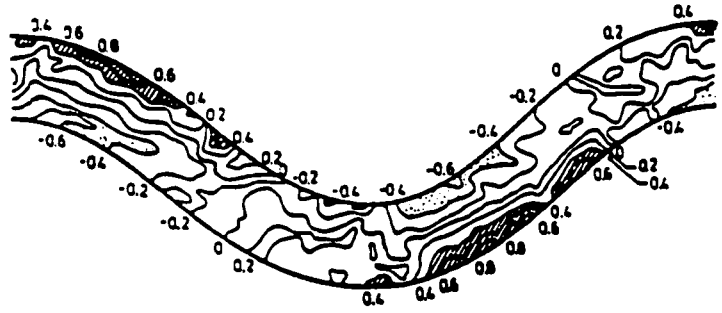

Figure 2.8: Measured bed topography for the 40°-channel (from Ikeda and Nishimira 1986)

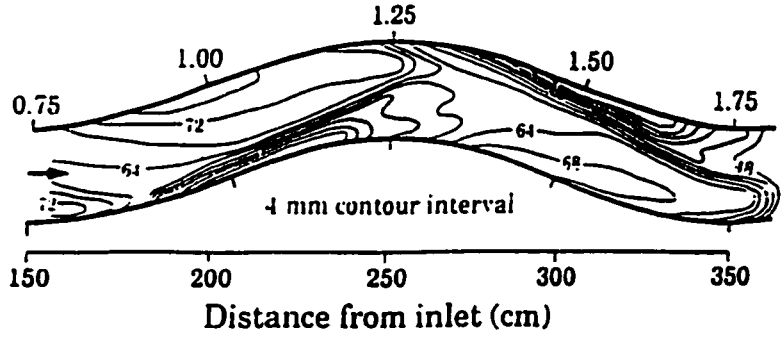

Figure 2.9: Measured bed topography for the 20°-channel (from Whiting and Dietrich 1993c)

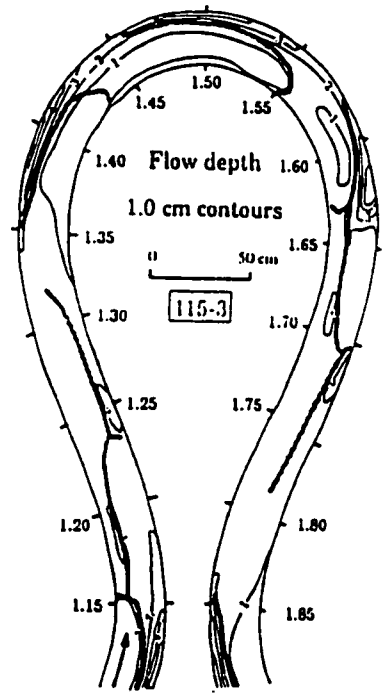

Figure 2.10: Measured bed topography for the 110°-channel (from Whiting and Dietrich 1993a)

Fig. 2.11. As expected the high velocity appears to be diverging from the inner bank throughout the loop and converging on the outer bank downstream of the apex section. This flow pattern is consistent with the defined behaviour of an outgoing flow, which has been identified with large sinuosity channels.

In the majority of the works mentioned above the measurements were carried out in the presence of a deformed (equilibrium) bed. Yet, little was known about the initial flow patterns of a channel were the bed is initially flat, which is of paramount importance to this work. It was not until 1995 that Silva conducted an investigation of the initial flow patterns in channels having two distinct values of sinuosity. As previously mentioned these channels were defined by θ_0 =30° and 110°.

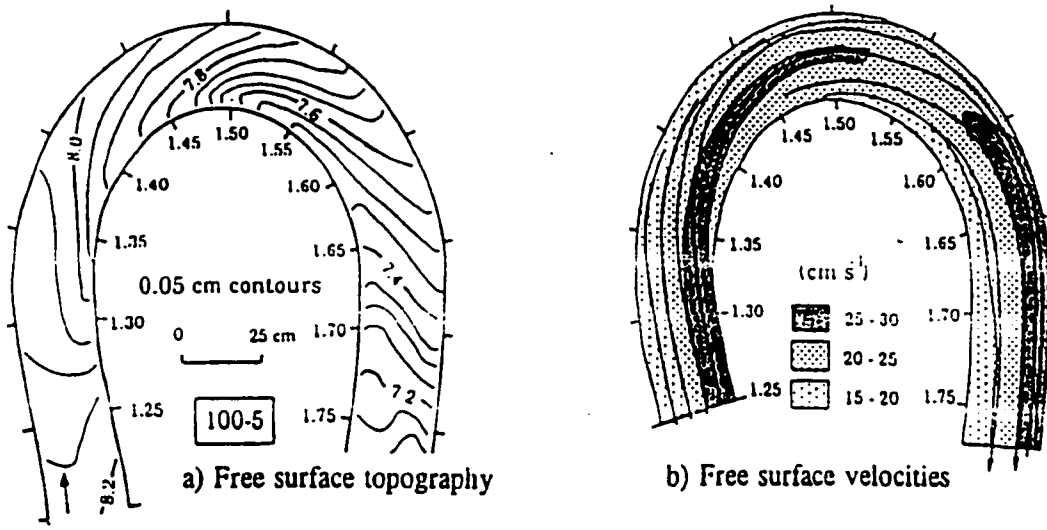

a) Free surface topography b) Free surface velocities

Figure 2.11: Free surface topography and computed free surface velocities in a 110°-channel with a flat bed (from Whiting and Dietrich 1993b)

The conditions used by Silva 1995 during her physical testing are given in Table 2.2. Of the experiments conducted runs $30_2/1^*$ and $110_2/3^*$ are of most interest to the current work. For these two tests the flow rate was maintained around 2 l/s; the channel averaged flow depth (h_m) was in the range of 3-3.2cm. These flow depths resulted in conditions which matched those of a wide channel ($B>>h_m$) where B/h_m is of the order of magnitude of 12.5 - 13.5. The conditions in these two tests also ensure that the Froude number[1] is small, and that the flow is rough turbulent[2].

In both channels, Silva 1995 took measurements at 25 cross-sections, the location of these cross-sections being shown in Fig. 2.12. The measurements recorded at each of these cross-sections for tests $30_2/1$ and $110_2/3$ consisted of the vertically-averaged velocity profiles ($\overline{u}$), the free surface profiles (h) and the vertically-averaged deviation angle ($\overline{\omega}_c$) at the channel centreline. The velocity measurements were taken at mid-

---

[1] Froude number is defined as $Fr = u_m^2 / gh_m$ where u_m is the channel averaged cross-sectional velocity, g is the gravitational constant = 9.81m/s^2 and h_m is the normal flow depth.

[2] Rough turbulent flow is defined by $Re_* > \approx 70$, where $Re_* = (v_* k_s)/\nu$ and v_* is the shear velocity, k_s is the bed roughness ($k_s = 2D_{50}$ for sands) and ν is kinematic viscosity = 1x10^{-6} m^2/s

Table 2.2: Parameters and dimensionless variables used by Silva 1995 (from Silva 1995)

RUN	Q (l/s)	D_{50} (mm)	B (m)	h_m (cm)	S_{bc}	u_m (cm/s)	v_* (cm/s)	c_m	$v_* k_s/\nu$	Re	$(Fr)_m$	B/h_m	h_m/k_s	Quantities measured
$30_2/1$*	2.10	2.2	0.40	3.2	1/1000	16.4	1.77	9.3	78	5250	0.086	12.5	7.3	$\overline{u}$, $\overline{\omega}_c$, h (a)
$30_1/2$	2.26	0.6	0.40	3.2	1/2000	17.7	1.25	14.2	15	5600	0.100	12.5	26.7	$\overline{u}$ (b)
$110_2/3$*	2.01	2.2	0.40	3.0	1/1120	16.7	1.62	10.3	72	5000	0.095	13.3	6.8	$\overline{u}$, $\overline{\omega}_c$, h (a)
$110_2/4$	5.92	2.2	0.40	6.0	1/1120	24.7	2.29	10.8	101	14800	0.104	6.7	13.6	$\overline{u}$ (a)
$110_1/5$	1.68	0.6	0.40	3.0	1/3230	14.0	0.09	14.7	11	4200	0.067	13.3	25.0	$\overline{u}$ (b)

(a) quantities indicated were measured for all l_c-sections (Fig. 6.11)

(b) quantities indicated were measured only for l_c-sections 1_l and 5_l

$u_m = Q/Bh_m$

$v_* = \sqrt{gS_{bc}h_m}$

$c_m = u_m/v_*$

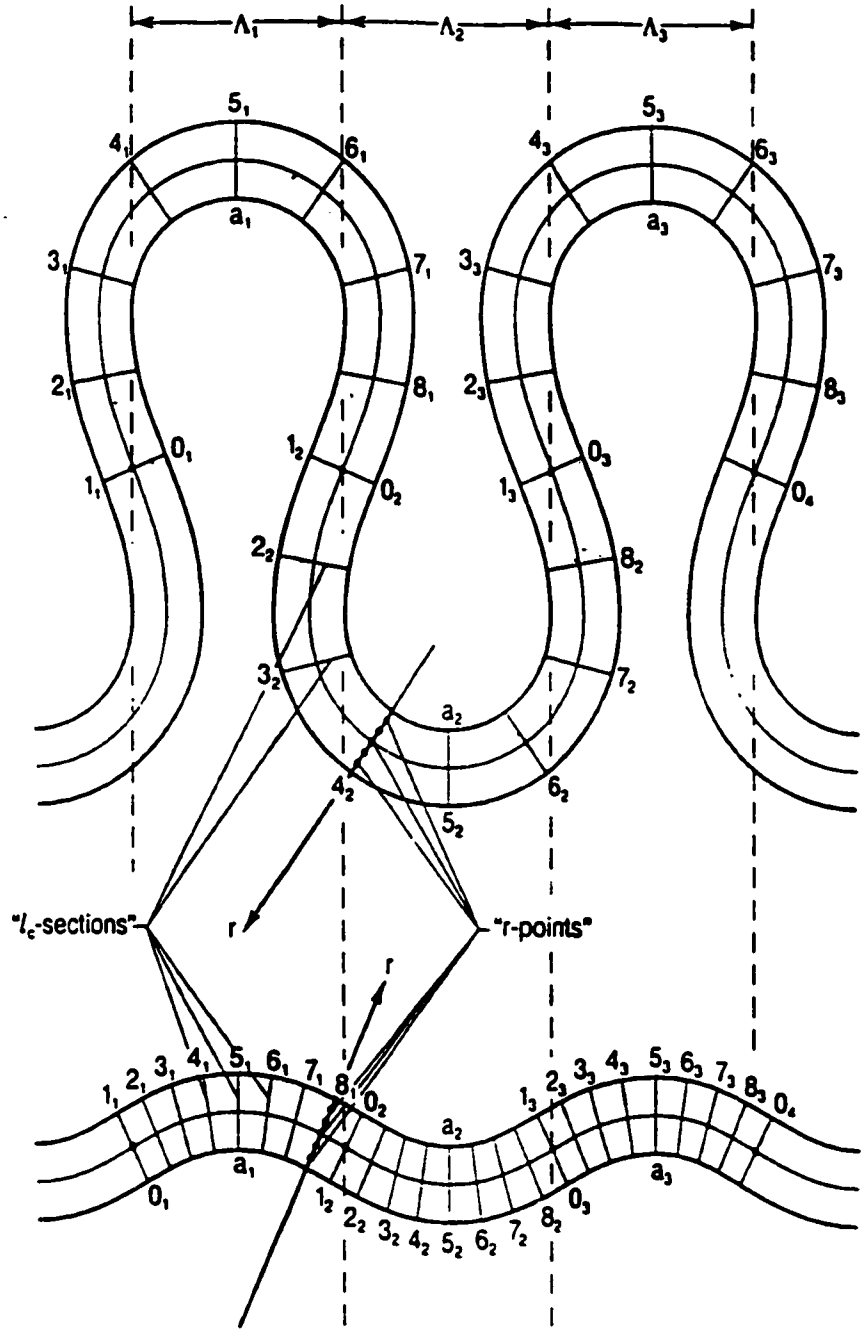

Figure 2.12: Location of measurement sections within Channels tested by Silva 1995 (from Silva 1995)

depth, as this location was assumed to be associated with the vertically-averaged flow velocity. The deviation angle was recorded at multiple depths at each cross-section resulting in profiles that resembled those shown in Fig. 2.13. A schematic of the device used to measure the deviation angle is shown in Fig. 2.14. To determine the vertically averaged deviation angle at a given cross-section an area weighted averaging method was employed. For the purpose of determining the behaviour of the free surface, measurements were taken at a number of locations across the channel's width.

As already mentioned in the Introduction, Silva 1995 recorded different flow patterns for large and small sinuosity channels. In the channel of small sinuosity where θ_0=30°, her measurements revealed the vertically-averaged deviation angle to follow the pattern shown in Fig. 2.15a: $\overline{\omega}_c$ is negative approximately between a crossover *O* and the apex *a* and positive between the apex *a* and the crossover *O'*. This behaviour is consistent with the velocity profiles shown in Fig. 2.16a, where the flow converges to the inner bank between *O-a* and then diverges from the inner bank between *a-O'*. As mentioned in Chapter 1 this flow type was termed ingoing. In the channel of large sinuosity (θ_0=110°), the measurements revealed $\overline{\omega}_c$ to follow the pattern shown in Fig. 2.15b: $\overline{\omega}_c$ is positive approximately throughout *OaO'*. These findings are supported by the measured velocity profiles shown in Fig. 2.16b. If the highest local velocity is traced in this figure as the water travels downstream it becomes clear that the flow is continuously diverging from the inner bank throughout the length of the loop. As previously mentioned in Chapter 1, this flow pattern was termed outgoing.

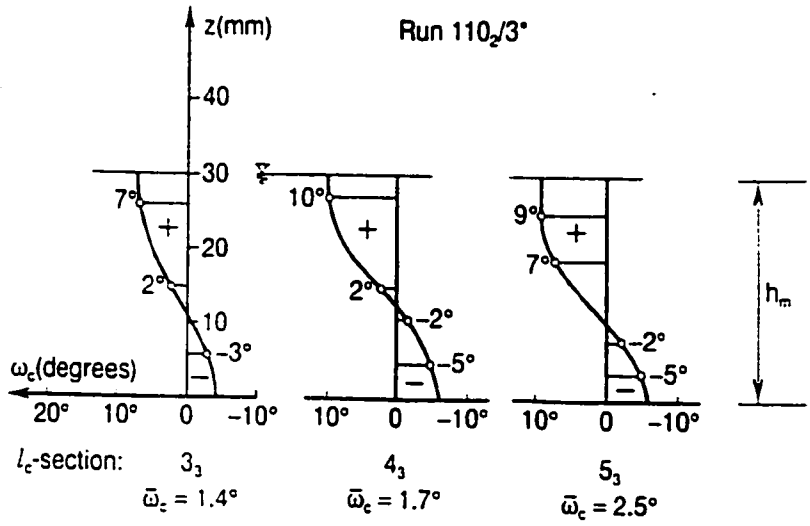

Figure 2.13: Examples of deviation angle profiles recorded by Silva 1995 (from Silva 1995)

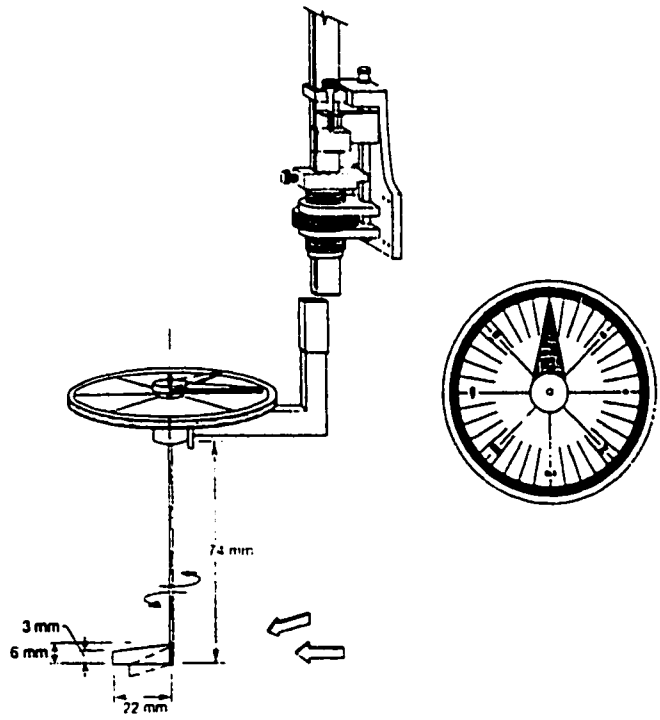

Figure 2.14: Schematic of device used by Silva 1995 to record flow deviation (from Silva 1995)

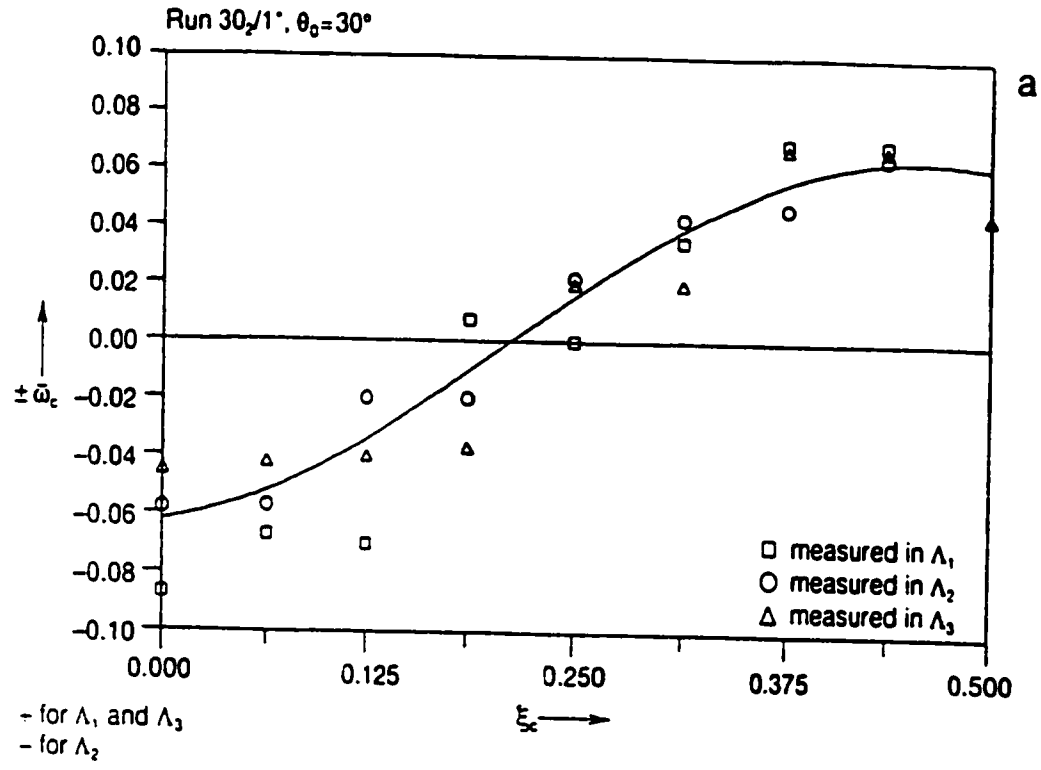

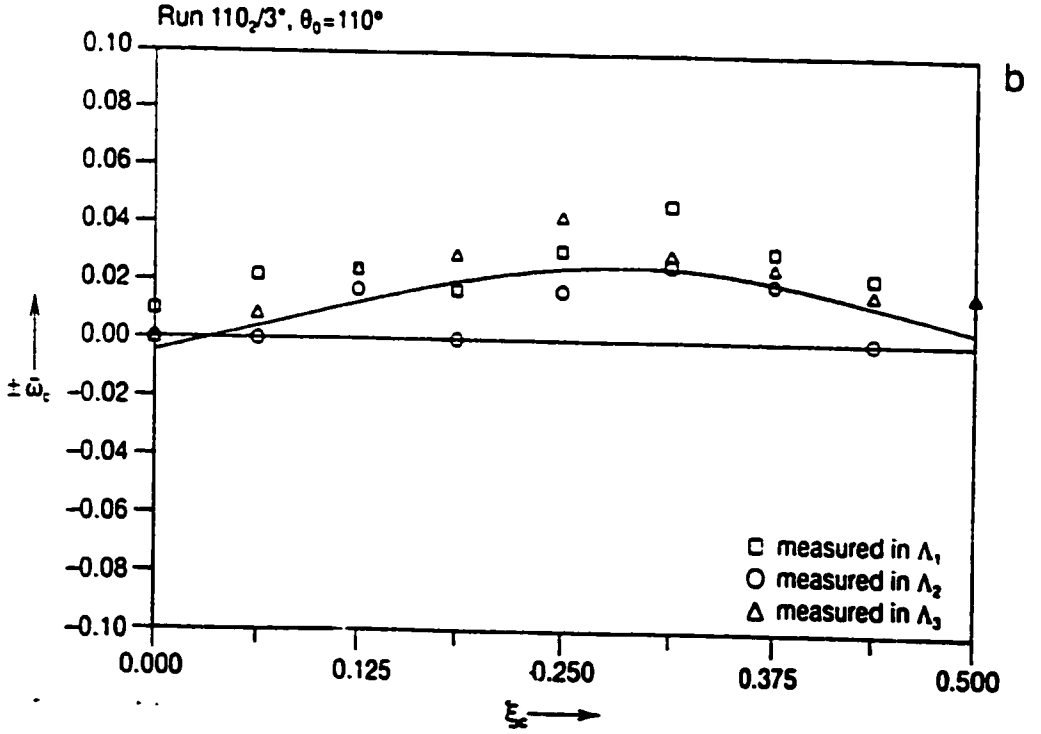

Figure 2.15: Variation of measured values of $\bar{\omega}_c$ along ξ_c (from Silva 1995)

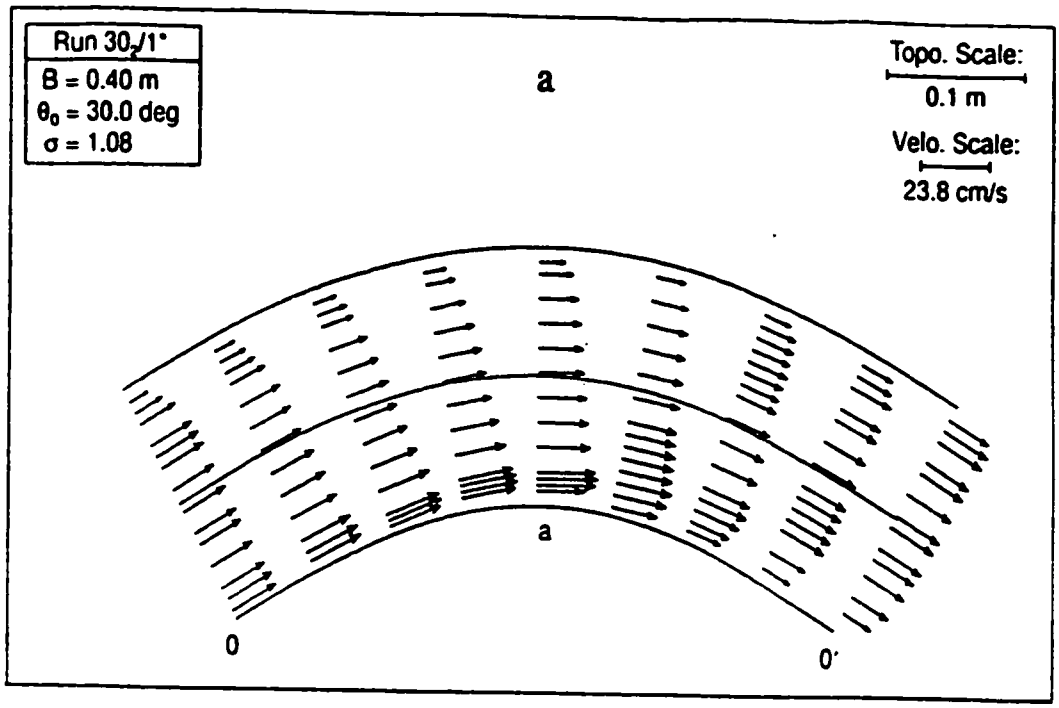

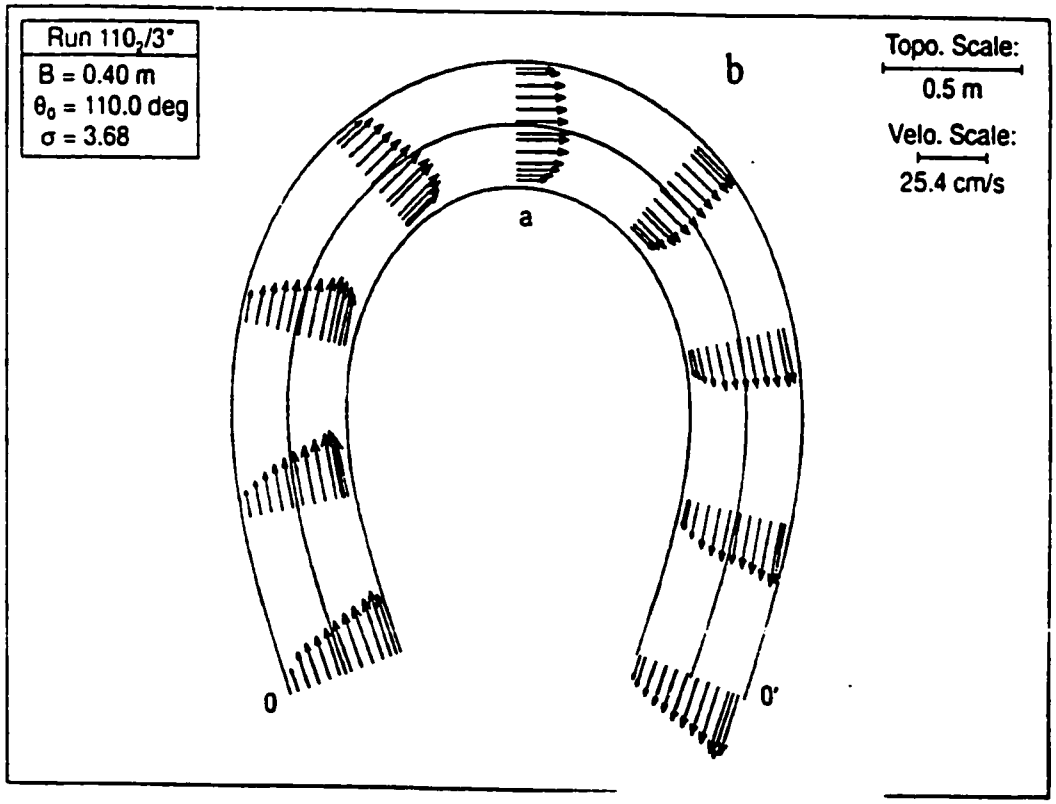

Figure 2.16: Measured fields of the flow velocity $\bar{u}$ (from Silva 1995)

Termini 1996 extended the work of Silva, conducting research in a sine-generated channel having θ_0=110°. The conditions used by this researcher are comparable to those used by Silva. However, the slope and size of grain used were significantly different. Measurements include initial conditions as well as equilibrium bed topography. It should be mentioned that the initial flow conditions recorded in this study supported the findings of Silva. In her experiments over a flat bed, Termini recorded values of flow depth and the vertically-averaged flow velocities. From these measurements she was able to compute the contours of the divergence of the sediment transport rate ∇q_s, which is shown in Fig. 2.17. Termini took further measurements, this time, of the equilibrium bed topography as shown in Fig. 2.18. From these plots it was observed that the zones of erosion/deposition associated with the initial flow (zones of positive ∇q_s correspond with zones of erosion and negative ∇q_s values correspond with zones of deposition, as shown in Fig. 2.17) do not experience any major shifts in their locations in the flow plan during the evolution of the bed topography.

2.4 Mechanics of Meandering Flows

2.4.1 Flow Structure

Yalin 1992 described the flow in a sine-generated channel as the sum of two components, which are superimposed onto each other. One component of the flow, which is associated with channel curvature (1/R), is a helicoidal motion referred to as cross-circulation. The second component of the flow, which is associated with the changes in curvature, occurs in the form of a laterally oscillating fluid mass. The laterally oscillating fluid mass can be considered the basic flow structure upon which the cross-circulation is superimposed.

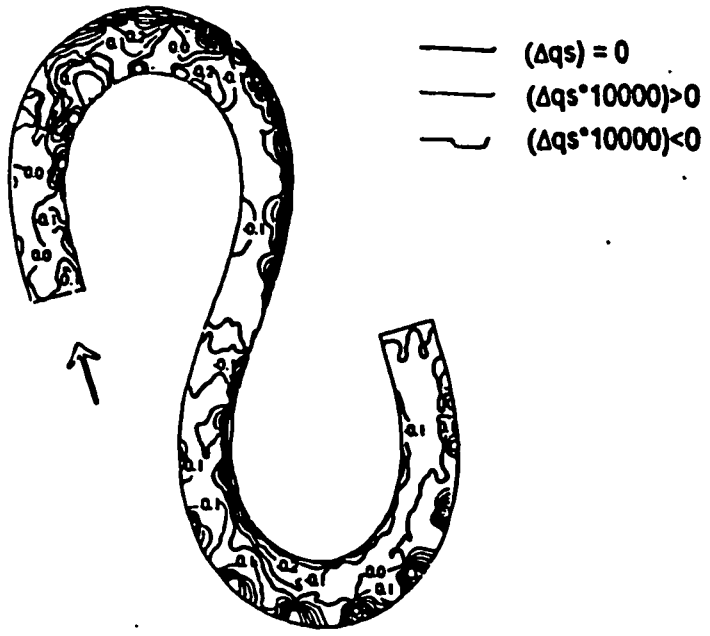

Figure 2.17: ∇q, over the flat bed of the 110°-channel (from Termini 1996)

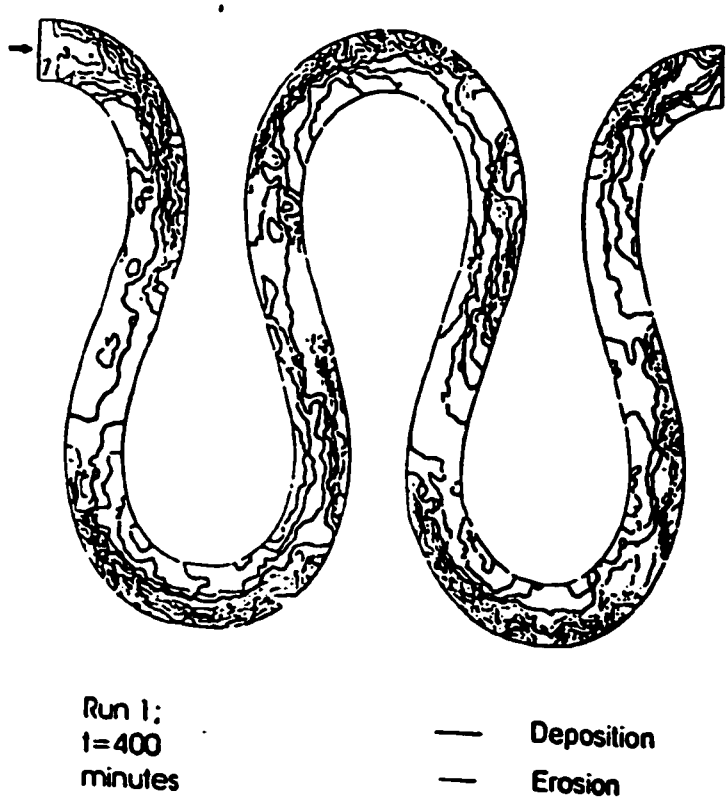

Figure 2.18: Measured equilibrium bed topography at t=400 minutes (from Termini 1996)

2.4.1.1 Basic Flow Structure

As the flow travels downstream in a meandering channel, it is subjected to changing forces due to changes in channel curvature. These forces create a condition which results in a lateral shift in the fluid mass as it is conveyed downstream, measured by a non-zero angle ω between the streamlines and the centreline. When discussing the basic structure of meandering flows, Yalin stated that "... it is formed by a fluid mass, which shifts (in all its thickness, i.e. flow depth) as it moves downstream". This motion is represented graphically in Fig. 2.19. Consider the vertical 1-2: since the fluid is being shifted as it moves downstream, the vertical 1-2 is deformed into 1'-2'. The radial velocity of the shift in Fig. 2.19 maintains a constant sign throughout the cross-section irrespective of its location as relates to the centreline of the channel.

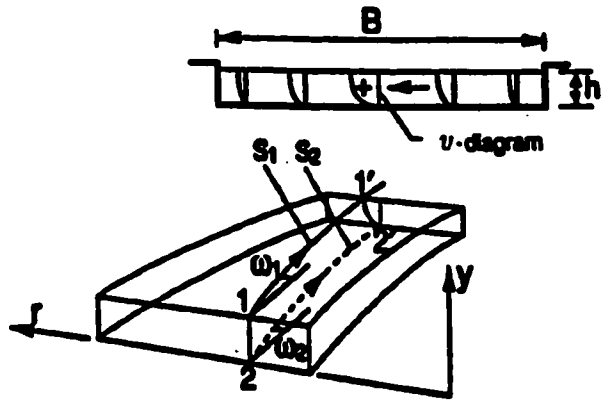

Figure 2.19: Convective streamlines of meandering flows (after Yalin 1992)

As shown in Fig. 2.19, ω_1 (at the free surface) and ω_2 (near the bed) are not equal. In fact, ω_1 is larger than ω_2 as the deviation of the streamline decreases as the bed is approached. However, if only wide channels (B>>h) are considered, the difference in magnitude between these two angles is not significant. Such is the case in the works of

Nelson and Smith 1989a,b, Smith and McLean 1984, Shimizu and Itakura 1989, Struiksma et al. 1985 and Silva 1995. Thus in all these works the vertically averaged flow was considered: and the deviation of the streamlines from the channel centreline can be associated with the vertically-averaged deviation angle.

2.4.1.2 Cross-circulation

Consider the free surface of the flow in a curved channel. This free surface is characterized by a change in elevation between the inner and outer bank (see Fig. 2.20). This elevation change is known as super-elevation Δh. In the case of a sine-generated channel, Δh increases as the apex is approached (being a maximum at or near the apex). The cause of super-elevation has been discussed, among others, by Henderson 1966, Graf 1971, and Chin 2000. Chin stated that the super-elevation can be predicted by the expression

$$\Delta h = \frac{u_{av}^{\ 2}}{g}\frac{B}{R}, \tag{2.13}$$

where B is the channel width, R is the channel radius (see Section 2.2), and u_{av} is the average cross-sectional velocity.

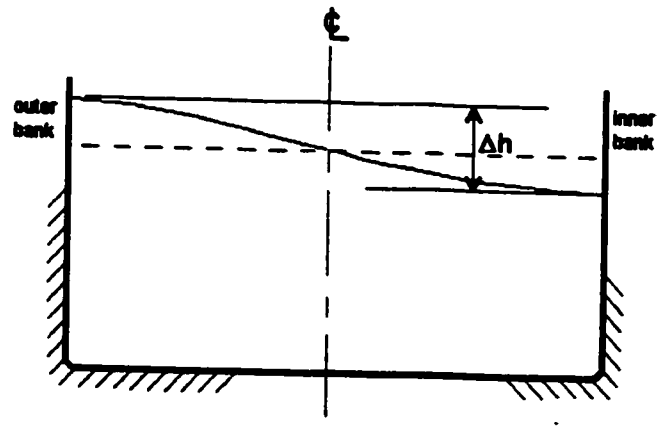

Figure 2.20: Super-elevation between inner and outer banks of meandering channels

This super elevation results in a cross-circulation (Γ) pattern within the flow. Cross-circulation can be associated with the presence of a pressure gradient (F_p) and the centrifugal forces (F_c) acting on the fluid body. Henderson 1966 stated that the pressure distribution is "very nearly hydrostatic" for any vertical within the flow field. He further explained that the presence of a super-elevation, however, results in a transverse pressure gradient which can be defined by $F_p=-\gamma\ \delta h/\delta r$, where δh is the difference in free surface elevation between two verticals and δr is the distance between those verticals. This force acts at all times towards the inner bank; on the other hand, the centrifugal force $F_c = \rho\ u^2/r$ increases along the vertical (as u increases as the free surface is approached), and always points towards the outer bank. Consider a point B located in the middle of a vertical AC (Fig. 2.21a). Below B, $F_p>F_c$, while above B, $F_p<F_c$. This condition will result in a helical motion of the flow known as cross-circulation (see also Chang 1988), which is shown in Fig. 2.21.

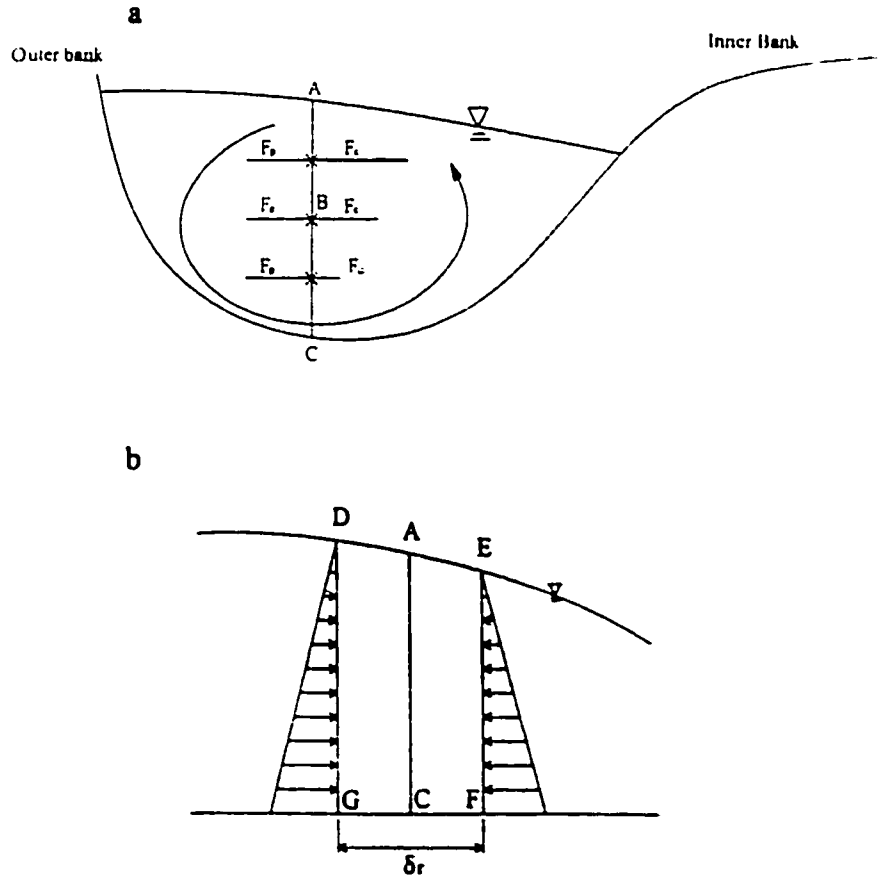

Figure 2.21: Origin of cross-circulatory flow (from Ackert 2000)

It was originally suggested that the cross-circulation was the main factor associated with bed deformation (Henderson 1966, and Leliavsky 1955 etc.). For this to hold true, a few conditions would have to exist in all deformed channels (see e.g. Hooke 1974, Yalin 1992, etc.). First, the maximum helix strength occurs at the apex section where the centrifugal force and thus the radial velocity is at its maximum (Rozovskii 1961, Engelund 1974, Zimmerman 1977, etc) This would lead to the most pronounced area of erosion/deposition being at the apex. Secondly, the helix strength would have to be of a high order of magnitude to transport large quantities of material across the channel as the B/h ratio increased. However, Yalin 1992 stated that "with the increment of B/h the cross-sectional circulation tends to lose its meaning", a view shared by Hooke 1974. These two conditions would lead to a standard erosion/deposition pattern as shown in Fig. 2.22. However, from laboratory testing and field measurements (Silva 1995, Whiting and Dietrich 1993b, Hasegawa 1983), this situation is not found to be true. Rather the erosion/deposition pattern can be associated with θ_0 and B/h_m. Further support for the case against a dominant cross-circulation, as relates to bed erosion/deposition, is based on extensive field observations made by Matthes 1941 who stated "sediment entering the stream from the scour of the concave banks becomes deposited on the downstream convex bank on the same side of the river, and only a small portion of the eroded material crosses the channel". Modeling conducted by Silva 1999, as well as, Banerjee 2000 accurately predicted the erosion/deposition pattern for large and small sinuosity channels without invoking cross-circulation. Therefore, the theory of cross-circulation controlling erosion and deposition cannot hold true. When speaking of the effect of cross-circulation in a sinuous channel Yalin 1992 stated that the role of cross-circulation is often "overstressed".

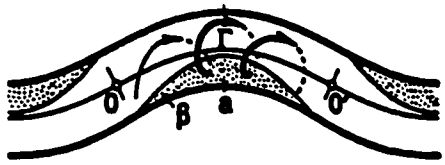

Figure 2.22: Standard deposition pattern due to cross-circulation (from Yalin 1992)

2.4.2 Periodic Property of Meandering Flows

Consider flow entering a long channel (from a reservoir, say). If the channel is sufficiently long, the flow in it will achieve a fully developed pattern. However, for a distance at the channel entrance, the flow will require a development region. Far away from the channel entrance, the flow in a sine-generated channel acquires periodic characteristics. This was explained by Silva 1995 with the aid of Fig. 2.23. Zone I is the channel entrance. When discussing this zone Silva 1995 stated "one can postulate that in zone I (viz $0 < x < x_e$) the flow is affected by the entrance conditions and it is thus not periodic". As the flow moves further down the channel it begins to exhibit a periodic behavior between loops (Zone II). By stating that the flow begins to exhibit a periodic behavior, it is meant that the flow appears to mirror itself between loops with L/2 defining one loop. It is because of this phenomenon that any loop within Zone II can be used to predict the flow patterns of all loops within the same zone. Silva 1995 stated "it follows that the study of a meandering flow, or of one of its consequences, in the semi-infinite (periodic) zone II can be reduced to its study within any of its regions of the length L/2".

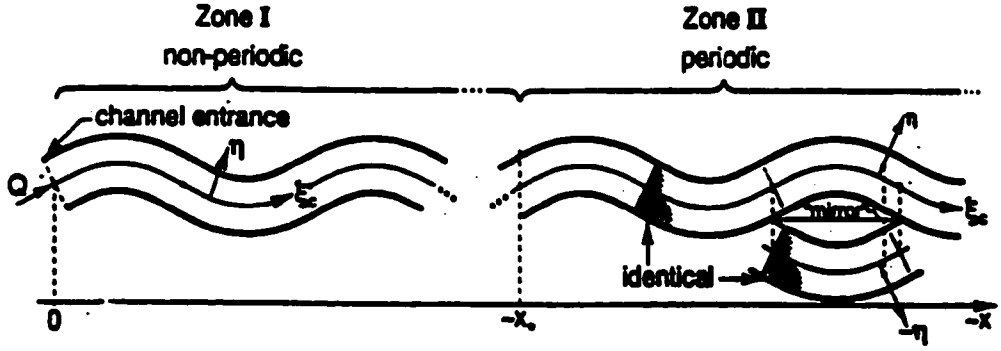

Figure 2.23: Periodic and Non-periodic zones in meandering channels (from Silva 1995)

3.0 EXPERIMENTAL SETUP

The experiments reported in this thesis were carried out in the meandering research facility of the Great Lakes Institute for Environmental Research (GLIER). A schematic of the facility, which was built in the fall of 1999, is shown in Fig. 3.1. The facility is similar to that used by Silva 1995, although some modifications, developed by the author and technical staff at the University of Windsor, were incorporated into the design.

The purpose of this chapter is to describe the meandering research facility, and in particular its hydraulic circuit. Some aspects of the design and construction of the facility are also presented.

3.1 Hydraulic Circuit of the Meandering Research Facility

The hydraulic circuit of the facility comprises of the following components:

1) a head tank
2) an entrance system
3) the meandering channel itself
4) the return channel.

In this section, the components above will be described in detail.

3.1.1 The Head Tank

The Head tank, shown in Fig. 3.2, consists of several components including a constant-head reservoir, a stilling basin and a V-notch weir. The head tank itself is constructed of standard 200mm concrete block. The exterior and interior of the head tank were waterproofed after construction to prevent leakage.

As indicated in Fig. 3.2, water is pumped (by a Hayward pool pump, maximum capacity of 10 l/s at 12.2m of lift) from the sump into the constant-head reservoir (see also Fig. 3.1). The water fills this reservoir up to the overflow spillway, which results in a constant head. Once full, excess water flows into the spillway and is discharged back

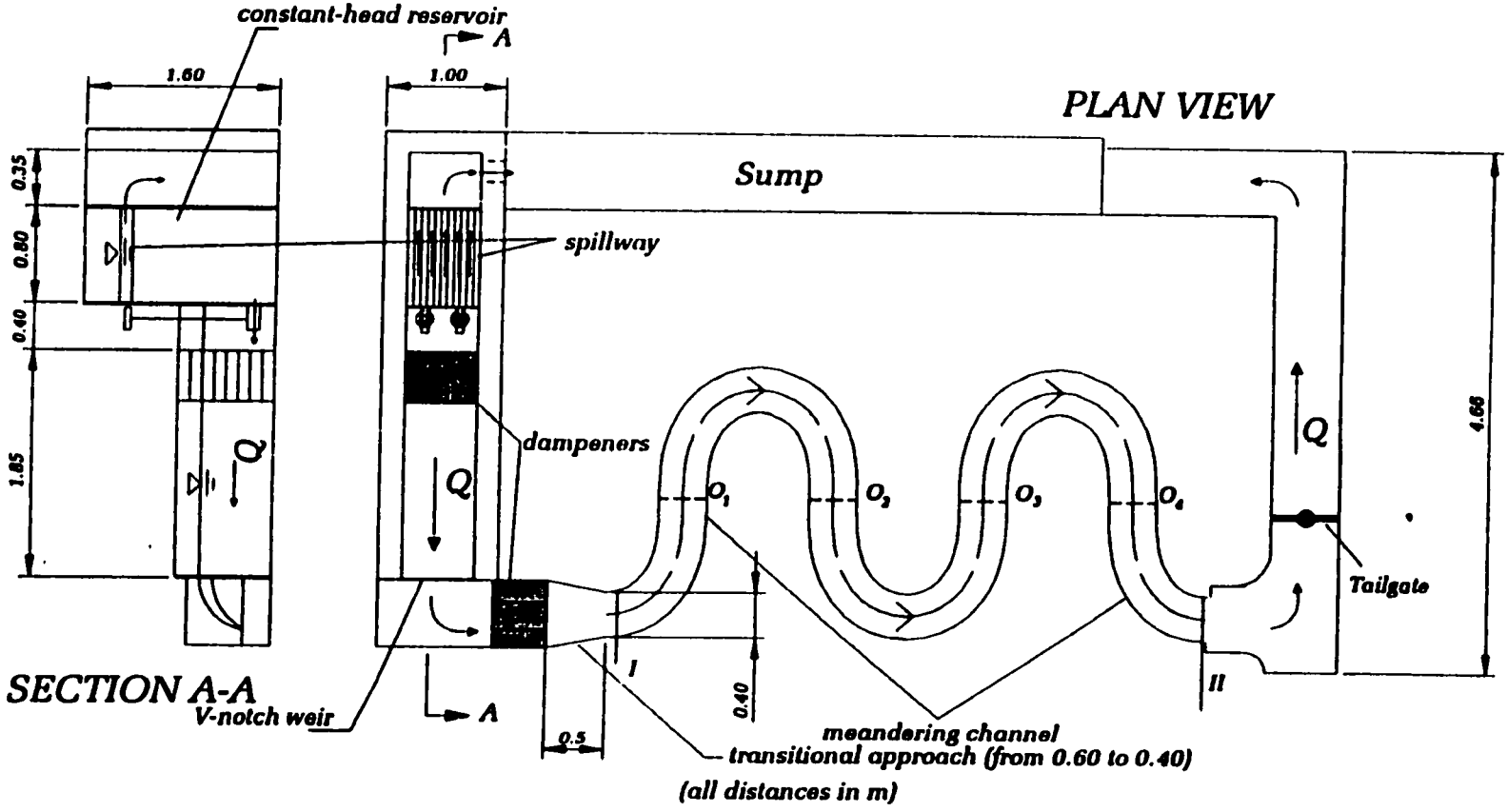

Figure 3.1: Experimental Set-up

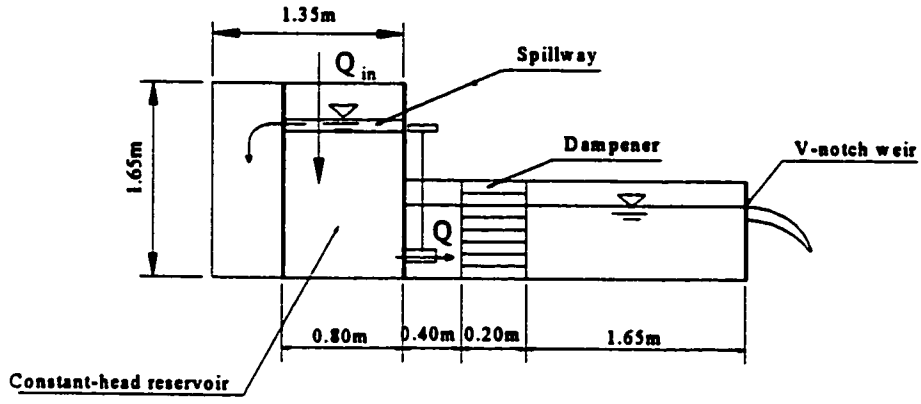

Figure 3.2: Flow directions within the head tank

into the sump. The water required for the experiments is discharged from the constant-head reservoir into a stilling basin by means of two outlets on the front face of the reservoir; the flow rate through these outlets is controlled by two gate valves. While in the stilling basin the flow passes first through a flow dampener, and then continues downstream for a short distance until it passes over a V-notch weir.

The overflow spillway consists of four channels, whose cross-sections are half-circles all 25mm in radius (see Fig. 3.3). These semi-circular sections are made of 50mm ABS pipes. These pipes were cut along their centrelines; the edges of the spillway were then sanded to an angle.

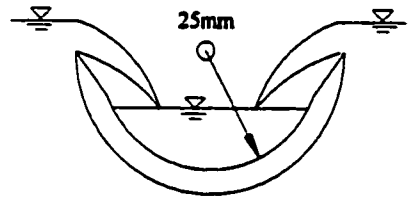

Figure 3.3: Cross-section of one channel of the overflow spillway

The water outlets at the front wall of the constant-head reservoir were circular (50mm diameter) and located at a height of 30cm from the bottom of the wall. This distance was selected to provide a head of 1m, allowing a better control of the flow rate in the range of 2 to 10 l/s.

The flow dampener was installed at a distance of 0.40m downstream from the front wall of the constant head tank. This system is used to calm and straighten the flow. The dampener is made of 25mm type-M (thin wall) copper pipe sections. Copper pipe was selected because of the minimal area obstructed by its wall and because of its availability. The pipes were cut to 20cm lengths, then placed across the width of the head tank with their longitudinal axis parallel to the flow direction. The pipes were secured to each other using silicone and stacked to a height of 70cm, as illustrated in Fig. 3.4.

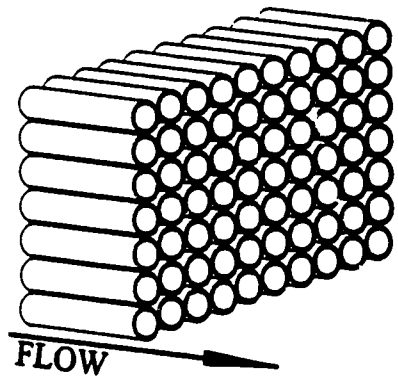

Figure 3.4: Configuration of pipes in dampener

The V-notch weir is positioned at the downstream end of the head tank, at a distance of 1.65m from the flow dampeners. The weir itself was designed so as to maximize the water depth upstream at flow rates in the range of 2 to 3 l/s. The V-notch was constructed from Plexiglas, with a top width of 0.50 m and a depth of 0.25 m, as shown in Fig. 3.5. After the "V" was cut, the front side of the weir was ground at an angle until the thickness of the wall at the edges of the "V" was negligible.

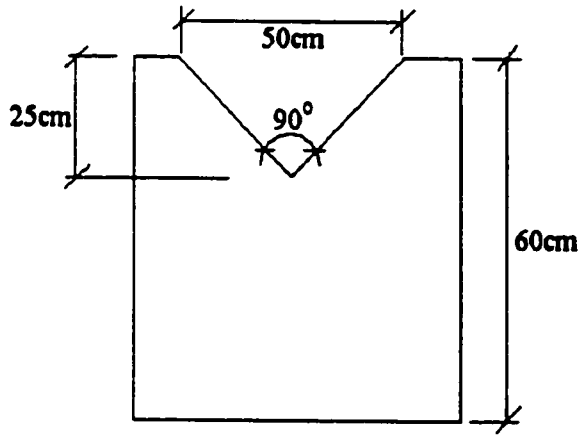

Figure 3.5: Dimensions of the V-notch weir

3.1.2 The Entrance System

The "entrance system" is the region between the V-notch weir and the meandering channel itself (see Fig. 3.1). It consists of a basin to receive the water discharged over the weir, a flow dampener, and a transitional approach. The dampener was constructed of the same materials and in the same pattern as the one in the head tank, however, its height was only 30cm (as apposed to 70cm for the dampener in the head tank). The transitional approach downstream of the dampener contracts the flow from a width of 0.60m to 0.40m over a distance of 0.50m.

3.1.3 The Meandering Channel

The meandering channels themselves were installed between sections I and II in Fig. 3.1. The design and the methods used to construct the meandering channels took into consideration the fact that three channels were to be tested, and thus the channels themselves should be removable.

The (21cm high) walls of the channel were made of 3 mm Plexiglas sheets. The sheets were cut in stripes 2.44m long and 21cm high, and held in place (so as to form the

channel walls) by an aluminum frame. This frame was made of 37.5mm x 4.8mm aluminum flat stock forming the top and bottom rails, and 50mm x 50mm x 4.8mm aluminum angle forming the supports for the rails. Sections of 37.5mm x 4.8mm flat stock were cut to 13.13cm lengths to sit between the top and bottom rails of the channel at the joints between the Plexiglas sheets. These 13.13cm plates added extra support to the Plexiglas thereby reducing the chance of buckling of the walls at the joints.

As previously mentioned, the aluminum rails were held in place by supports made of 50 x 50x 4.8mm aluminum angles which were cut and welded in the shape of an "L". For each support, two angles each of 21cm in length were placed together and welded at 90 degrees to each other. The front and bottom faces of the support were then drilled to allow them to be attached to the rails and to the floor. Fig. 3.6 below shows one of the supports.

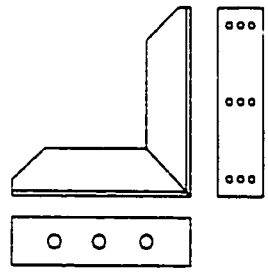

Figure 3.6: Support for meandering channel

Before installing the main channel, a 19mm (3/4") plywood floor was installed. The plywood was used so that the channel support did not have to be anchored to the concrete floor. In order to prevent the infiltration of water, both the faces and the edges of the plywood were painted. To ensure a water tight seal the plywood sheets were siliconed along the edges where they abutted each other. Once in place this new floor was painted again. All edges were screwed to the concrete floor to insure they sat flush to each other.

For the purpose of channel assembly, it was necessary first to draw an outline of the proposed meandering channel on the plywood sheets. The coordinates of several points along the centreline of the meandering channel were determined with the aid of the computer program LOOP, Fortran 77 (Silva 1995). Once all the centreline points were marked on the plywood sheets, they were connected by straight lines. In order to mark the position of the walls, an adjustable square was then set to 20cm and held square to the midpoint of the lines connecting the coordinates, and a point was marked at the end of the square. This procedure was repeated until the position of both walls were marked.

Before installing the frame, the supports were attached to the aluminum rails. One end of this frame was then secured up against the wall of the entrance and then screwed to the plywood floor. The frame was then bent to follow along the previously marked wall location points. As the frame was bent, the supports were secured to the floor. The Plexiglas sheets where then clamped to the frame and drilled at the same locations as holes previously drilled in the rails. The Plexiglas sheets were drilled after the installation of the frame to insure the holes lined up and to minimize stresses in the Plexiglas. Once all the sheets were drilled, the holes were countersunk to allow the heads of the screws to rest flush with the face of the wall. This was done to avoid interference with the flow. Fig. 3.7 shows graphically the assembly of the channel at a joint. Figs. 3.8a,b,c show pictures of the completed 90°-,70°- and 50°-channels, respectively.

The installation of the channel walls using the method outlined resulted in some error in the distance between walls. The standard deviation in distance between the walls, with respect to the desired width B of 40cm, was +/- 0.60cm in the 90°-channel, +/- 0.60cm in the 70°-channel and +/- 0.40cm in the 50°-channel. For all channels the standard deviation of the width was based on 25 measurements, one measurement was taken at each of the cross-sections used for testing.

Refer to appendix E for pictures taken during the assembly of the meandering channel.

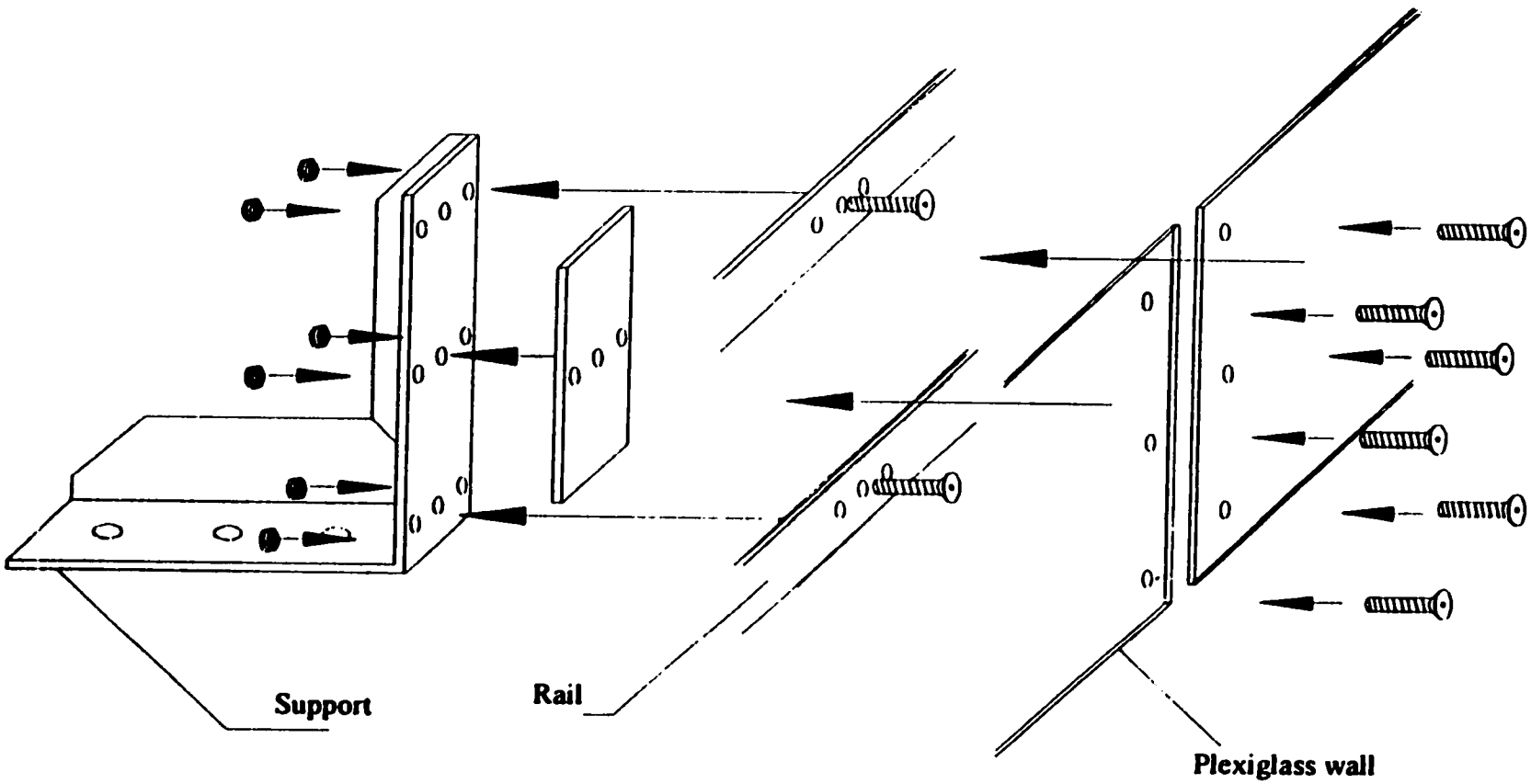

Figure 3.7: Channel assembly at a joint and a support

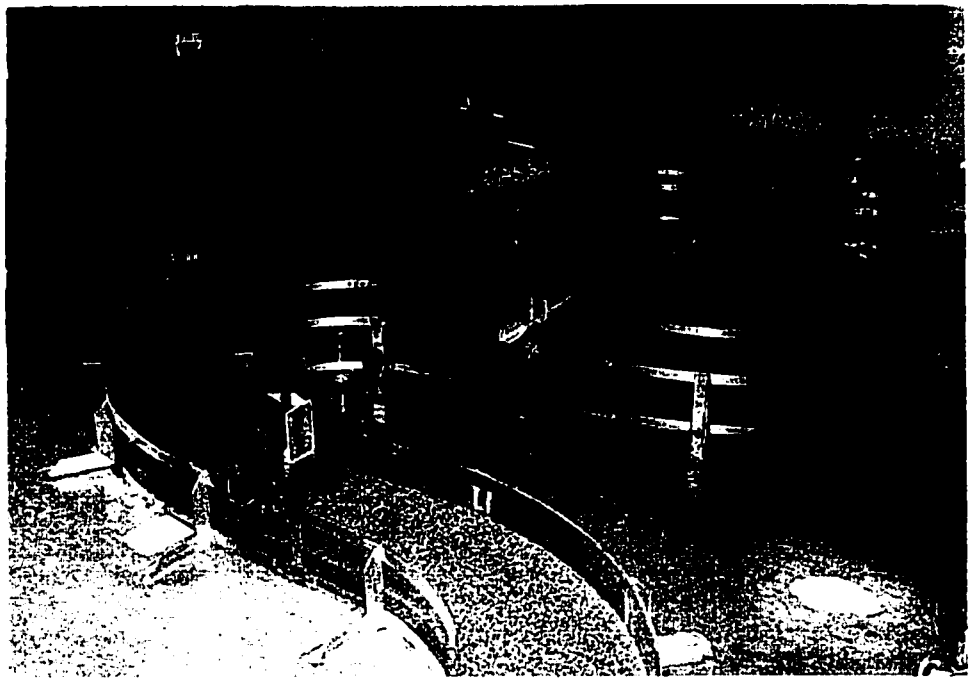

Figure 3.8a: Picture of completed 90°-channel.

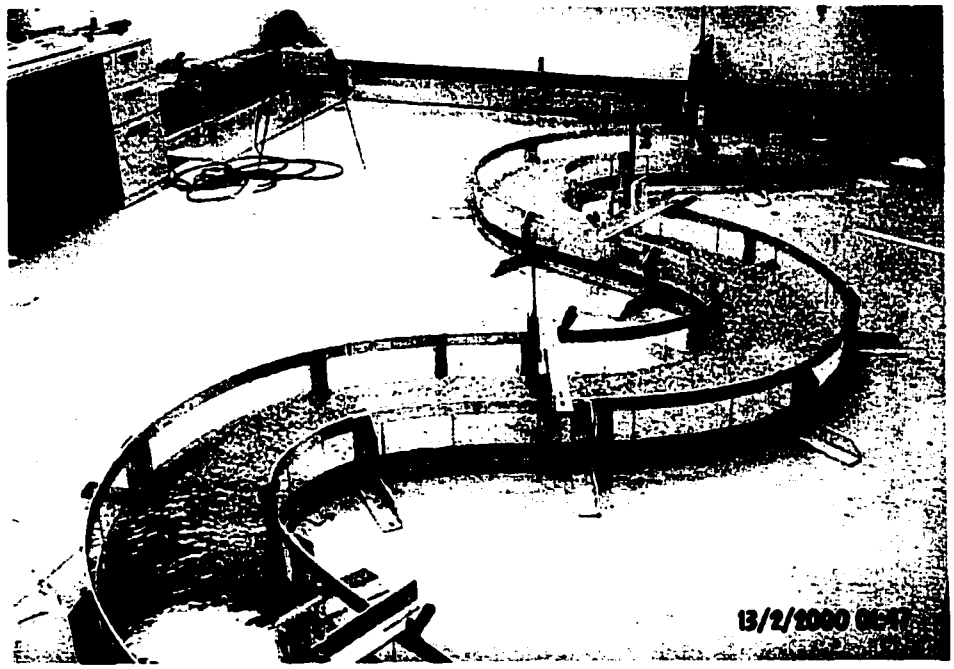

Figure 3.8b: Picture of completed 70°-channel

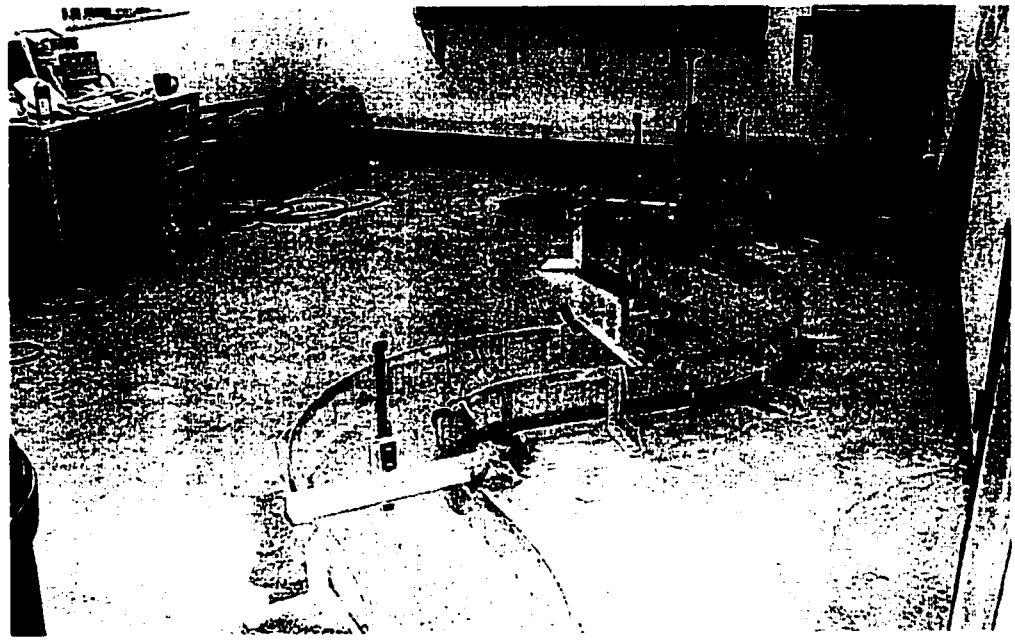

Figure 3.8c: Picture of completed 50°-channel

3.1.4 The Return Channel

The final section in this recirculating system is the return channel (Fig. 3.9). The width of this channel is 60cm measured wall to wall; its walls are 20cm high.

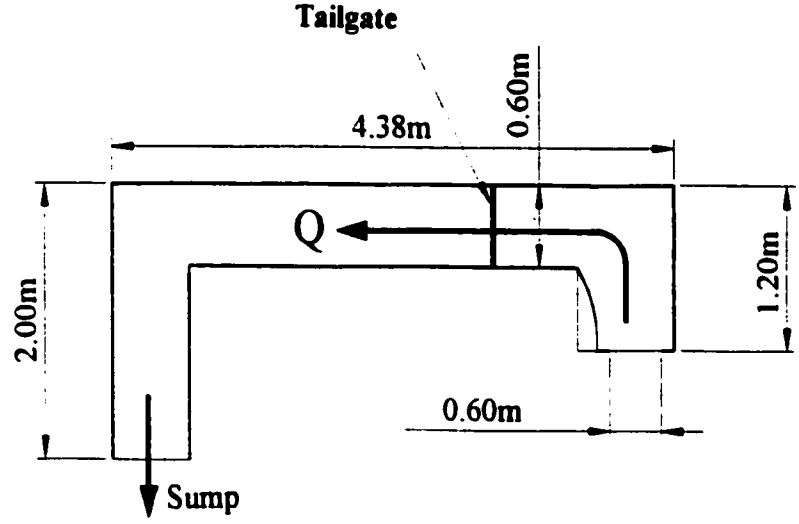

Figure 3.9: The return channel

The tailgate is placed in the return channel at a distance of 125 cm downstream from the end wall. It is held in place by an aluminum frame. The frame is attached to the tailgate with a pivoting joint, which is attached to a stainless steel threaded rod. A handle is attached to the end of this rod for its operation. To prevent the rotation of the tailgate the sides of the return channel were milled to a depth of 6mm. The tailgate itself is made of 1.25cm Plexiglas with a size of 61.25cm x 20cm. Fig. 3.10 shows a diagram of the tailgate.

3.2 Channel Bed and Roughness

The beds of all three channels were made of a 5cm to 10cm layer of compacted cohesionless granular material. This material was also used to form an entrance ramp at the transitional approach located just upstream of the working section. Before installing

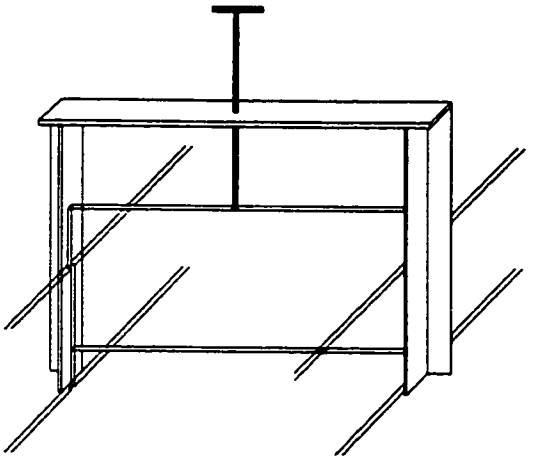

Figure 3.10: The tailgate assembly

the channel bed, the locations corresponding to 1mm changes in the channel bed elevation at the centreline (dictated by the required channel slope) were located and marked. To place the bed in the working section, a base of granular material was laid along the channel and then sprayed with water to aid in compaction. The base layer was then compacted by placing a small square section of plywood approximately 20cm x 20cm, on top of the loose granular material and striking the plywood with a standard proctor hammer. This plywood square was moved around the channel until the entire base layer was compacted. A finishing layer of the granular material was then placed on top of the base layer. This layer was scraped approximately to the required bed slope. To ensure a uniform slope a Sokki Set 3 total station was employed. The total station provided the ability to measure a 1mm vertical drop at the previously marked locations. The total station and a small spirit level were both used to ensure a zero slope across the channel width providing a perfectly rectangular cross-section. Once the slope was set, a varnish solution of 50% water based varnish (Flecto brand) and 50% water was sprayed onto the channel's bed to immobilize the grains and thus maintain a constant slope. This, as well as similar methods of immobilizing the movable bed, are known not to affect the proportionality between the grain size and the effective bed roughness (see. e.g. Khalil

1972, Krishappan 1977). Accordingly, throughout this thesis the proportionality $k_s \approx 2D$ is adopted (Yalin 1992, Kamphuis 1974, etc).

The granular material used to form the bed was selected so as to closely match that used by Silva 1995. This granular material ensures also that the flow is in the rough turbulent regime, and that the Froude number, $Fr = u_m/(gh_m)^{1/2}$, where g is acceleration due to gravity, u_m is channel averaged flow velocity and h_m is the channel averaged flow depth, is low. Accordingly, a material with a D_{50} of 2.2mm was selected. To form this material a Geotechnical Engineering Firm was contracted to combine two different materials in equal amounts, resulting in the required grain size. Table 3.1 shows the characteristics of the two different sands selected as well as the characteristics for the mixture. In Fig 3.11, a grain size analysis of the resulting mixture is shown.

Table 3.1: Cohesionless Granular Material

Description	D_{50} (mm)	Uniformity (D_{90}/D_{10})
Sand 1	1.83	1.60
Sand 2	2.46	1.74
Mixture *	2.20	2.44

* used in this thesis

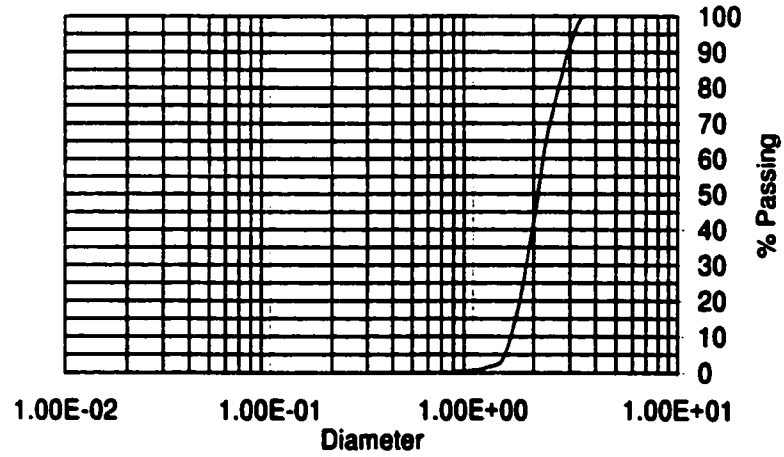

Figure 3.11: Sieve analysis of cohesionless granular material

4.0 EXPERIMENTAL RUNS AND DATA COLLECTION

4.1 General

As mentioned in Chapters 1 and 3, the present experiments were conducted in three sine-generated channels having θ_0=90°, 70°, and 50°. All channels had the width B=0.40m. Each channel had a length L_{total}=2L, where L is one meander length (see Fig. 1.5); the entrance and exit sections were in coincidence with apex sections (as can be inferred from Fig. 3.1). The geometric characteristics of the channels are given in Table 4.1.

Table 4.1: Geometric Properties of Experimental Channels

θ_0	$\Lambda=2\pi B$ (m)	L (m)	σ	L_{Total} (m)
90°	2.513	5.325	2.12	10.650
70°	2.513	3.807	1.51	7.614
50°	2.513	3.071	1.22	6.142

4.2 Instrumentation and Measurement Techniques

In each channel measurements of the vertically averaged flow velocity ($\overline{u}$), flow depth (h), and the vertically averaged deviation angle $\overline{\omega}$ were carried out at various locations (l_c,n) of the flow. The present sections concerns the description of instrumentation and techniques used to determine $\overline{u}$, h, and $\overline{\omega}$.

4.2.1 Measurement of Local Longitudinal Flow Velocities $\overline{u}$

The local time-averaged longitudinal flow velocities (u) were measured with a miniature propeller meter (403 Streamflo Low Speed Probe, commercialized by HR Wallingford). The probe consists of a five-blade rotor which is mounted on a stainless

steel spindle with jewel bearings. The signal is routed through an insulated gold wire which is 1mm from the rotor and transferred through a co-axial cable to a digital indicator. This probe allows measurement of velocities in the range of 2.5 cm/sec to 150 cm/sec. The probe has been calibrated with the following accuracy:

+/- 5% (in the u-range of 2.5 - 7.5cm/sec)
+/- 2% (in the u-range of 7.5 - 15cm/sec)
+/- 1% (in the u-range of 15 - 150cm/sec)

This probe also has a maximum immersion length of 430mm.

The aforementioned digital indicator (type 402/412, HR Wallingford) provides a frequency range of 0 to 99Hz at the 1 second range and 0 to 99.9Hz at the 10 second range. The display has a three-digit LED output. The 402/412 digital indicator allows for 1 sec or 10 sec intervals or for continuous data output.

For the purpose of the present work, the indicator was routed to a data acquisition system which was set to record two readings per second for 60 seconds. The time of 60 seconds was selected by plotting a running average of recorded values, taken over a 1.5 minute period, versus time (Fig. 4.1). From this plot it was determined that the average obtained at 60 seconds corresponded with the time-averaged flow velocity.

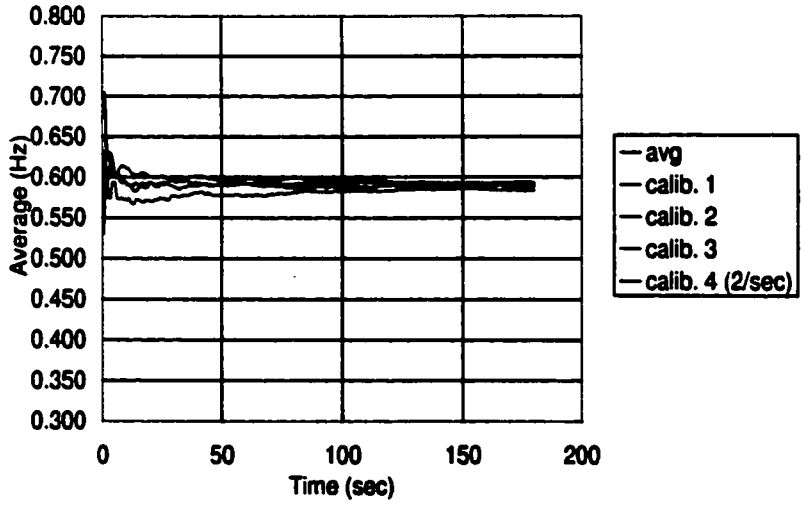

Figure 4.1: Time calibration of probe recordings

Measurements of the longitudinal flow velocity were carried out at the mid-depth of the flow. The vertically-averaged flow velocity $\bar{u}$ at any location (l_c, n) of the flow was identified with the velocity measured at the mid-depth of the flow (at that location). Mid-depth was determined with respect to the depth of flow at the centreline. In order to position the propeller meter at this depth it was attached to the end of a point gauge. The probe was set such that the distance measured from the point of the gauge to the centre of the propeller was equal to half the flow depth at the centreline.

4.2.2 Measurement of Local Flow depths h

Measurements of the free surface profiles (and thus of h) at the various cross-sections were carried out with the Wavo Mk II precision liquid-level transmitter (designed and commercialized by Delft Hydraulics). This instrument is shown in Fig. 4.2. A needle is mounted in a housing which is located at the end of a chain and wire. This needle is connected directly to a 24 Volt power supply which results in the vibration of the needle. The free-surface location is determined by the device based on the needle being in the water only 50% of the time. To identify the water location, the instrument uses a grounding rod which must be placed into the water in order to complete the circuit.

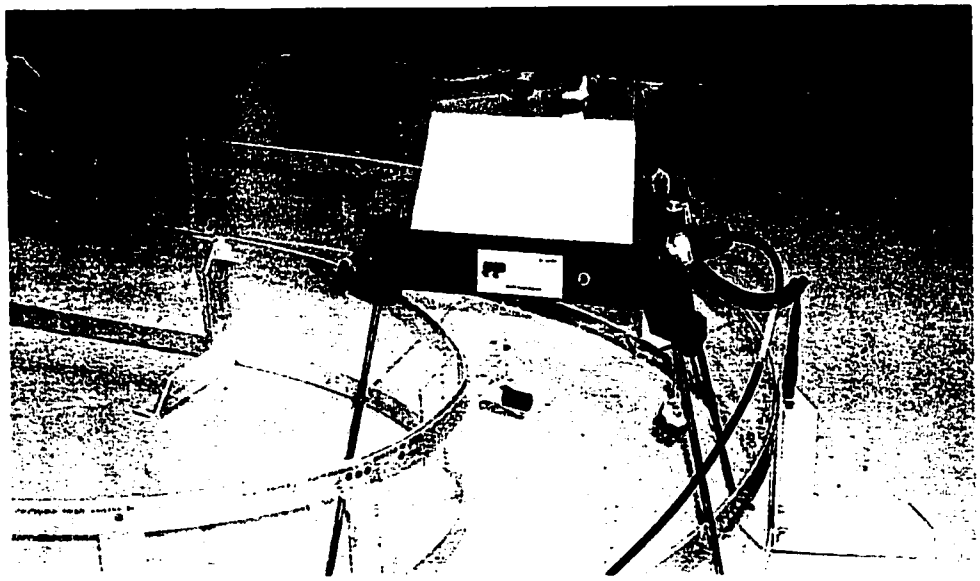

Figure 4.2: Wavo Mk II precision liquid-level transmitter

The motor and pulley system for the chain, which controls the needle, was located in a housing of triangular dimensions of 35 x 40 x 25cm. It should be noted that the Wavo uses a needle current of up to 0.1mA with a Needle amplitude of 1-3 mm (adjustable). This device has a sensitivity of greater than 0.1mm and a repeatability of 0.1mm as specified by the manufacturer.

The signal from the Wavo is relayed to a remote control unit via a 10m long 7 core 0.25mm, shielded cable. The remote control unit which contains the Wavo's 24 VAC power supply reports the results in terms of +/- 5 VDC. The remote control unit routes the output voltage to a data acquisition system which was set to record two reading per second for 60 seconds. The time of 60 seconds was selected by plotting a running average of recorded values, taken over a 3 minute period, versus time, as shown in Fig. 4.3. From this plot it was determined that the average obtained at 60 seconds corresponded to the average free surface location.

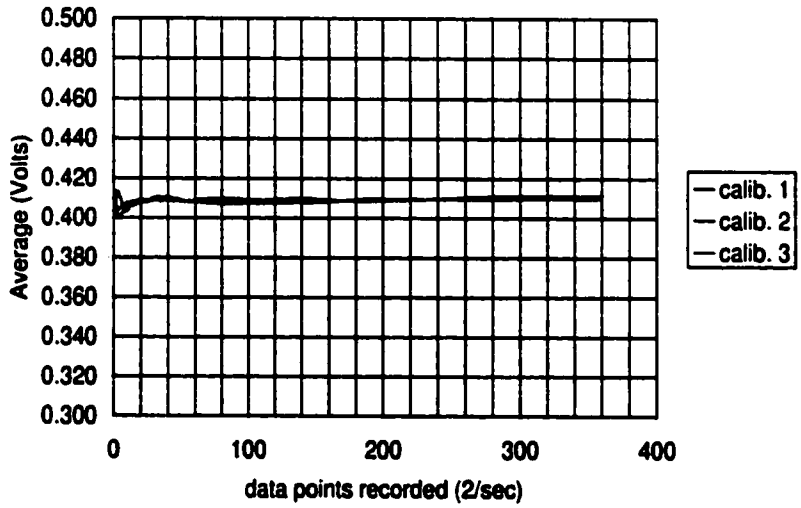

Figure 4.3: Time calibration for Wavo recordings

4.2.3 Measurement of Local Deviation Angles ω

The deviation angle between the flow direction and the longitudinal direction was measured with the device shown in Fig. 4.4. This device, which is similar to that used by Silva 1995 was designed and constructed at the University of Windsor. The device consisted of a 3.2 mm brass rod of 74mm in length. At the lower end of the rod, a flag, which is made of 0.5 mm thick aluminum, measuring 22mm in length, and 3mm to 6mm in height, is attached. The top of the rod was secured to a cap, which sat on a set of bearings. The bearings attached to an aluminum frame, which connected to a point gauge. To measure the angle at which the flag was pointing a needle was attached to the cap and a protractor was secured to the aluminum frame. When constructing this device great care was given to ensure that the flag was exactly 90° to the needle. A photograph and schematic of this device is shown in Fig. 4.4. The deviation angle was measured only at the channel centreline (i.e. only ω_c was measured). At any centreline location, the deviation angles ω_c were recorded throughout the flow depth, at distance of 5,10,15, 20, and 25mm from the bed. The recorded values were then plotted with respect to z to provide profiles such as the ones shown in Fig. 4.5. The areas under these curves were determined, maintaining the corresponding signs, i.e. negative values of ω_c resulted in negative area values, then they were divided by the flow depth. The resulting value from this process is the vertically averaged deviation angle $\overline{\omega}_c$.

4.2.4 Measurement of Flow Rate Q

As previously mentioned in Chapter 3, the flow rate Q was measured with the aid of the V-notch weir located at the end of the head-tank (see Fig. 3.1). To measure the head of water over the weir (h_w) a point gauge was placed at a distance of 0.80m upstream from the weir. The gauge was then zeroed at the free surface elevation associated with the vortex of the weir.

To calibrate the weir a series of different flow rates were used. The actual flow rate each time was determined by recording the time required for a know volume to

Figure 4.4: Device for the measurement of the deviation angle

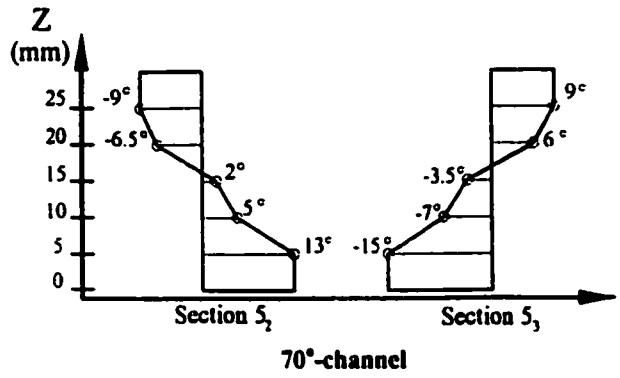

Figure 4.5: Example profiles of the flow deviation from the centreline

completely fill with water. The head over the weir was then recorded. From these measurements, it has been found that Q and h_w are interrelated as

$$Q = 2.32 h_w^{2.49}. \tag{4.1}$$

4.3 Experimental Tests

4.3.1 Specifications of Tests

In each meandering channel, one experimental test was carried out. All three tests were conducted with a constant flow rate Q (steady flow). Prior to testing, the point gauge behind the V-notch weir was adjusted to the zero position if necessary. The pump was then turned on allowing the water to buildup in the constant head reservoir. Once the water reached the overflow spillway, the valve(s) were slowly opened. The valve(s) was adjusted until the flow rate was approximately in the range of 1.5 to 3 l/s. The tailgate and valve(s) were then manipulated until a flow depth h_m in the range of 3.0 to 3.2 cm was achieved. The flow depth was determined by using four point gauges located on the centreline of the channel, at each of the crossovers. Each point gauge had a fine adjustment screw, located below a digital output screen, for the purposes of improved accuracy during flow depth measurements. The digital output itself displayed the

measured height, with reference to a datum selected by the user, in this case the bed, with an accuracy of 0.01mm. The point on each gauge was placed in contact with the free surface after each adjustment of the tailgate and valves to determine the flow depth. This procedure was repeated until the $h = h_m$ at the centreline of the four crossovers. Table 4.2 shows the particulars of the three tests which were carried out.

The experimental conditions (grain size, slope, flow depth) were selected so as to match those of Silva 1995 (see also Table 2.2). It should be noticed that these conditions result in a rough turbulent flow ($Re_* = v_* k_s / \nu > 70$), and in a low Froude number, which are typical of natural meandering streams. The low Froude number also ensured that the free surface was calm (i.e. free of waves) which facilitated the measurement of flow depth.

4.3.2 Location of Measurements

The measurements were carried out in the three consecutive loops shown in Fig. 4.6. Henceforward, these three loops will be distinguished by the nomenclature $\Lambda_1, \Lambda_2, \Lambda_3$ for all channels. In each loop (Λ_i), eight cross-sections were defined for the purpose of measurement, with the fifth cross-section always being located at the apex section and the first cross-section located at the crossover. The cross-sections are numbered k_i, where k is the section number in the range of 1 to 8, and i represents the loop number (i = 1, 2, 3, 4). Figs. 4.6a,b,c show a detailed drawing of the location and numbering of the cross-sections in the 90°-, 70°-, and 50°-channel, respectively. The distance between adjacent cross-sections measured along the centreline is as follows: 33.3 cm in the 90°-channel, 23.8cm in the 70°-channel, and 19.2cm in the 50°-channel.

Table 4.2: Parameters and dimensionless variables of experimental runs

TEST	Q (l/s)	D_{50} (mm)	B (cm)	h_m (cm)	S_{bc}	u_m (cm/s)	v_* (cm/s)	c_m	v_*k_s/ν	Re	Fr_m	B/h_m	h_m/k_s
50°-channel	2.53	2.2	40	3.14	1/1000	20.1	1.76	11.5	77	6300	0.131	12.8	7.1
70°-channel	1.84	2.2	40	3.08	1/1000	14.9	1.74	8.6	76	4600	0.074	13.0	7.0
90°-channel	2.21	2.2	40	3.05	1/1000	18.1	1.73	10.5	76	5500	0.110	13.1	6.9

$u_m=Q/Bh_m$

$v_*=(gS_{bc}h_m)^{1/2}$

$c_m=u_m/v_*$

$Re=vh/\nu$

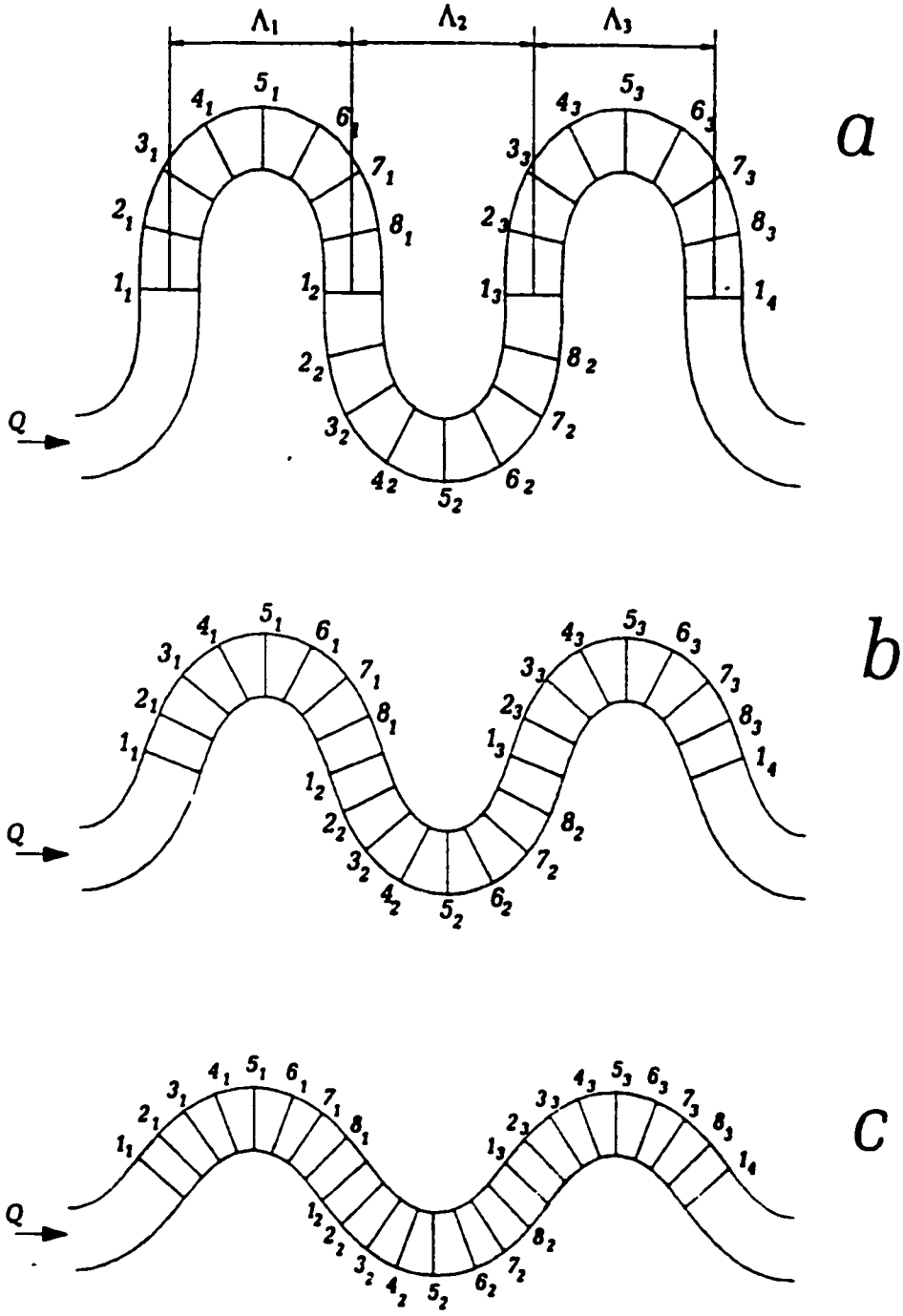

Figure 4.6: Plan view and cross-section numbering for all channels

The vertically-averaged longitudinal flow velocity $\bar{u}$ was measured at various points along each cross-section, so that the velocity profile can be inferred. Near the walls, a close spacing between points was maintained, so as to ensure a better understanding of the velocity behavior near the wall (where the local velocities fluctuated the most). The largest spacing used between any two measurement points in a given cross-section was kept to 2cm.

The velocity profile was recorded three times at each apex (section 5_i). This was done for the purpose of determining repeatability. The velocity profiles at the apex were then retaken with a different probe at the end of the test to ensure the original probe was still operating correctly.

The free surface profile was also recorded at each cross-section. The instrument was located near the inner bank and moved across the channel at spacings of 3 cm until the probe reached the opposite bank. As was the case for the velocity profile, the free surface profile was recorded three times at each apex for the purpose of determining repeatability. The Wavo was calibrated after every test to ensure the equipment was still operating correctly.

The deviation angle of the flow was measured only at the centreline of each cross-section. At the apex-sections the deviation angle was recorded three times to determine repeatability. Refer to appendix F for pictures taken during testing.

5.0 RESULTS AND DISCUSSION

5.1 General

In this chapter, the measurements carried out in all three channels are presented and discussed.

The dimensionless counterparts ϕ_u and ϕ_h of the recorded quantities $\bar{u}$ and h will often be used (instead of $\bar{u}$ and h), ϕ_u and ϕ_h are defined as follows:

$$\phi_u = \frac{\bar{u}}{u_m} \quad \text{and} \quad \phi_h = \frac{h}{h_m}. \tag{5.1}$$

Here u_m and h_m are the channel-averaged flow velocity and depth, respectively. The dimensionless coordinates $\eta = n/B$ and $\xi_c = l_c/L$ (see Section 1.4) will be used. Fig. 5.1 shows the sign convention for the present channels.

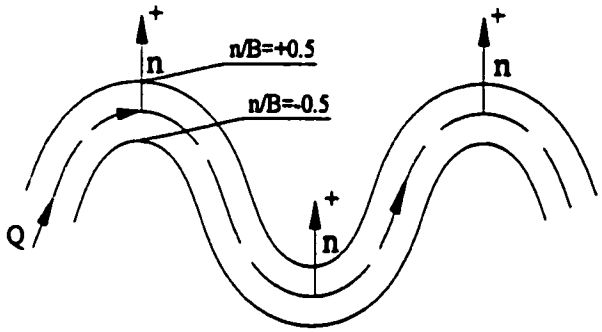

Figure 5.1: Sign convention for n/B

The entire sets of measurements (raw data) of $\bar{u}$, h, and $\overline{\omega_c}$ carried out in the 90°-, 70°- and 50°-channels are given in Appendixes A, B and C, respectively. The full set of measurements of ω_c at various levels z of a centreline vertical are shown in Appendix D.

As follows from the Introduction an ingoing flow is distinguished by the fact that its $\overline{\omega}_c$-values are negative for most part of the region between the crossover O and apex a, and they are positive for most part of the region between the apex a and crossover O' (i.e. $\overline{\omega}_c<0$ if $\approx 0 \le l_c/L <\approx 0.25$ and $\overline{\omega}_c>0$ if $\approx 0.25 < l_c/L <\approx 0.5$). The $\overline{\omega}_c$-values of an outgoing flow maintain their sign almost throughout OaO' (i.e. $\overline{\omega}_c>0$ if $\approx 0 < l_c/L <\approx 0.5$).

5.2 Measurements in the 90°-Channel

5.2.1 Deviation angle $\overline{\omega}_c$

Fig. 5.2 shows the measured values of $\overline{\omega}_c$(in radians) versus ξ_c (=l_c/L). The data collected in all three loops are reported on a single graph; due to the anti-symmetry of the flow the values recorded for the loop Λ_2 are reported in terms of their opposite sign so as to provide the same sign as in Λ_1 and Λ_3. The data collected at the equivalent sections of the three loops, sections 1_1, 1_2, 1_3, for example, were averaged; the sold line in Fig. 5.2 is the best-fit line (third order polynomial function) to these averaged data.

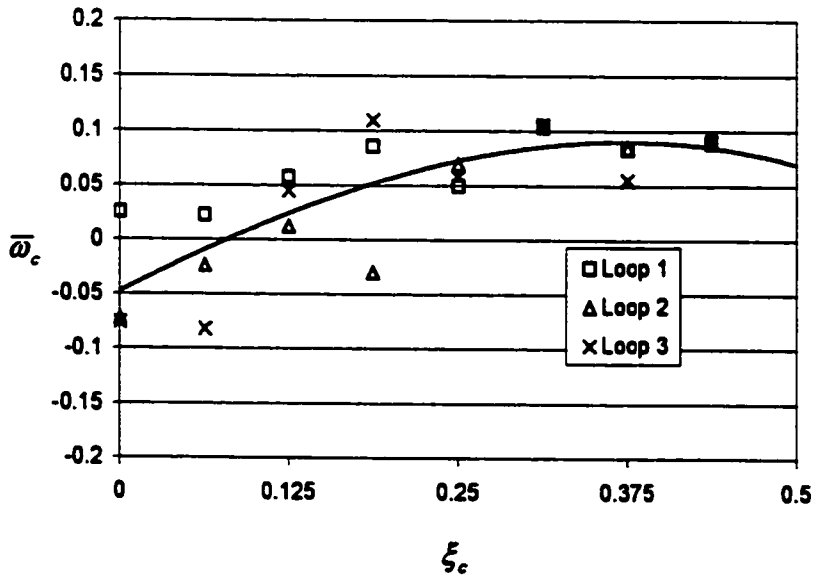

Figure 5.2: Deviation angles for the 90°-channel

The graph in Fig. 5.2 shows that the maximum absolute value of the average deviation angle is approximately 0.09 radians. $\overline{\omega}_c$ changes from negative to positive at $\xi_c \approx 0.08$. That is the $\overline{\omega}_c$-values are positive almost throughout *OaO'*- and thus the flow in this channel is clearly outgoing.

For a better understanding of the flow deviation angle and its variation with respect to an axis normal to the bed refer to Fig. D.1 (in Appendix D), which shows the profiles of the deviation angle at each cross-section. From this Figure it can be inferred that the local deviation angles recorded at the apex have a clearly defined cross-circulation component. This component is hardly noticeable in any section other than the apex. To put it in other words the intensity of the cross-circulation is the largest at the apex and quickly becomes negligible when moving towards the crossovers. This is understandable, for the intensity of cross-circulation is proportional to curvature – and the curvature is maximum at the apex and zero at the crossovers (see Eqs. (2.11) and (2.12)).

5.2.2 Longitudinal Flow Velocity $\overline{u}$

Fig. 5.3 shows the field of longitudinal flow velocity $\overline{u}$. The flow pattern in this Figure is also consistent with that of an outgoing flow. Indeed, in each loop the maximum flow velocity occurs at the inner bank near the crossover, in fact from the Figure it appears that $\overline{u}_{max}$ occurs at $\xi_c \approx 0.0625$, which is in agreement with the value $\xi_c \approx 0.08$ obtained from the measurements of $\overline{\omega}_c$.

Figs. 5.4a through h show the cross-sectional velocity profiles measured in the sections 1_i to 8_i. The data measured in the equivalent sections of each loop are plotted together in one graph. In each of these graphs the periodic character of the flow is evident from the fact that the data collected in the three different loops are similar.

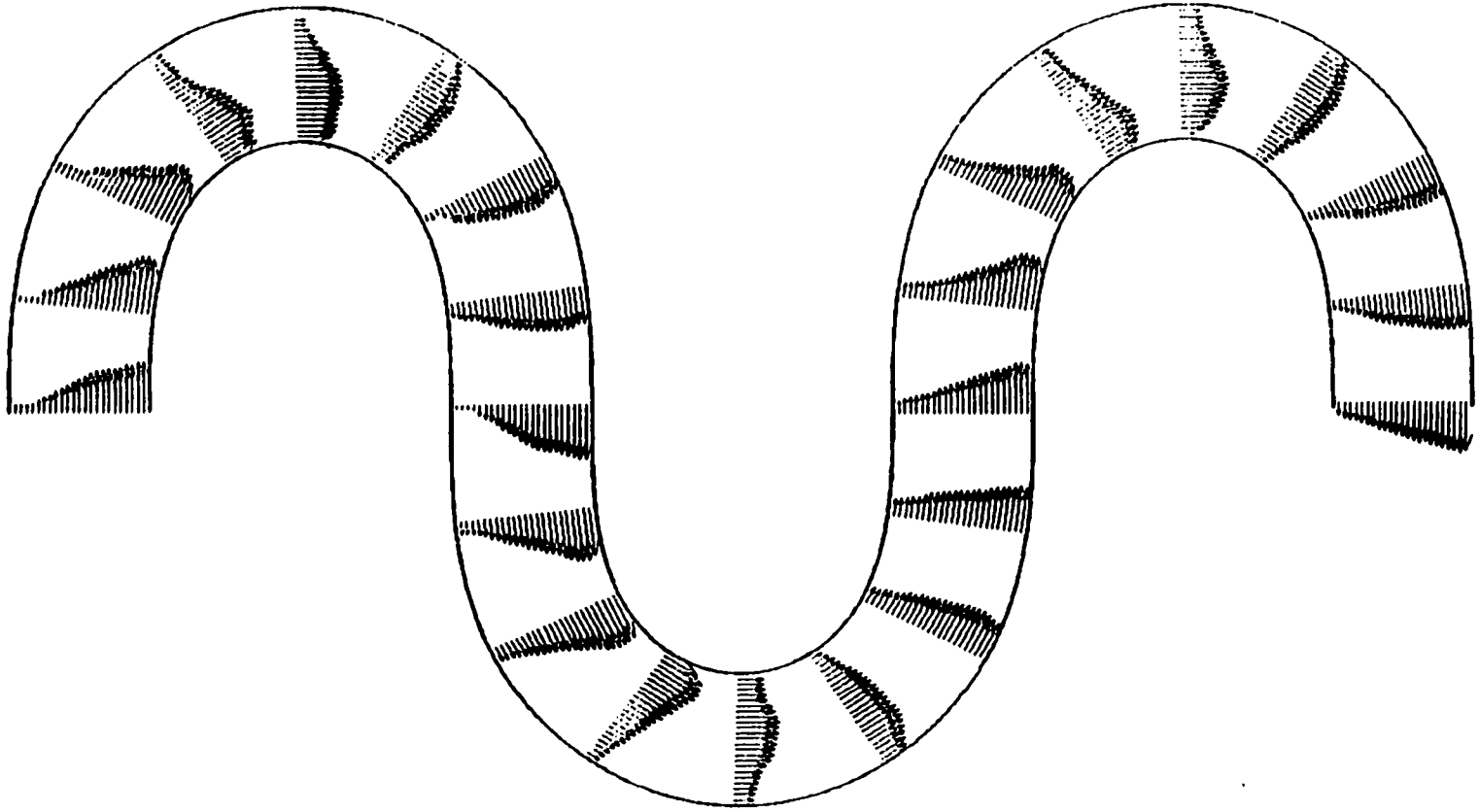

Figure 5.3: Longitudinal velocity field $\bar{u}$ for the 90°-channel

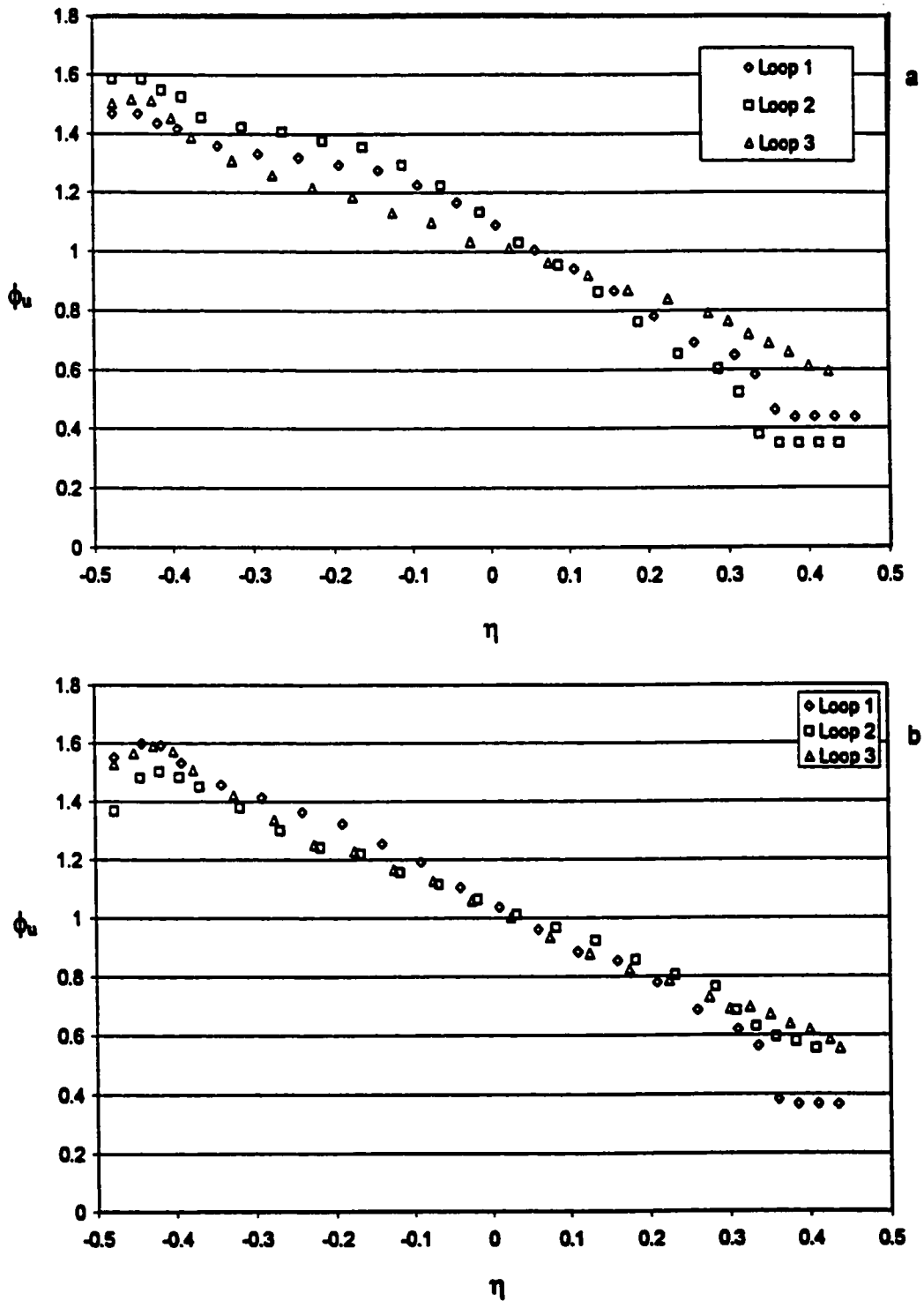

Figure 5.4: Measured dimensionless longitudinal flow velocity ϕ_u versus η (90°-channel)

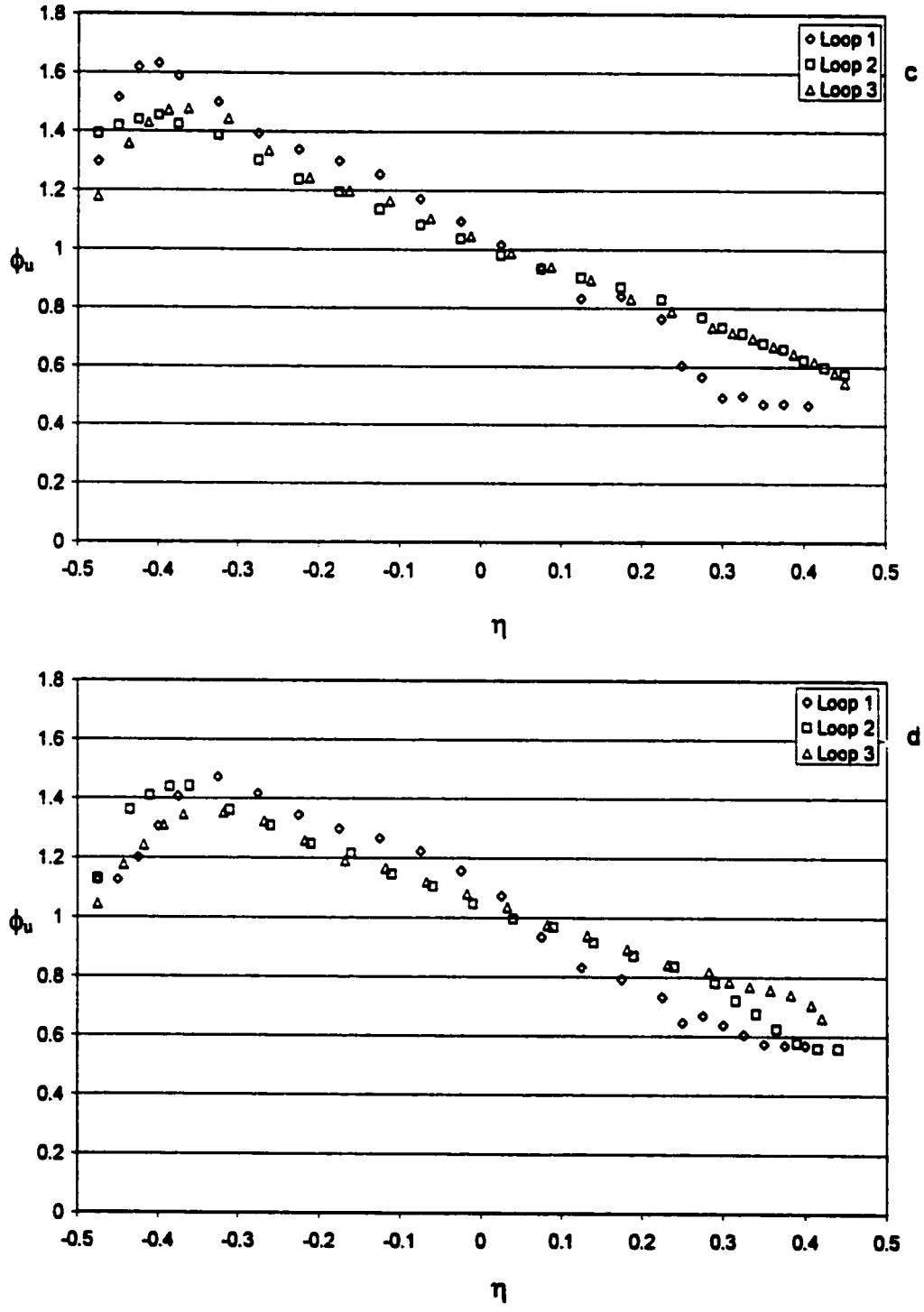

Figure 5.4: Measured dimensionless longitudinal flow velocity ϕ_u versus η (90°-channel)

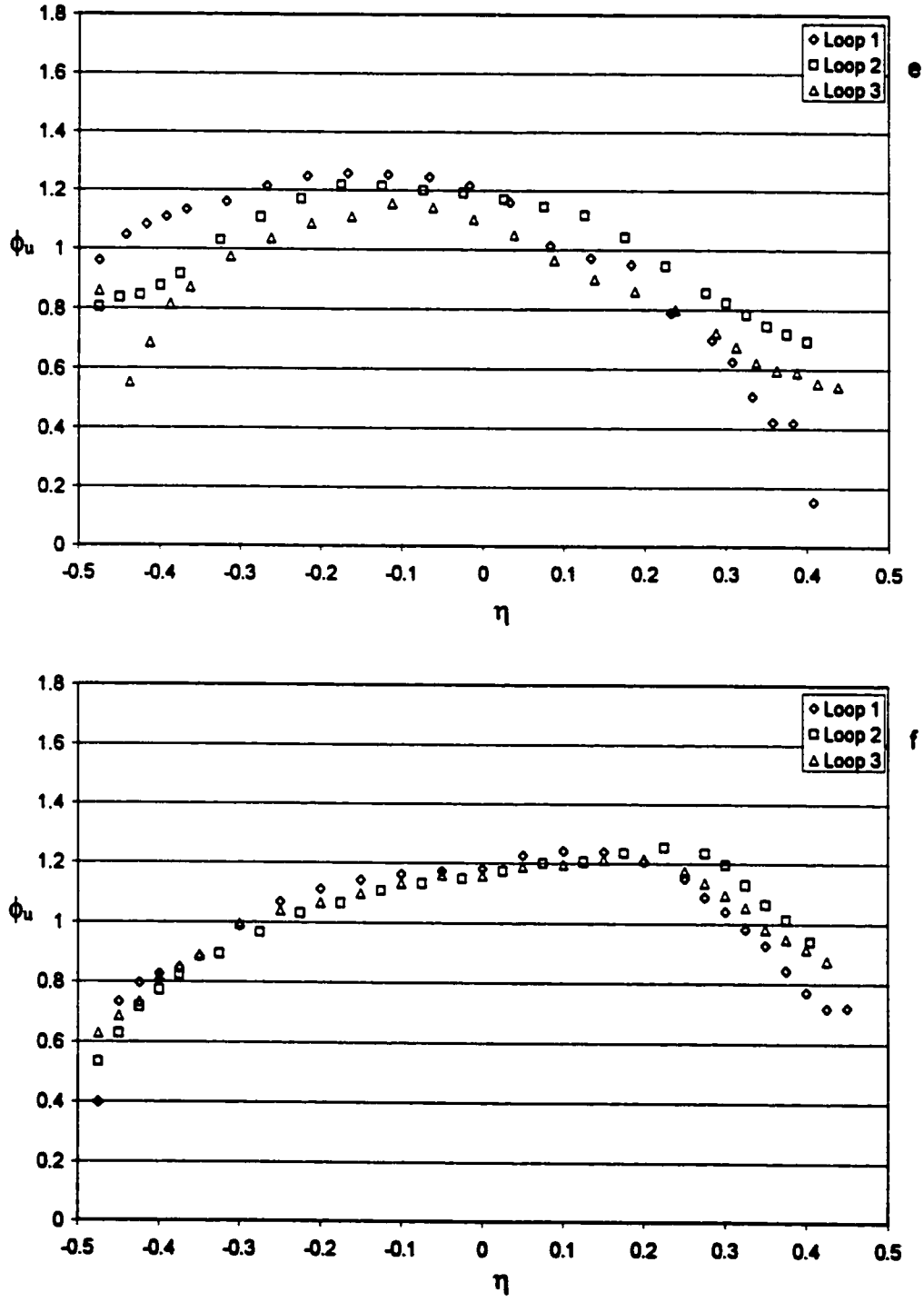

Figure 5.4: Measured dimensionless longitudinal flow velocity ϕ_u versus η (90°-channel)

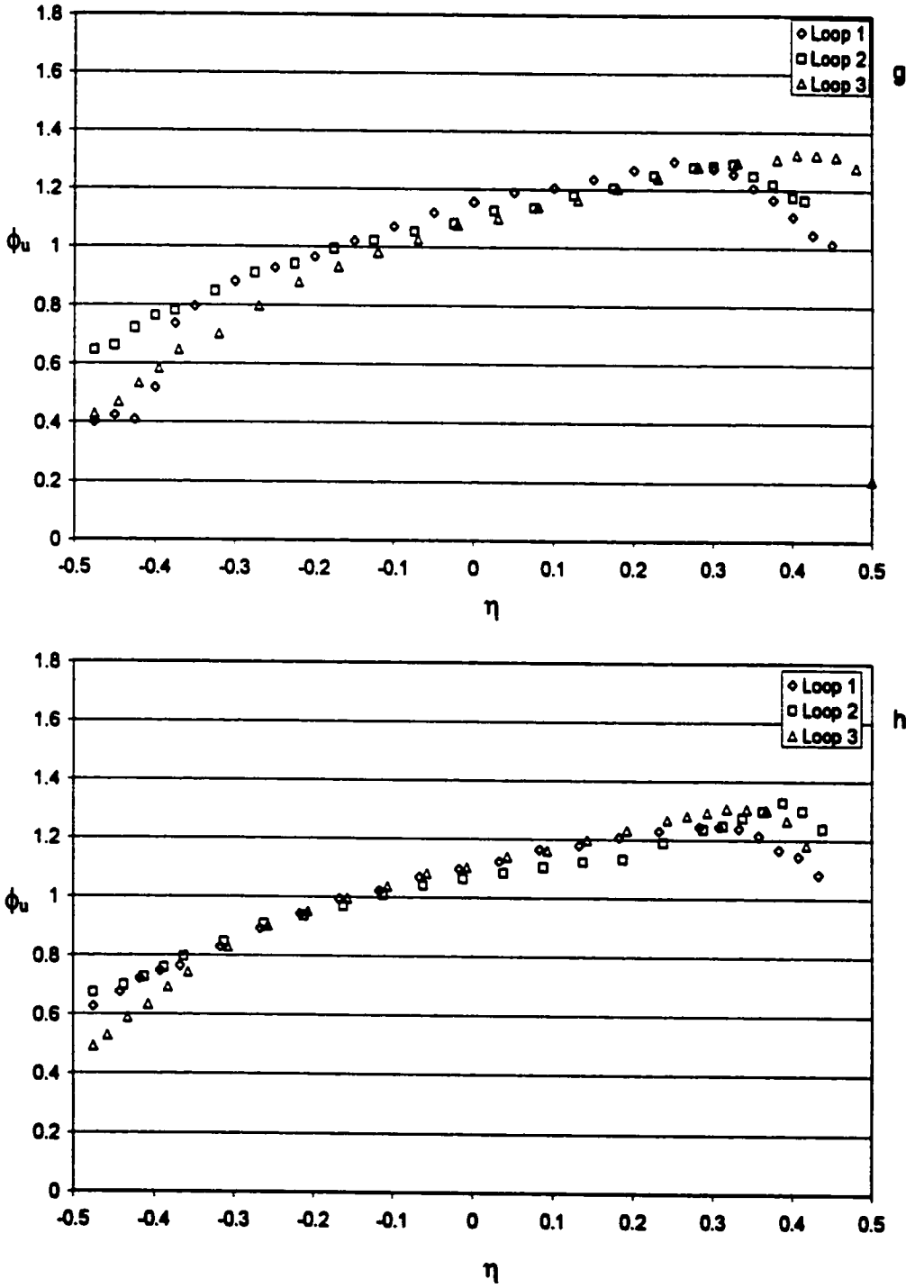

Figure 5.4: Measured dimensionless longitudinal flow velocity ϕ_u versus η (90°-channel)

5.2.3 Flow Depth h

The recorded free surface profiles are shown in Figs. 5.5a to h. The data corresponding to the equivalent sections of the three meander loops are very similar- which is another confirmation of the periodicity of the flow.

From these graphs it can be observed that the free surface is nearly horizontal at the crossovers, with the maximum super-elevation being at the apexes; moreover the free surface profiles exhibit an *S* like shape, which is in agreement with the experimental observations of other authors.

Consider now the Eq. (2.13) for super-elevation namely:

$$\Delta h = \frac{u_{av}^2}{g}\frac{B}{R}. \tag{5.2}$$

Strictly speaking, this equation is valid only for flows in circular channels (where B/R=const), and not for sine-generated channels (where B/R is a function of ξ_c -among others). In spite of this Eq. (5.2) is the only existing expression for Δh, and in practice it is commonly, used to estimate super-elevation in curved channels of any shape. Thus it can be applied to a sine-generated channel in order to acquire an idea of the magnitude of the super-elevation. The values of Δh measured at each section of a sine-generated channel should not deviate substantially from those given by Eq. (5.2), provided that B/R is computed with the aid of Eq. (2.11),

$$\frac{B}{R} = \frac{B}{R_a}\sin(2\pi\xi_c) \tag{5.3}$$

Table 5.1 shows the recorded values of $\Delta h/h_m$ for each cross-section, based on a visual average of the three loops. The values of $\Delta h/h_m$ computed from Eq. (5.2) (with B/R given by Eq. (5.3)) are also shown. The recorded values were on average within 0.011 of those predicted by Eq. (5.2).

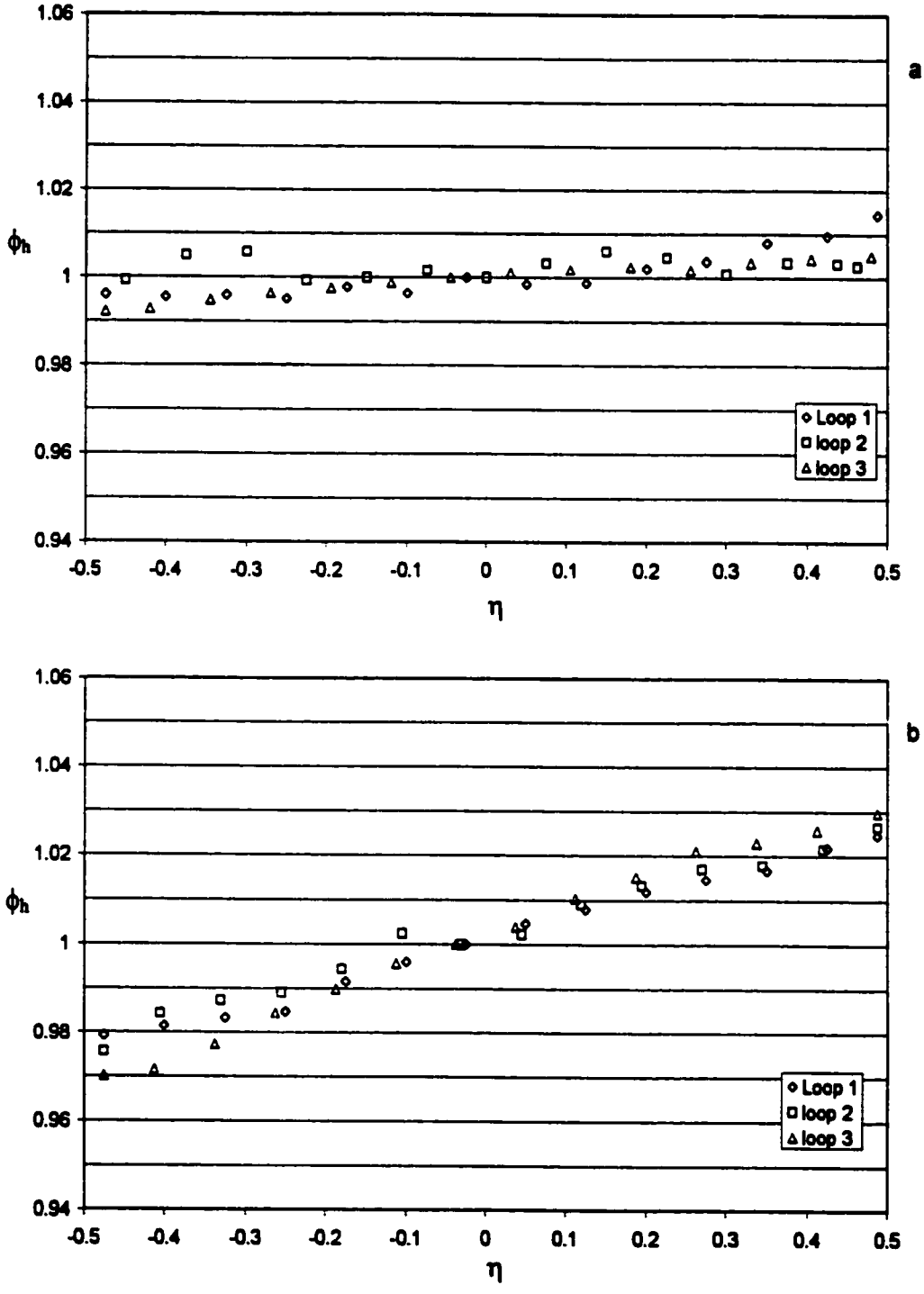

Figure 5.5: Measured dimensionless flow depth ϕ_h versus η (90°-channel)

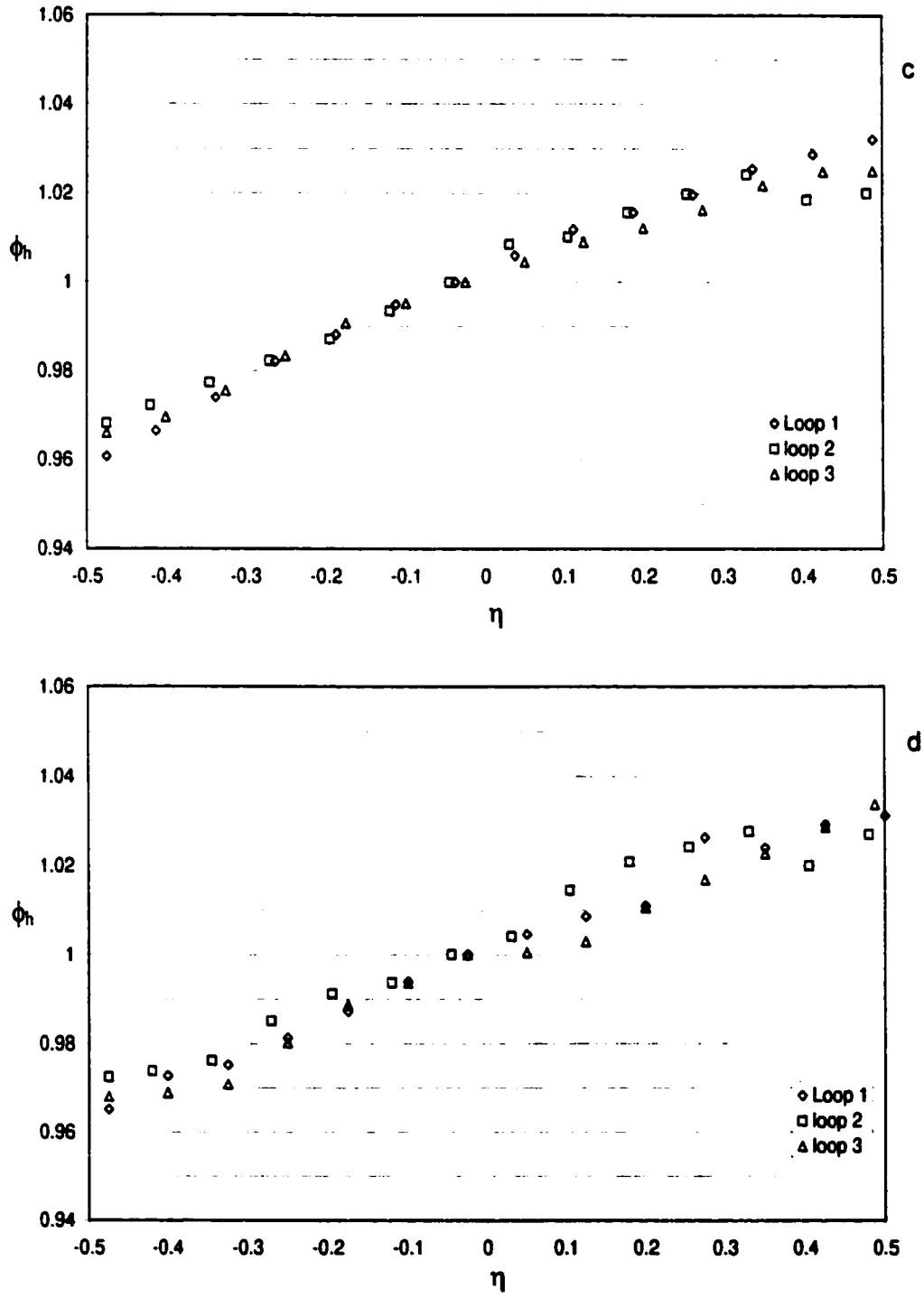

Figure 5.5: Measured dimensionless flow depth ϕ_h versus η (90°-channel)

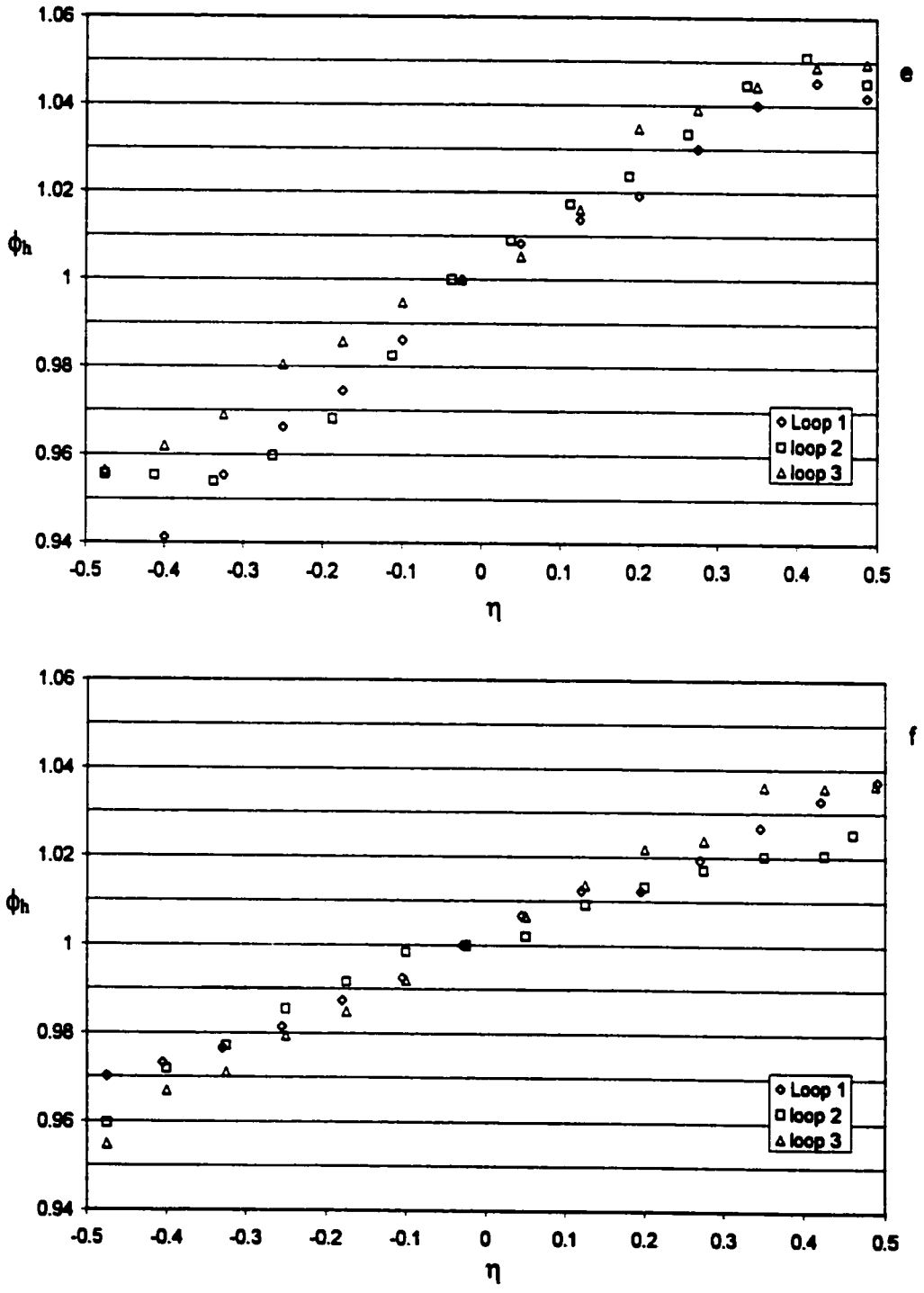

Figure 5.5: Measured dimensionless flow depth ϕ_h versus η (90°-channel)

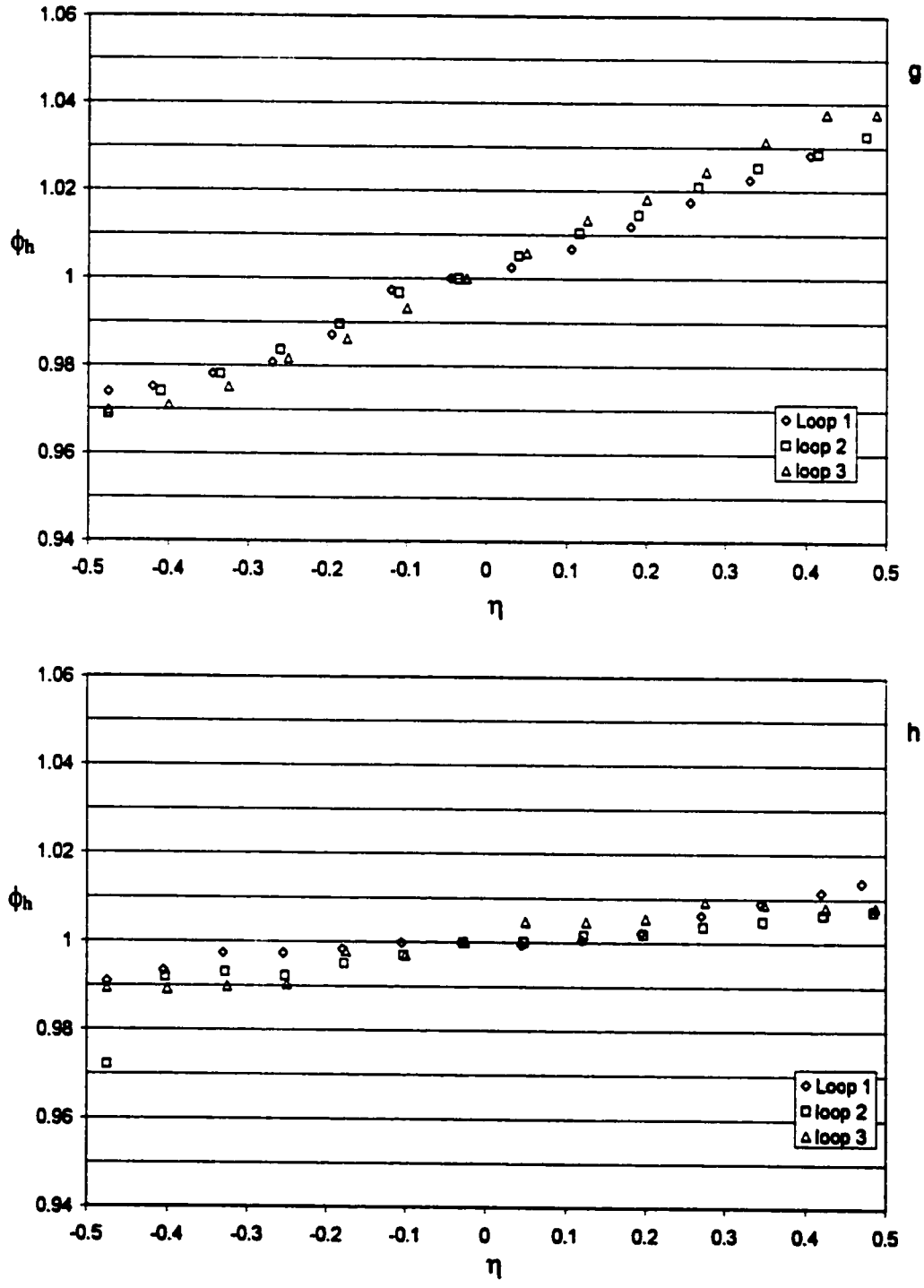

Figure 5.5: Measured dimensionless flow depth ϕ_h versus η (90°-channel)

Table 5.1: Recorded versus theoretical values of free surface super-elevation

Section	Recorded $\Delta h/h_m$ (Average)	$\Delta h/h_m$ Eq. (5.2)
1*i*	0.022	0.000
2*i*	0.042	0.027
3*i*	0.059	0.050
4*i*	0.062	0.065
5*i*	0.09	0.070
6*i*	0.069	0.065
7*i*	0.06	0.050
8*i*	0.024	0.027

5.3 Measurements in the 50°-Channel

5.3.1 Deviation angle $\overline{\omega}_c$

Fig. 5.6 shows the measured values of $\overline{\omega}_c$ versus ξ_c plotted in the same way as that used earlier for the 90°-channel. Here too the recorded values of $\overline{\omega}_c$ for Λ_2 were plotted with the opposite sign. The data from all equivalent sections of the three loops were averaged, the solid line in Fig. 5.6 being the best-fit line (a third order polynomial function) to the averaged data.

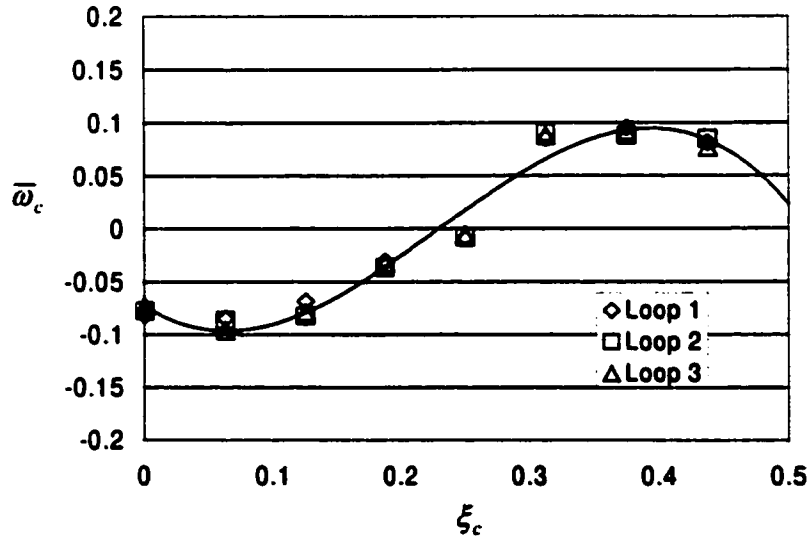

Figure 5.6: Deviation angles for the 50°-channel

From this Figure it should be noticed that the values of $\overline{\omega}_c$ measured at the equivalent section of loops Λ_1, Λ_2, and Λ_3 are very similar-which did not happen in the 90°-channel (see Fig. 5.2). This is probably the result of the fact that in the 50°-channel the flag was oscillating much less than in the 90°-channel. The author has no justification for this fact; it is, however, thought that this fact is due to the different internal structure of turbulence in both channels.

From the graph in Fig. 5.6, one can infer that the maximum deviation angle is approximately 0.10 radians. $\overline{\omega}_c$ changes from negative to positive at $\xi_c \approx 0.23$. Therefore, the $\overline{\omega}_c$-values are negative for most of the region $0 \leq \xi_c < 0.25$ and positive for most of the region $0.25 \approx< \xi_c \leq 0.5$ - and thus the flow in this channel is clearly ingoing.

Fig. D.2 (in Appendix D) shows the variation of ω_c along the vertical direction z for each measured cross-section. Just like in the case of the 90°-channel, here too the most defined cross-circulatory pattern can be found at the apex (as is to be expected). However, from Fig. D.2 it also follows that the flow maintains a noticeable cross-circulation pattern in all sections from, and including, the apex through to the following loop.

5.3.2 Longitudinal Flow Velocity $\overline{u}$

The field of longitudinal flow velocity $\overline{u}$ for this channel is shown in Fig. 5.7. The observed flow pattern in this channel is consistent with that of an ingoing flow. In each loop the maximum flow velocity occurs near the inner bank somewhere near the apex section. From this figure it appears that $\overline{u}_{max}$ occurs when $\xi_c \approx 0.25$. This is in agreement with the findings from the measurements of the deviation angle (where $\overline{\omega}_c = 0$ at $\xi_c \approx 0.23$) (section 5.3.1).

The cross-sectional velocity profiles for the 50°-channel are shown in Figs 5.8 a to h. From each of these graphs the periodic characteristic of the flow is visible, as the data collected from the three different loops appear to closely resemble each other.

5.3.3 Flow Depth h

Figs. 5.9a through h show the recorded cross-sectional free surface profiles. In support of the previously observed periodic behavior of the flow, in this channel the free surface profiles from all three loops also display close similarities to each other.

The free surface displayed a similar behaviour to that observed in the 90°-channel: the free surface was nearly horizontal at the crossovers and the super-elevation was maximum at the apex. The characteristic S-shape of the free surface was once again observed.

The measured values of the super-elevation $\Delta h/h_m$ compared with the values of $\Delta h/h_m$ given by Eq. (5.2), with B/R determined with the aid of Eq. (5.3), are given in Table 5.2. The visual averages of the recorded values were on average within 0.008 of those predicted by Eq. (5.2).

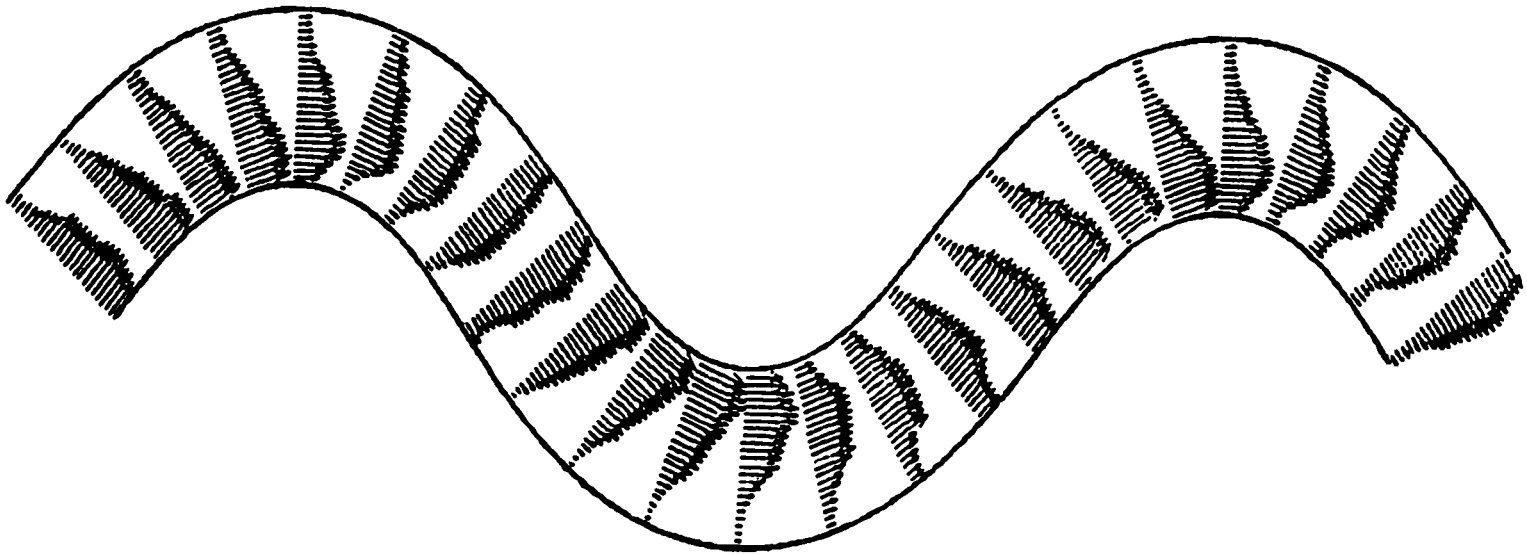

Figure 5.7: Longitudinal velocity field $\bar{u}$ for the 50°-channel

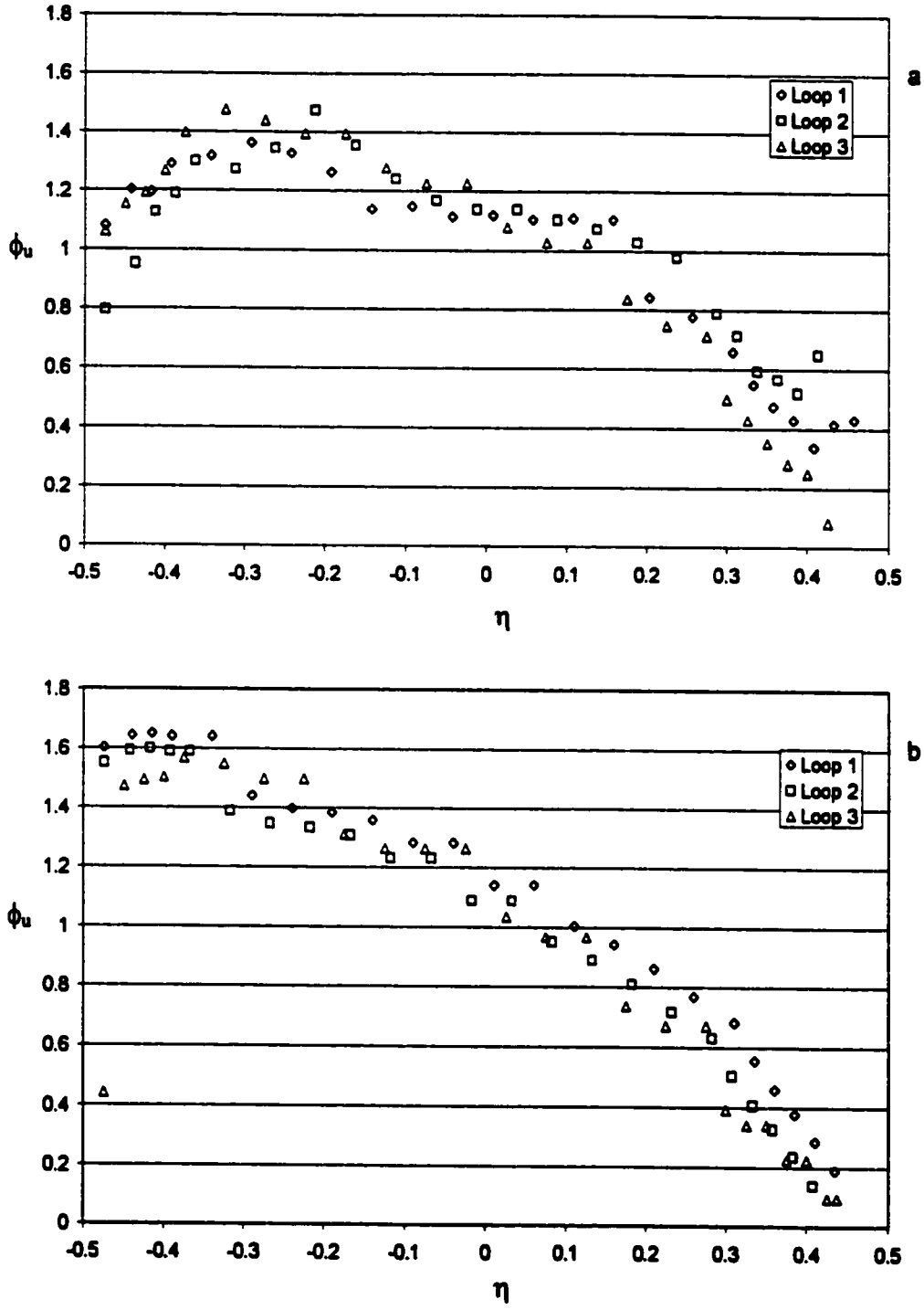

Figure 5.8: Measured dimensionless longitudinal flow velocity ϕ_u versus η (50°-channel)

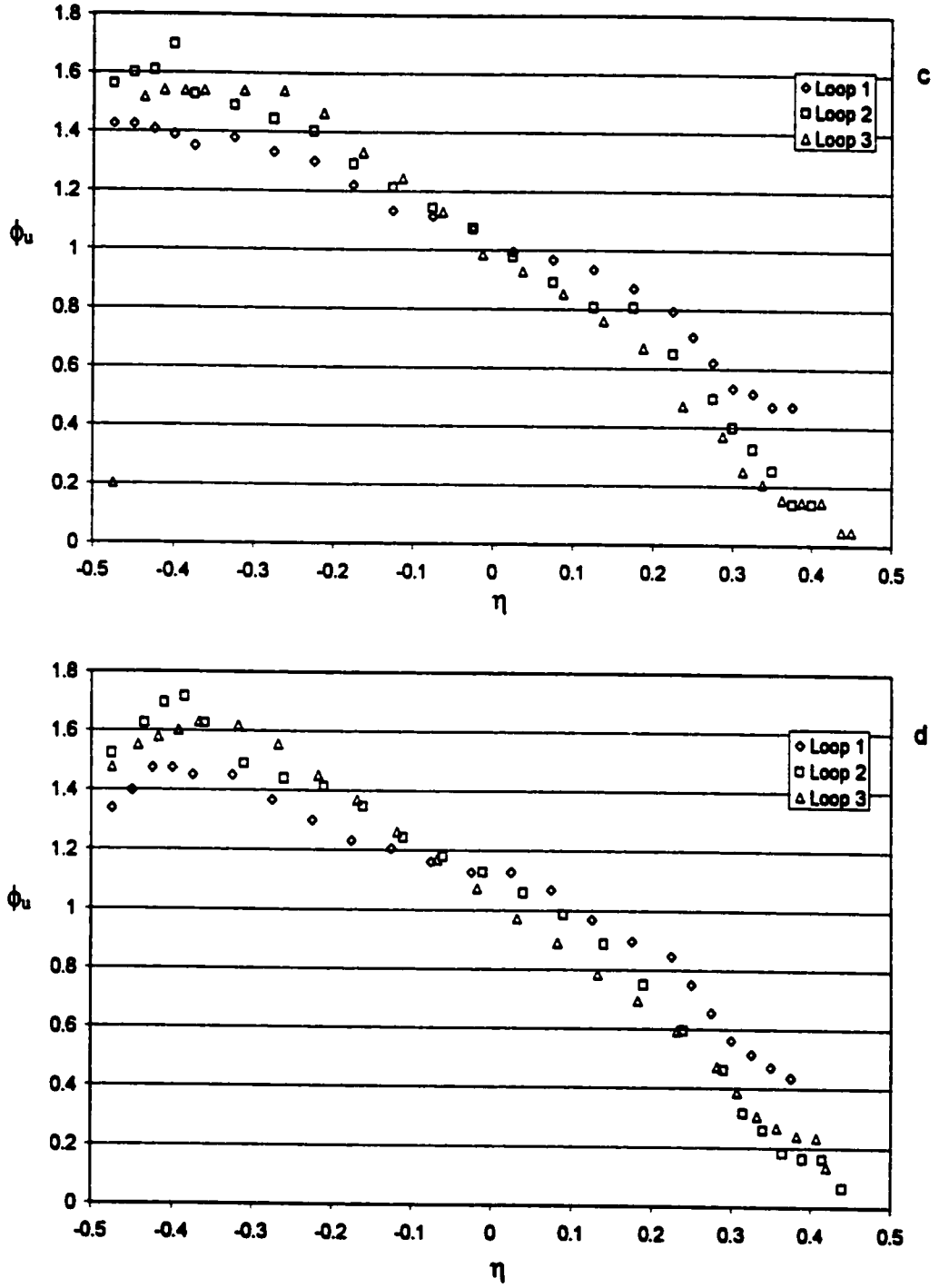

Figure 5.8: Measured dimensionless longitudinal flow velocity ϕ_u versus η (50°-channel)

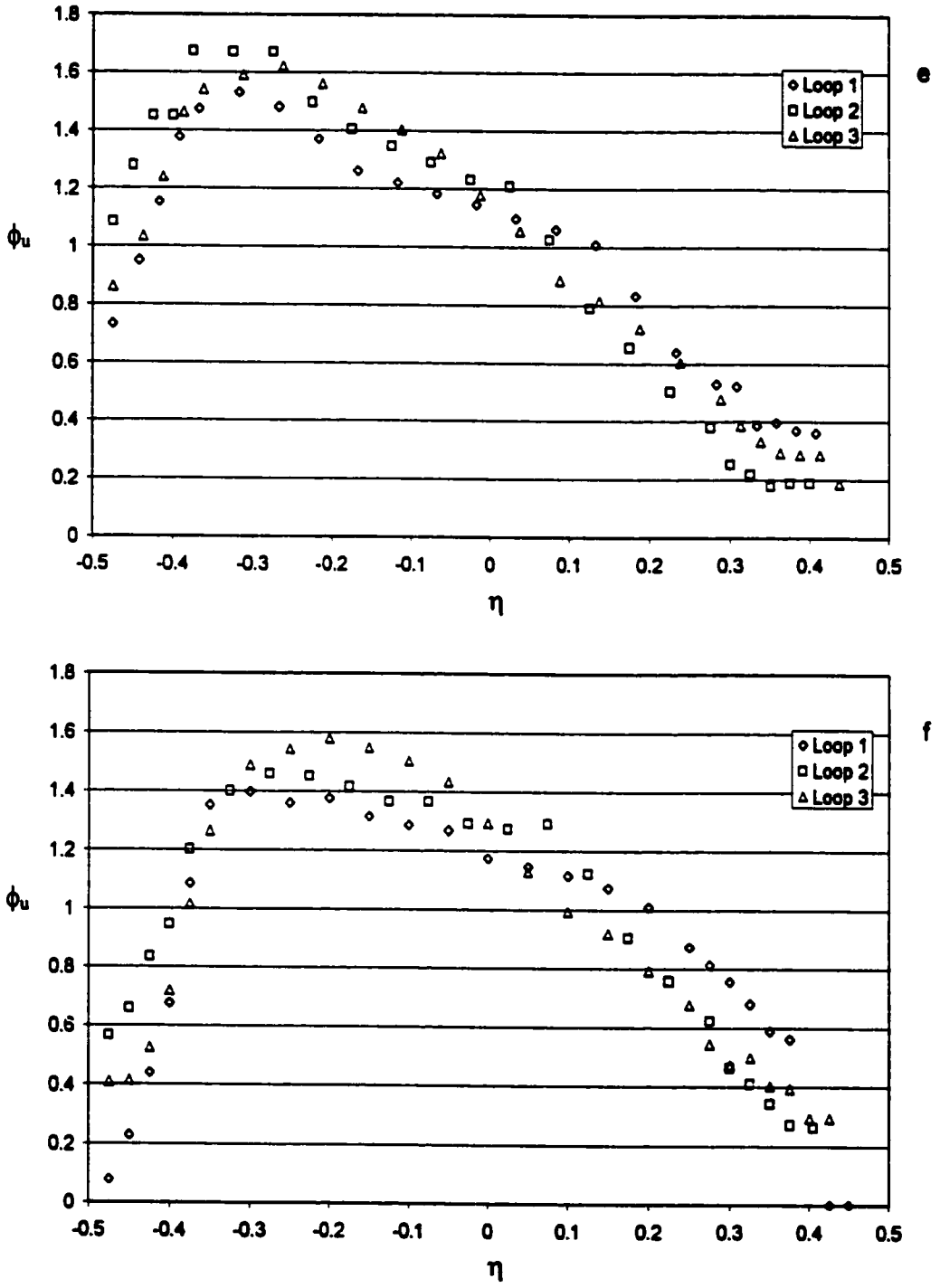

Figure 5.8: Measured dimensionless longitudinal flow velocity ϕ_u versus η (50°-channel)

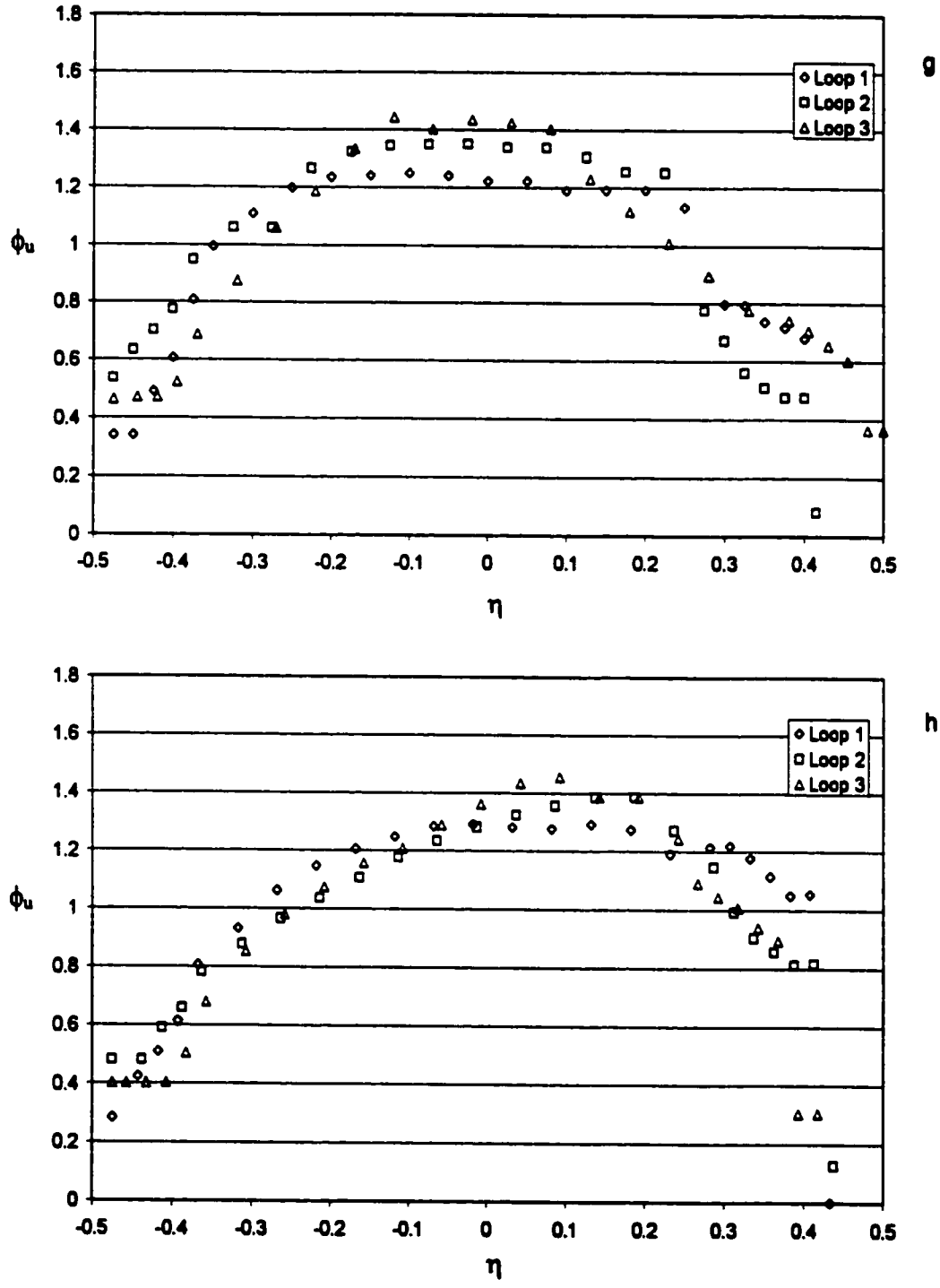

Figure 5.8: Measured dimensionless longitudinal flow velocity ϕ_u versus η (50°-channel)

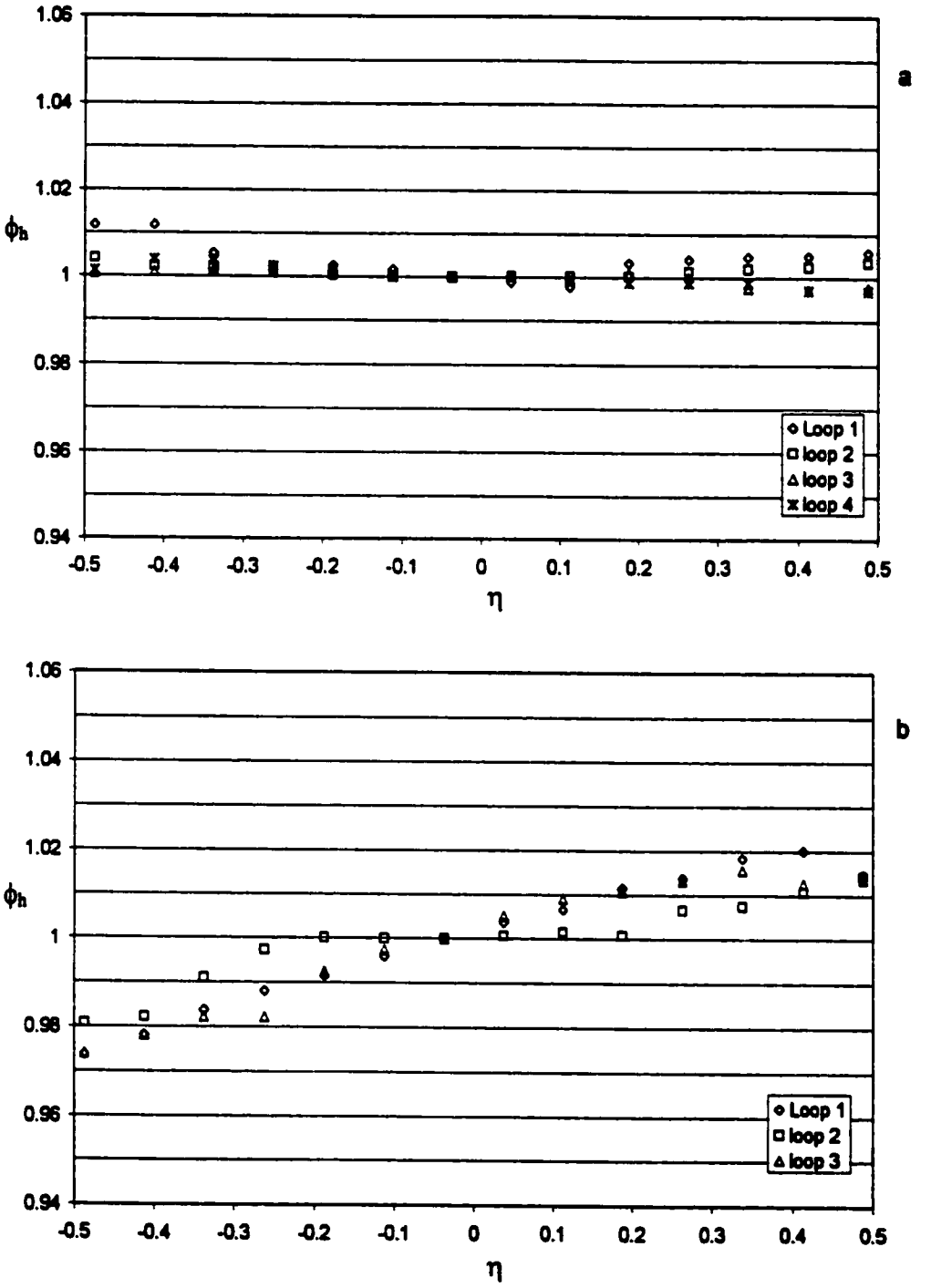

Figure 5.9: Measured dimensionless flow depth ϕ_h versus η (50°-channel)

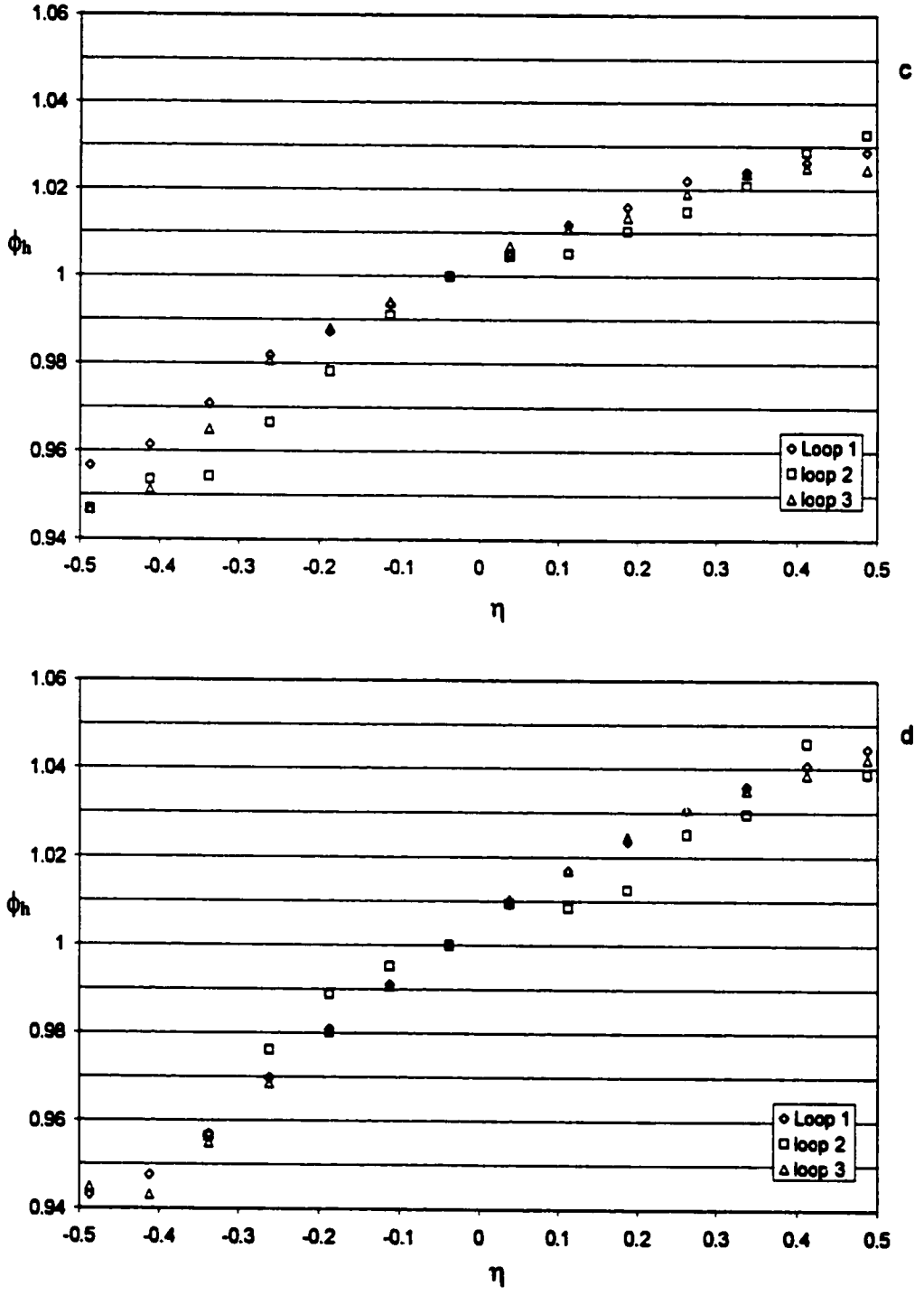

Figure 5.9: Measured dimensionless flow depth ϕ_h versus η (50°-channel)

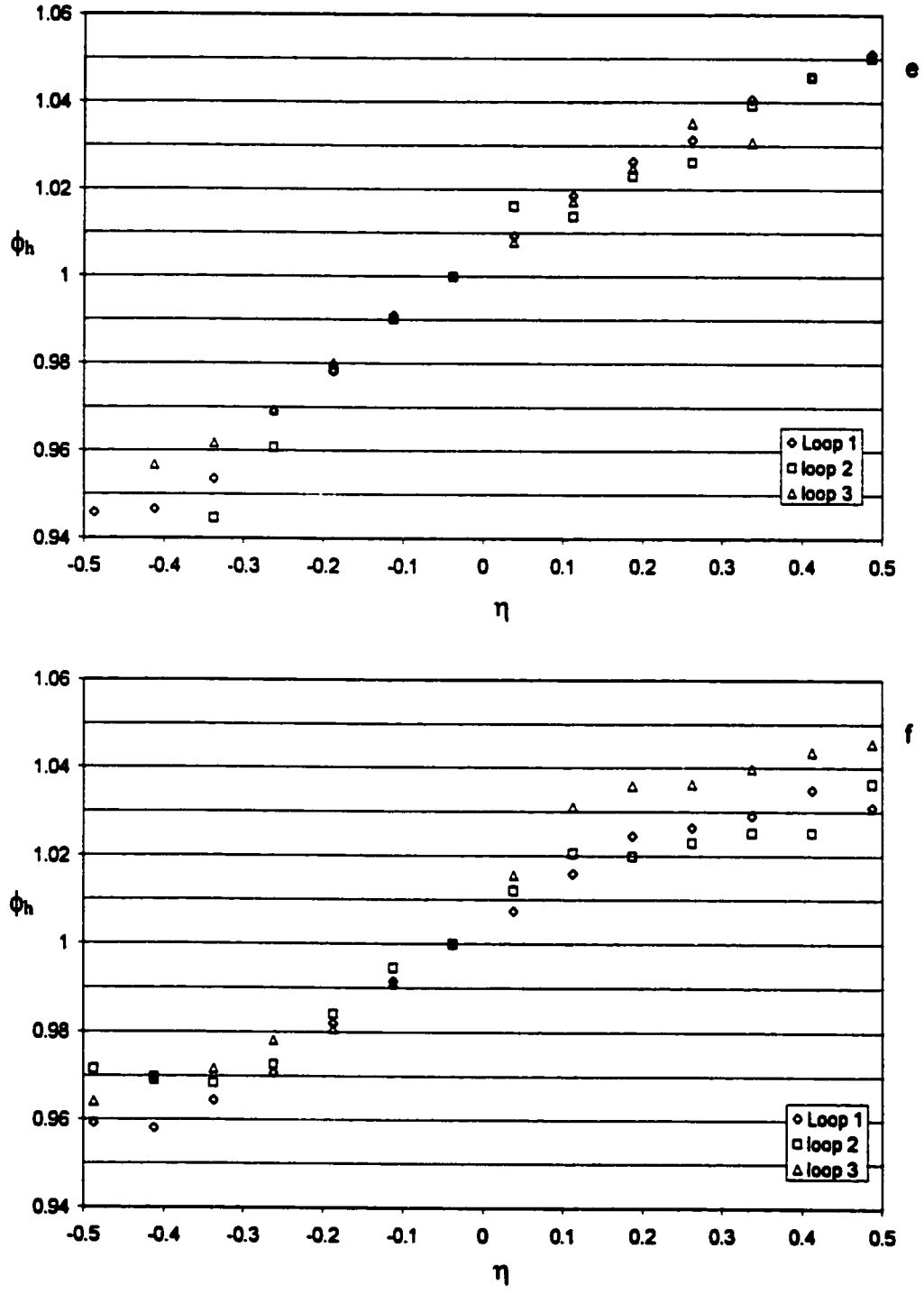

Figure 5.9: Measured dimensionless flow depth ϕ_h versus η (50°-channel)

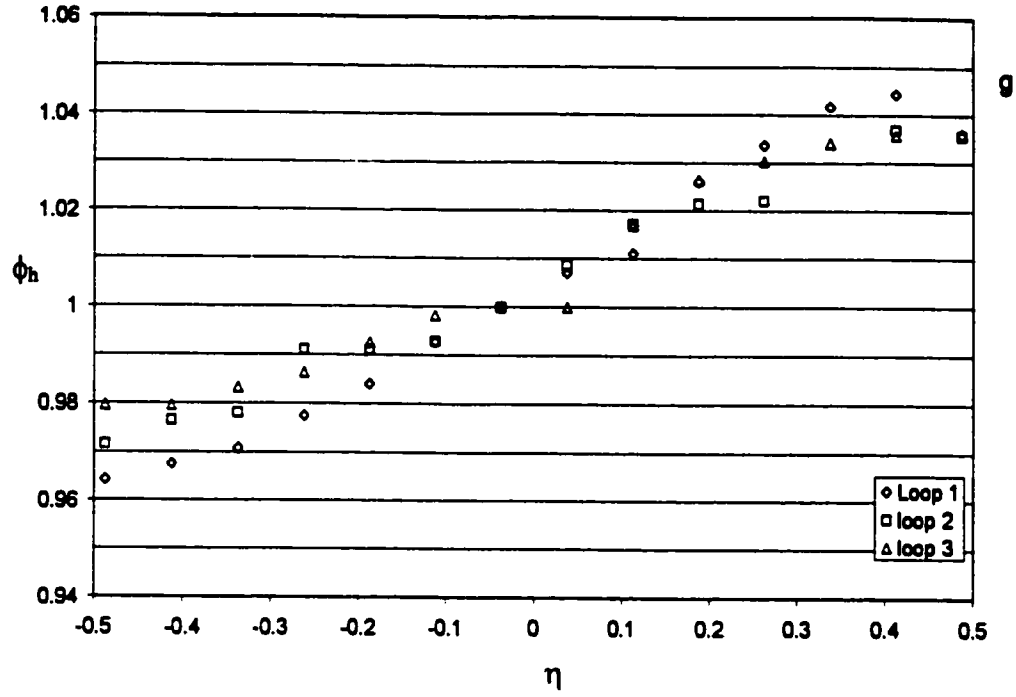

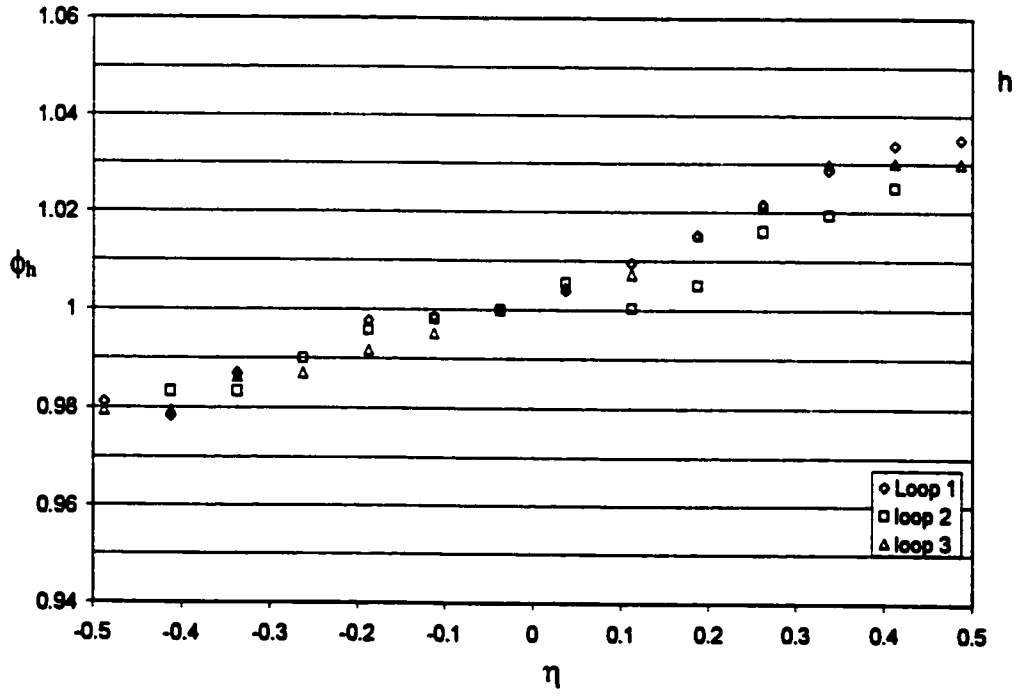

Figure 5.9: Measured dimensionless flow depth ϕ_h versus η (50°-channel)

Table 5.2: Recorded versus theoretical values of free surface super-elevation.

Section	Recorded $\Delta h/h_m$ (Average)	$\Delta h/h_m$ Eq. (5.2)
1*i*	0.003	0.000
2*i*	0.044	0.041
3*i*	0.076	0.075
4*i*	0.102	0.098
5*i*	0.105	0.106
6*i*	0.074	0.098
7*i*	0.067	0.075
8*i*	0.05	0.041

5.4 Measurements of the 70°-Channel

5.4.1 Deviation angle $\overline{\omega}_c$

Fig. 5.10 shows the measured values of $\overline{\omega}_c$ versus ξ_c. As was done for the previous two channels, the data from all three loops are plotted on a single graph (with the values for Λ_2 being plotted in terms of the opposite sign of the recorded values).

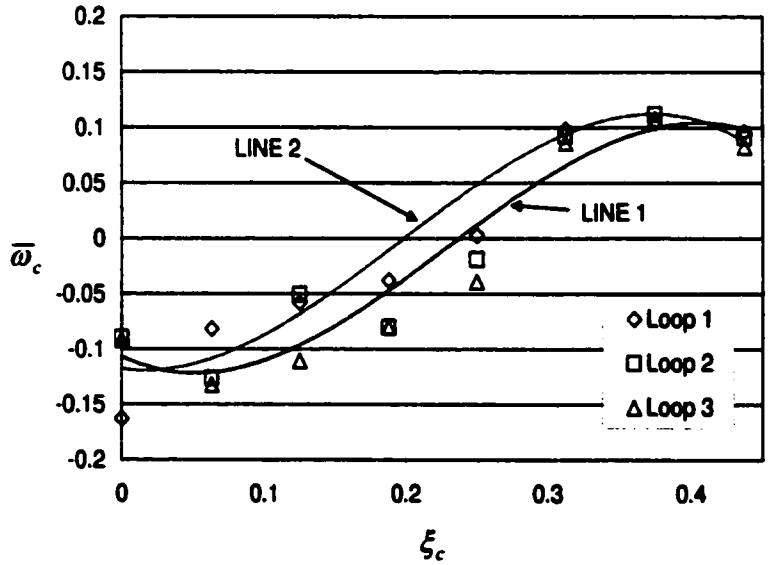

Figure 5.10: Deviation angles for the 70°-channel

From the graph in Fig. 5.10 it can be observed that the maximum deviation angle is approximately 0.12 radians.

Line 1 in Fig. 5.10 is the line of best fit (third order polynomial function) based on the average of the data. According to this line $\overline{\omega}_c = 0$ at $\xi_c \approx 0.23$, since the cross-section where $\overline{\omega}_c = 0$ is approximately in coincidence with the cross-section where $\overline{u}_{max}$ occurs, one would therefore expect $\overline{u}_{max}$ to occur at $\xi_c \approx 0.23$ (i.e. near the apex). However from the $\overline{u}$ field shown later on (see Fig. 5.11) in section 5.4.2 $\overline{u}_{max}$ appears to occur somewhere in between cross-sections 3_i and 4_i (i.e. for $\xi_c \approx 0.16$).

Let us now disregard the data collected at sections 4_i and 5_i, and fit a line to the average of the data collected in all other sections. The result, using a third order polynomial function, is line 2 in Fig. 5.10. According to this line $\overline{\omega}_c = 0$ at $\xi_c \approx 0.19$. This value of ξ_c is consistent with value $\xi_c \approx 0.16$ obtained from the velocity profiles. It is thus very likely the data measured in cross-sections 4_i and 5_i were effected by a considerable error. This should not seem strange, as the cross-circulation is the most intense in these sections, while the vertically averaged deviation is zero where the flag was oscillating the most.

Adopting line 2 as the most representative of the deviation angle pattern in this channel, one infers from Fig. 5.10 that in the range of $0.19 \approx < \xi_c < 0.5$, the deviation angle is positive. In this 70°-channel $\overline{\omega}_c = 0$ is clearly between the crossover and apex sections albeit it is closer to the apex then the crossover. Thus this flow cannot but be classified as the transitional flow between ingoing and outgoing.

Fig. D.3 (in Appendix D) shows the variation of ω_c along the z direction for all cross-sections. From this Figure it follows that, just as in the previous channels, the most

intense cross-circulation is at the apex. Like in the 50°-channel, the presence of a clearly defined cross-circulation is found at 6_i and 7_i, beside from the apex.

5.4.2 Longitudinal Flow Velocity $\overline{u}$

Fig. 5.11 shows the field of longitudinal flow velocity $\overline{u}$. As previously mentioned (section 5.4.1) the flow pattern in this Figure is consistent with the trend of line 2 in Fig. 5.10. Indeed, in each loop the maximum flow velocity occurs near the inner bank somewhere between sections 3_i and 4_i, from this Figure it appears that $\overline{u}_{max}$ occurs at $\xi_c \approx 0.16$, which agrees with line 2 and not line 1 of Fig. 5.10. Figs. 5.12a through h show the cross-sectional velocity profiles measured in the sections 1_i to 8_i. The data from all three loops for a given section are reported in the same graph. From these graphs it is evident that the flow maintains a periodic characteristic throughout the channel.

5.4.3 Flow Depth h

Fig. 5.13 a to h show the measured free surface profiles. Once again, the data corresponding to the equivalent sections of the three meander loops appear to be in agreement with each other, further indicating the periodicity of the flow.

As was the case in the previous two channels, the maximum super-elevation occurred at the apex section, and the free surface at the crossovers was nearly horizontal. Further, the characteristic S-shape taken by the super-elevated free surface was once again observed.

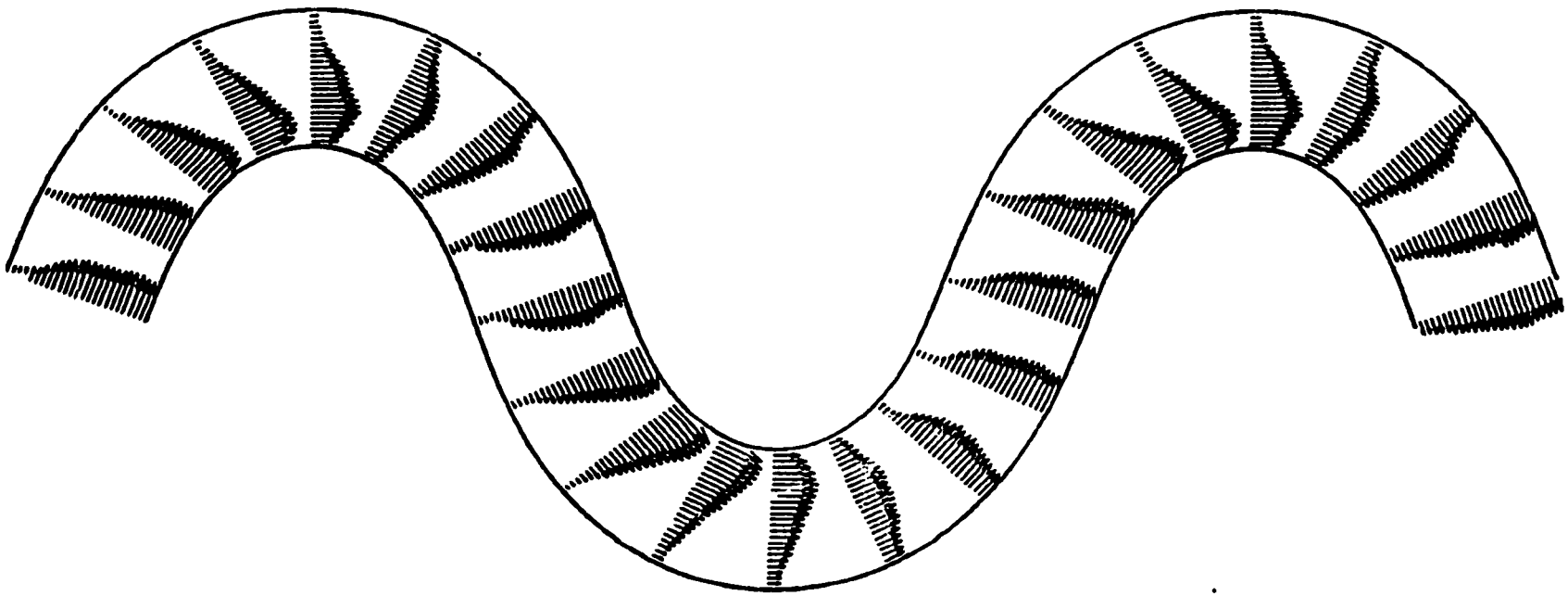

Figure 5.11: Longitudinal velocity field $\bar{u}$ for the 70°-channel

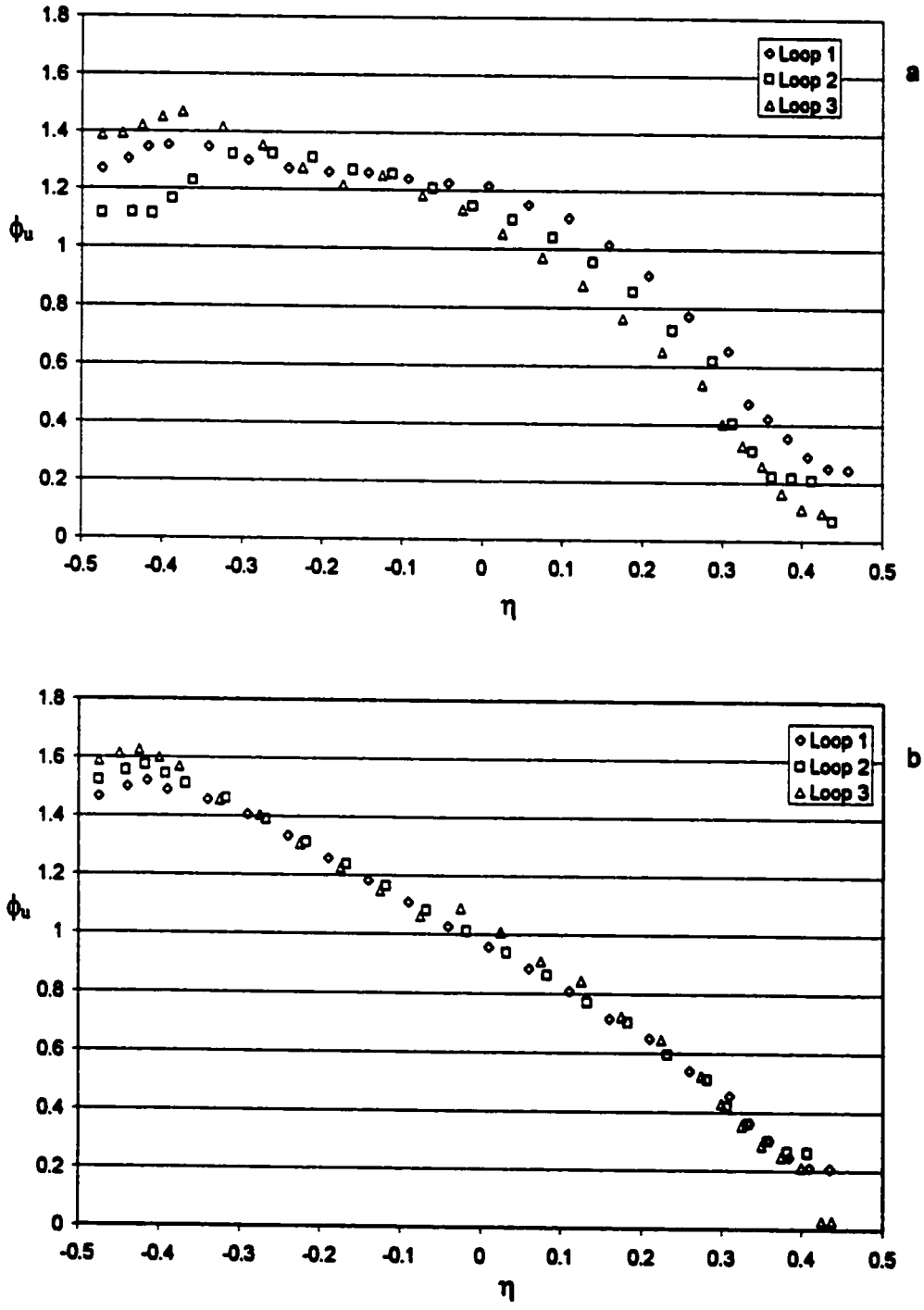

Figure 5.12: Measured dimensionless longitudinal flow velocity ϕ_u versus η (70°-channel)

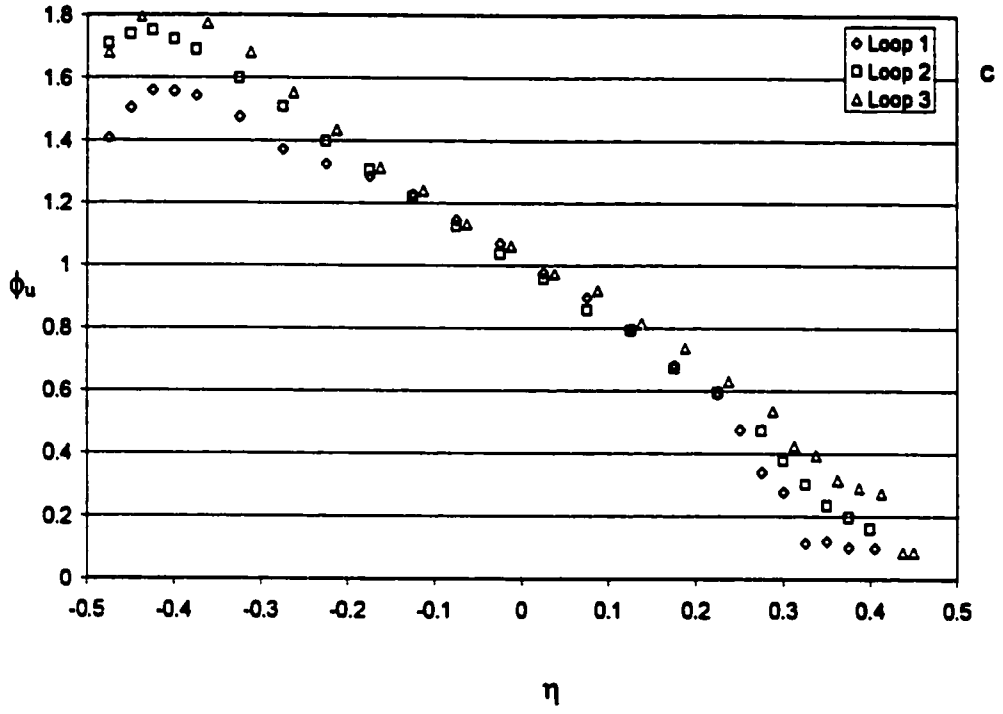

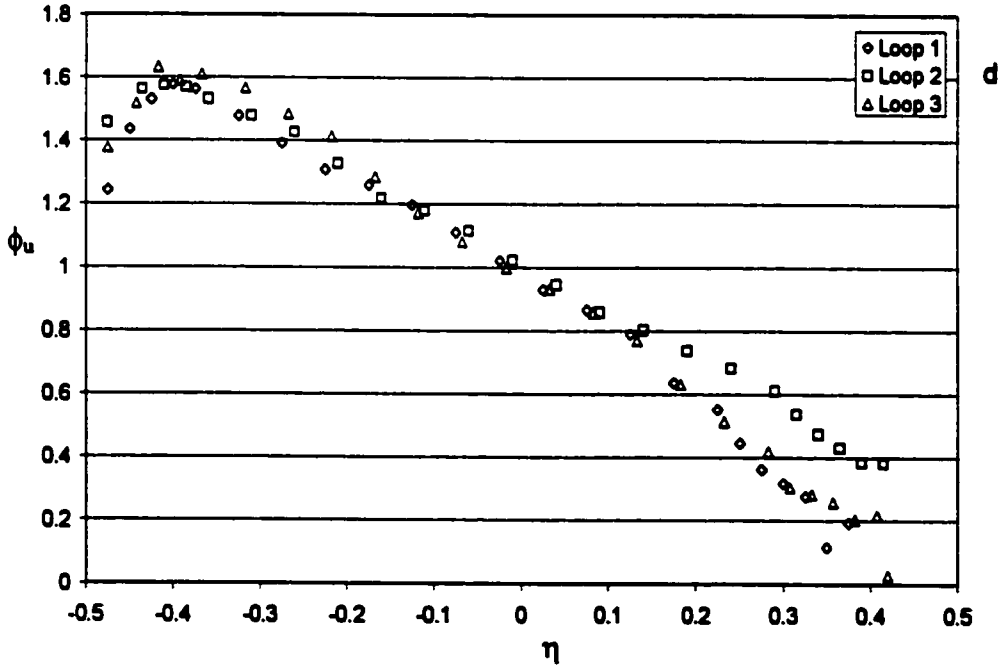

Figure 5.12: Measured dimensionless longitudinal flow velocity ϕ_u versus η (70°-channel)

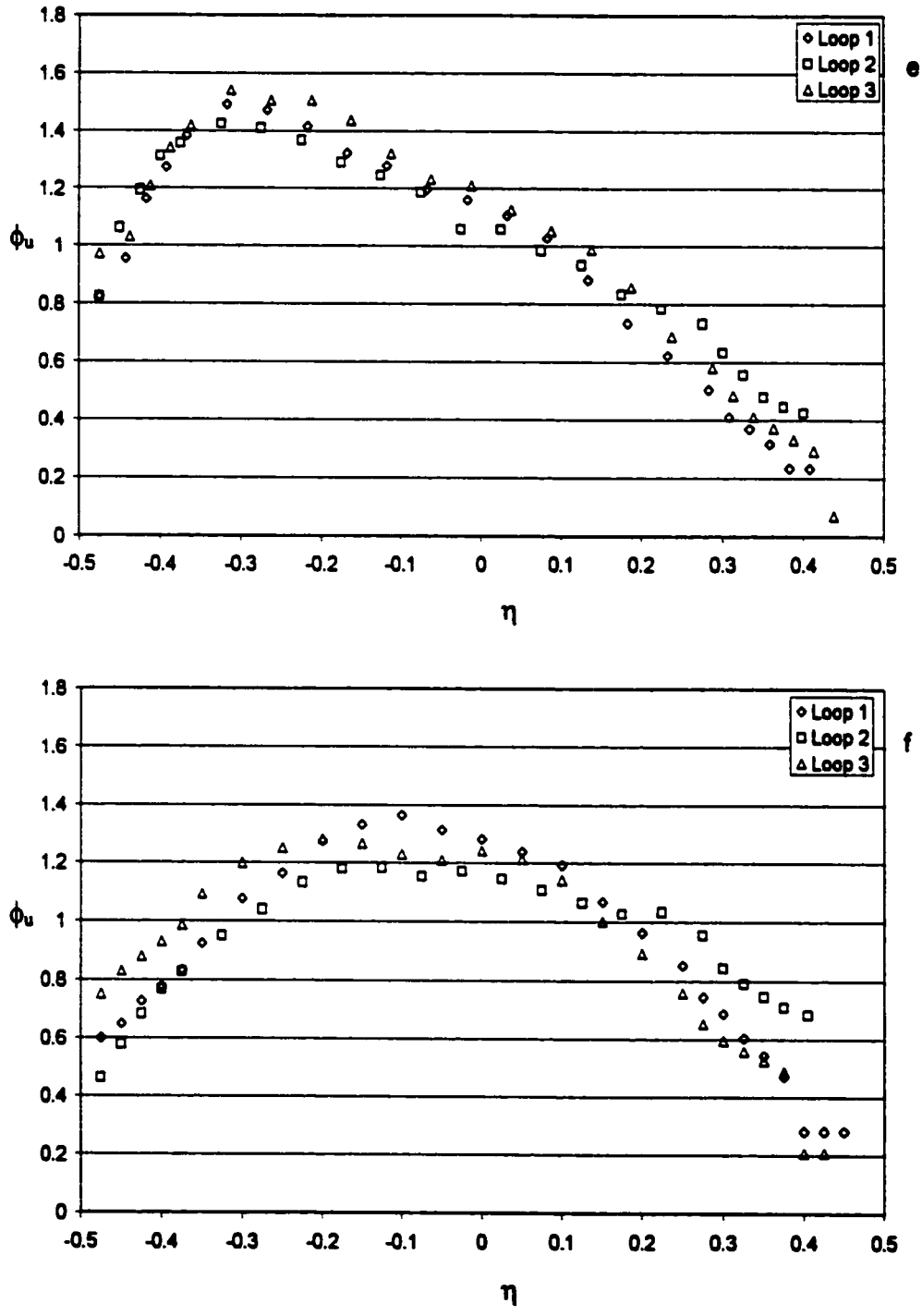

Figure 5.12: Measured dimensionless longitudinal flow velocity ϕ_u versus η (70°-channel)

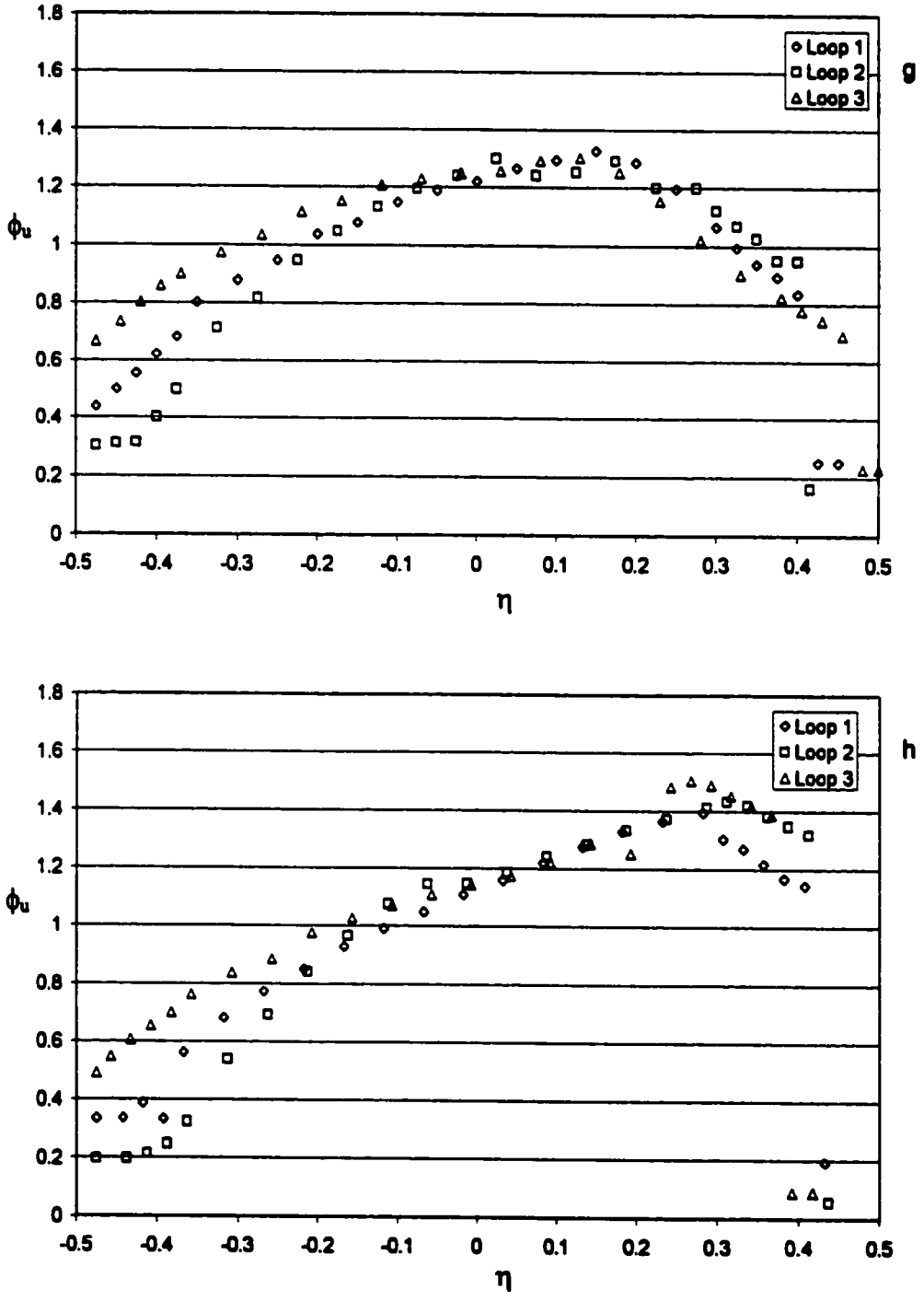

Figure 5.12: Measured dimensionless longitudinal flow velocity ϕ_u versus η (70°-channel)

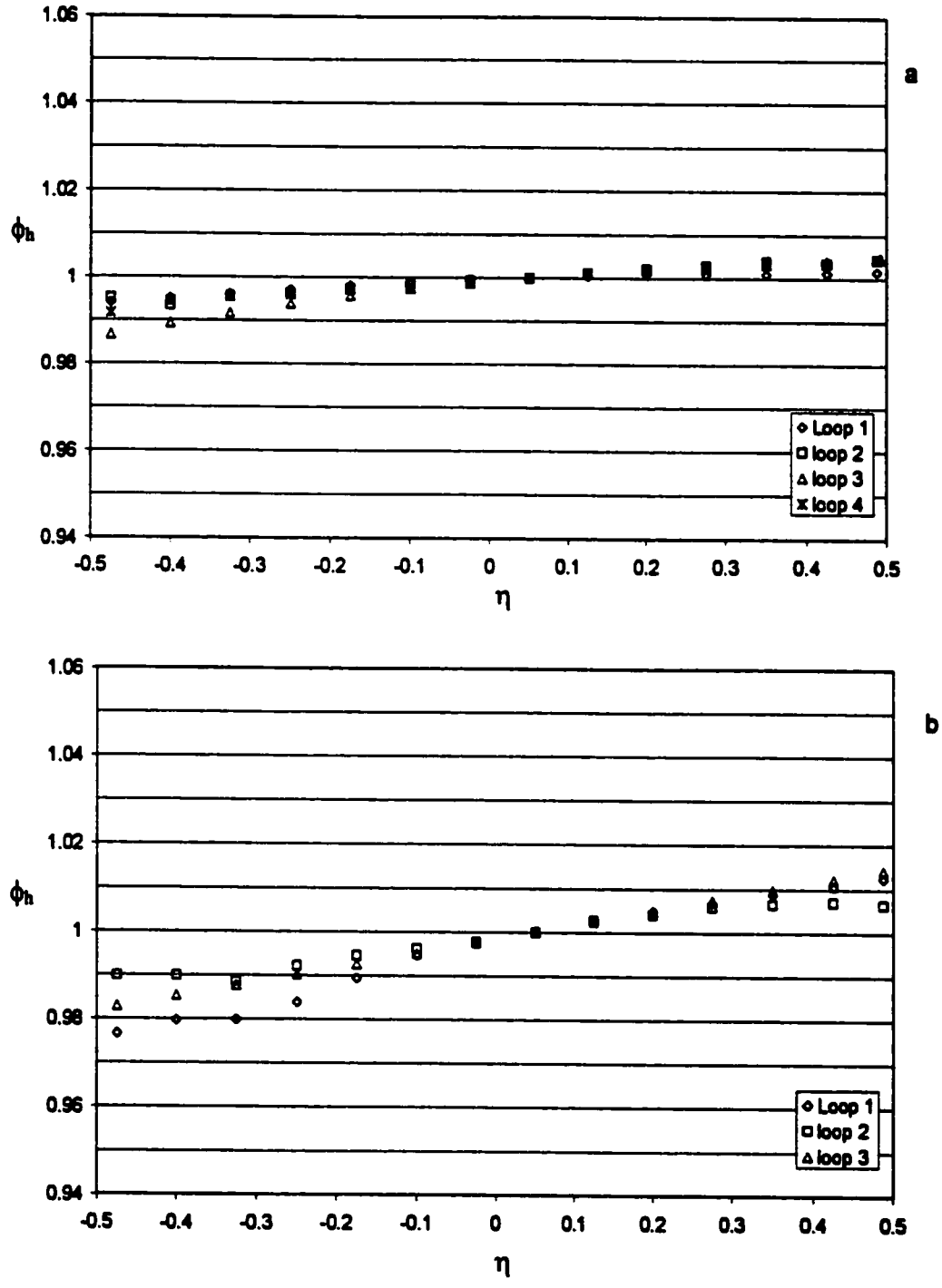

Figure 5.13: Measured dimensionless flow depth ϕ_h versus η (70°-channel)

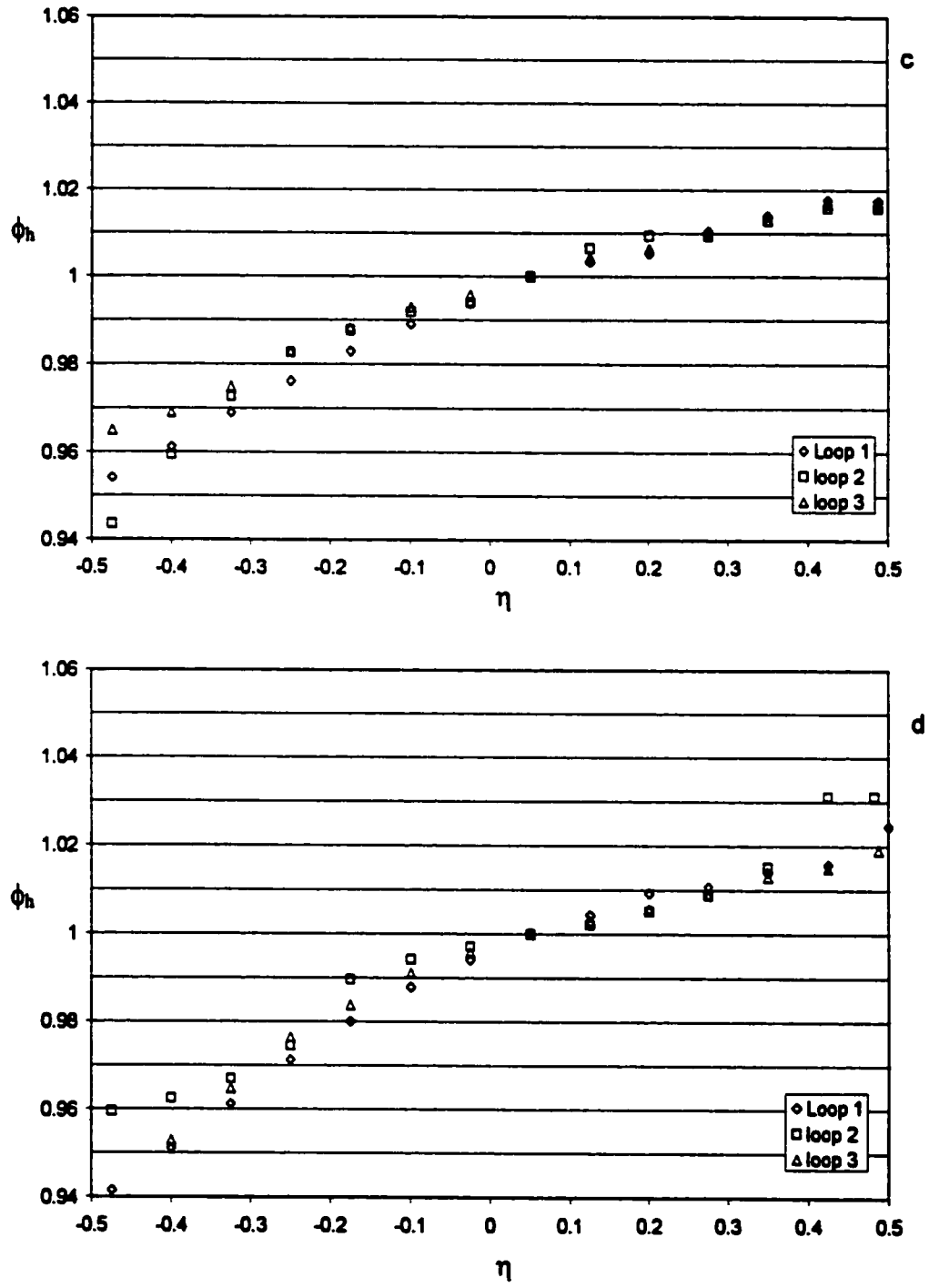

Figure 5.13: Measured dimensionless flow depth ϕ_h versus η (70°-channel)

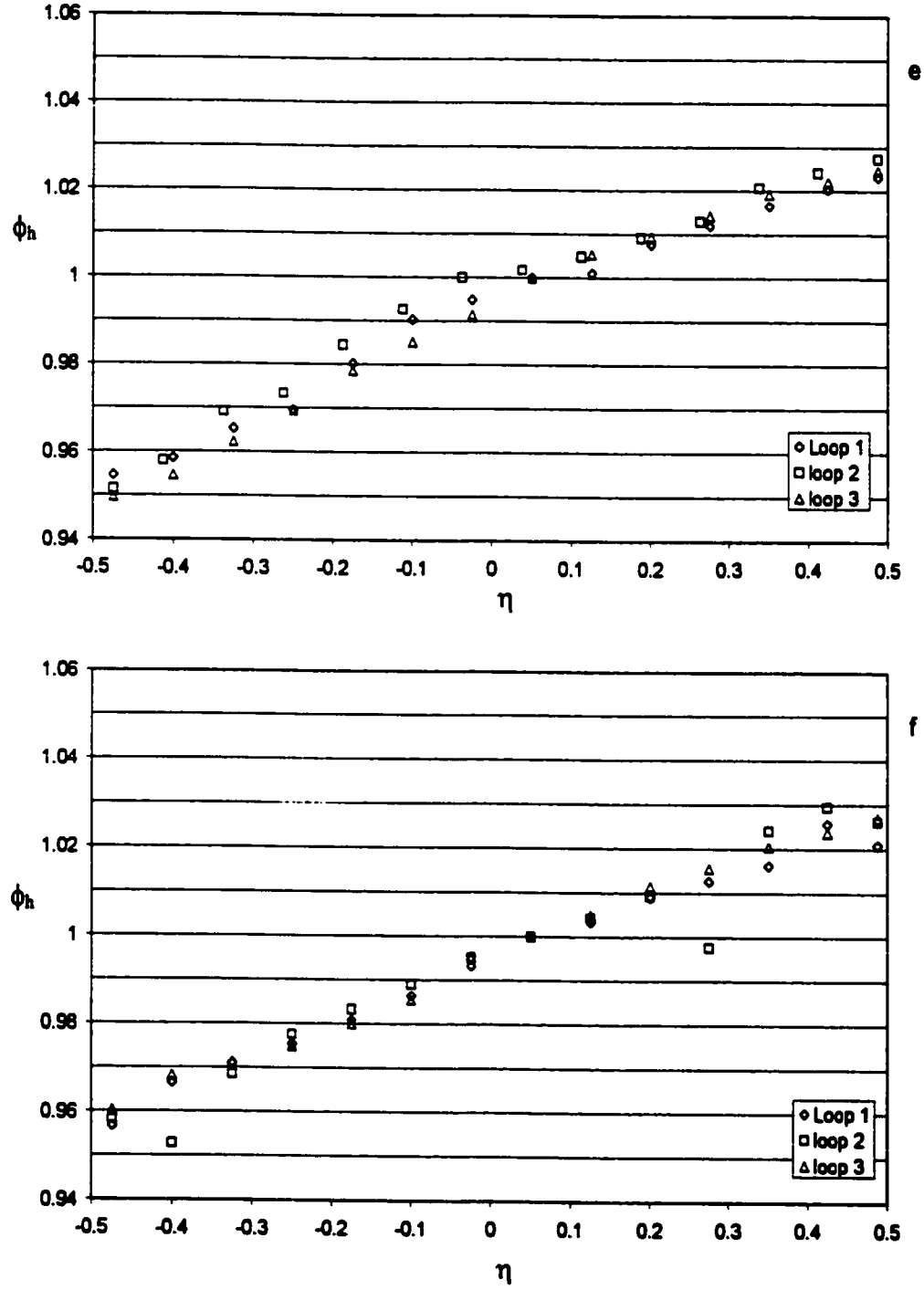

Figure 5.13: Measured dimensionless flow depth ϕ_h versus η (70°-channel)

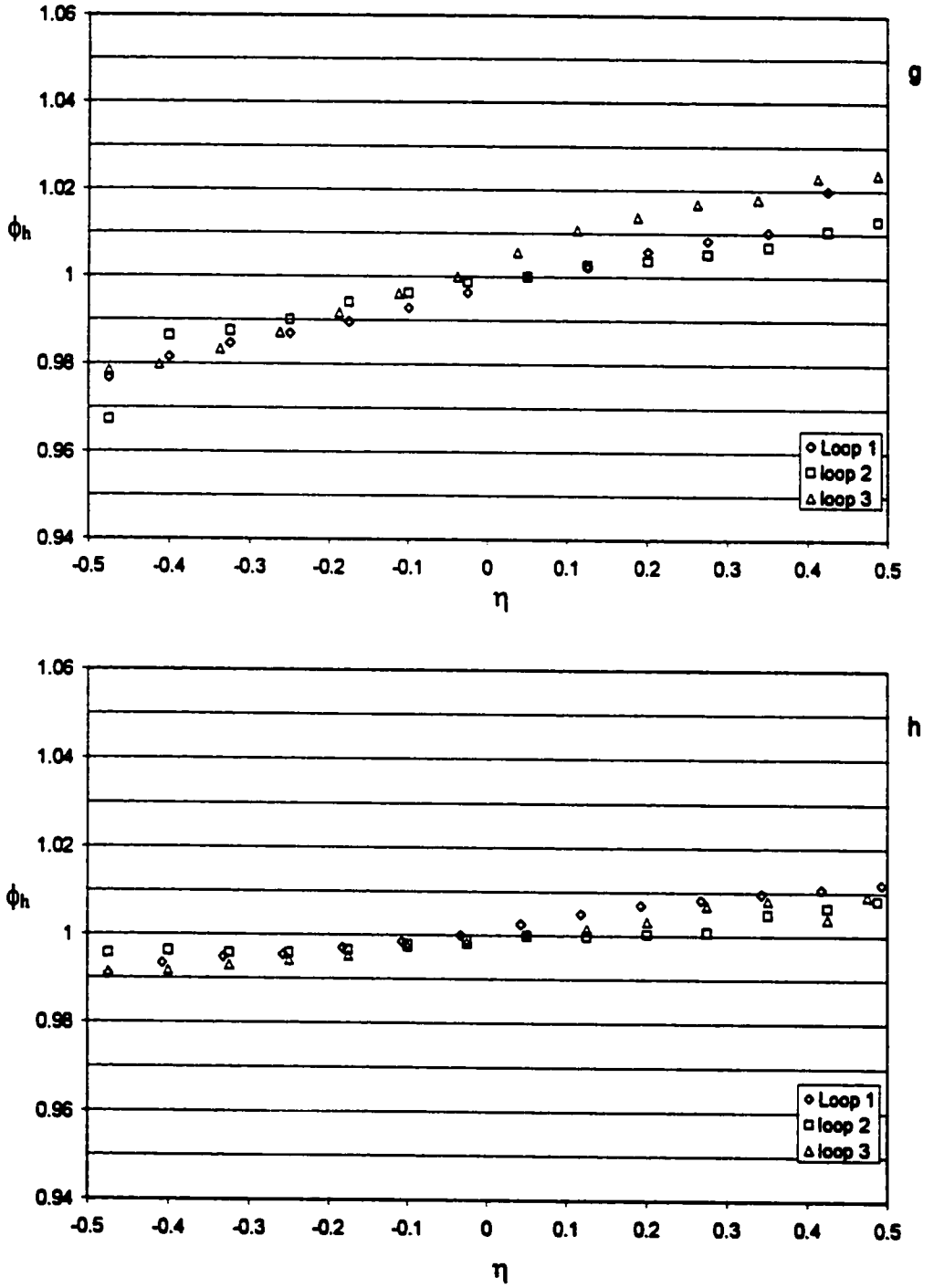

Figure 5.13: Measured dimensionless flow depth ϕ_h versus η (70°-channel)

The measured super-elevation $\Delta h/h_m$ was compared with the values of $\Delta h/h_m$ given by Eqs. (5.2) and (5.3). A comparison of the visual average of the recorded values $\Delta h/h_m$ versus those calculated are presented in Table 5.3. It was observed that on average the visual average of the recorded values differed from the calculated values by 0.007.

Table 5.3: Recorded versus theoretical values of free surface-elevation

Section	Recorded $\Delta h/h_m$ (Average)	$\Delta h/h_m$ Eq. (5.2)
1*i*	0.011	0.000
2*i*	0.024	0.022
3*i*	0.054	0.042
4*i*	0.067	0.054
5*i*	0.074	0.059
6*i*	0.068	0.054
7*i*	0.038	0.042
8*i*	0.016	0.022

5.5 Statistical analysis of Repeatability of Data

5.5.1 General

For the purpose of determining the repeatability for a specific set of measures a statistical analysis was preformed. As mentioned in section 4.3.2 all measurements (flow depth, velocity, and deviation angle) were recorded three times at each apex section. When recording all three sets of data the same spacing was used to ensure the measurements were recorded at approximately the same spot each time.

Consider three time-averaged velocity profiles taken at the same cross-section, in a given channel, under the same flow conditions such as the schematically shown set of measurements in Fig. 5.14. If steady state conditions are met all three profiles should be identical. However, for the turbulent flows under investigation the instantaneous velocity u_{inst} varies with time as shown in Fig. 5.15 the recorded velocity u being but the average over a period of time of 1 minute. Thus it should not be surprising that if the velocity is

measured at a given point three separate times, then the result should be three slightly different values for the flow velocity.

Suppose now that the velocity was measured at 23 points across the channel's width, and that this procedure was repeated three times. Thus for each one of these 23 points there are three values of flow velocity. The repeatability of the measurements will be given in terms of standard deviations of the measurements, determined as explained below.

Consider the average of the three different values of velocity collected at a given location,

$$\overline{U}_{x_i} = \frac{\left(u_{i_1} + u_{i_2} + u_{i_3}\right)}{3} . \tag{5.4}$$

Here x_i defines the location of a given point in the cross-section as shown in Fig. 5.14, and in u_{i_j}, i defines the location of the point in the cross-section and j defines the profile number. Using the average local velocity $\overline{U}_{x_i}$ for a given point the standard deviation of the three measurements can be determined as

$$S_{x_i}^2 = \frac{1}{n-1} \sum_{j=1}^{J} (u_j - \overline{U}_{x_i})^2 , \tag{5.5}$$

where n is the number of points, in this case 3, and j corresponds to the profile number (1, 2 or 3). Application of Eq. (5.5) to all 23 points in a cross-section results in 23 standard deviations, which can be averaged. This average defines the average standard deviation (S_m) of the three profiles with respect to their average profile. However, to understand how all points sit with respect to the average standard deviation, the highest (S_h) and lowest (S_l) local standard deviations within the cross-section will also be reported.

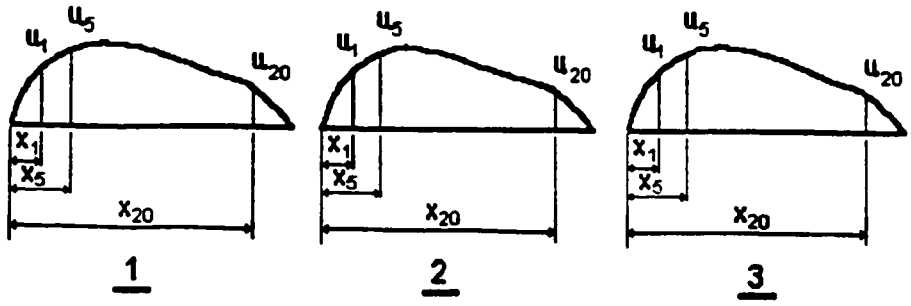

Figure 5.14: Examples of repeated velocity profiles

Figure 5.15: Fluctuation of u with respect to time, in turbulent flow

The above example outlined the procedure taken to analyze the repeatability of the velocity measurements. However, the exact same procedure is applied to the measurements of flow depth and deviation angle.

5.5.2 Repeatability of Velocity Measurements

Table 5.4a shows the values of S_l, S_m and S_h for the measurements of velocity taken at the apexes of loops Λ_1, Λ_2 and Λ_3, for all channels. The high and low standard deviations appear to be randomly distributed throughout the cross-sections. To provide some insight into the standard deviations presented in Table 5.4a consider the high and low standard deviations for Λ_1 of the 90°-channel, these standard deviations correspond to errors, with respect their average local longitudinal flow velocity, of 7.0% and 2.5% respectively. From this Table it can be noticed that the standard deviations for the

Table 5.4: Repeatability of all Measurements

Velocity :

	90°-Channel			70°-Channel			50°-Channel		
	S_l (cm/s)	S_m (cm/s)	S_h (cm/s)	S_l (cm/s)	S_m (cm/s)	S_h (cm/s)	S_l (cm/s)	S_m (cm/s)	S_h (cm/s)
Λ_1	0.581	1.153	1.355	0.090	0.234	0.747	0.049	0.580	1.570
Λ_2	0.322	0.379	0.557	0.027	0.266	0.665	0.413	0.880	1.571
Λ_3	0.088	0.130	0.117	0.130	0.322	0.669	0.023	0.600	1.672

Flow Depth:

	90°-Channel			70°-Channel			50°-Channel		
	S_l (mm)	S_m (mm)	S_h (mm)	S_l (mm)	S_m (mm)	S_h (mm)	S_l (mm)	S_m (mm)	S_h (mm)
Λ_1	0.449	0.541	0.667	0.055	0.159	0.307	0.132	0.205	0.290
Λ_2	0.270	0.351	0.379	0.005	0.049	0.282	0.060	0.200	0.523
Λ_3	0.198	0.248	0.302	0.012	0.199	0.473	0.030	0.230	0.707

Deviation Angle:

	90°-Channel			70°-Channel			50°-Channel		
	S_l (deg.)	S_m (deg.)	S_h (deg.)	S_l (deg.)	S_m (deg.)	S_h (deg.)	S_l (deg.)	S_m (deg.)	S_h (deg.)
Λ_1	0.0	1.1	1.4	0.6	0.8	1.2	0.0	0.4	0.5
Λ_2	0.3	1.1	1.4	0.6	1.1	1.2	0.3	0.6	0.9
Λ_3	0.4	0.9	1.4	0.6	1.1	1.5	0.3	0.6	1.0

90°- channel continuously decrease from Λ_1 to Λ_3. No apparent justification for such a phenomenon could be found by the author.

5.5.3 Repeatability of Flow Depth Measurements

Table 5.4b shows the values of S_l, S_m and S_h for the measurements of flow depth taken in all three channels. No correlation between the high and low standard deviation and a specific location within the cross-section is apparent. For a better understanding of the standard deviations in Table 5.4b considering the high and low standard deviations for Λ_1 of the 90°-channel, these standard deviations correspond to errors, with respect to the average local flow depth, of 2.3% and 1.5% respectively. The standard deviations are slightly higher in the 90°-channel when compared with the other two channels. The values of the standard deviation in this channel decreased from Λ_1 to Λ_3. During testing of the 90°-channel the formation of waves on the free surface at the channel entrance was observed. These waves appeared to be dampened out along the length of the channel. It is thus the opinion of the author that this phenomenon is the cause of the discrepancies in the standard deviations.

5.5.4 Repeatability of the Deviation Angle Measurements

Table 5.4c shows the values of S_l, S_m and S_h for the measurements of the deviation angle taken in all three channels. As was the case in both the flow depth and flow velocity measurements, the high and low standard deviations do not appear to correspond with any common location within a vertical. From this Table it appears also that the standard deviations are fairly consistent for all channels.

5.6 Final Remarks

i.) The curves representing $\overline{\omega}_c$ as a function of ξ_c for all channels (third order polynomial functions) in the present work are plotted together with those for the

channels tested by Silva 1995 in Fig. 5.16. It is interesting to notice that for the 30°- and 50°-channels the location of $\overline{\omega}_c = 0$ correspond approximately to the same ξ_c–value ($\xi_c \approx 0.23$). It was also observed that the values of ξ_c corresponding to $\overline{\omega}_c = 0$ for the 90°- and 110°-channels were within close proximate to each other. The curve for the 70°-channel is clearly sitting at an intermediate location between the 90°- and 50°-channels.

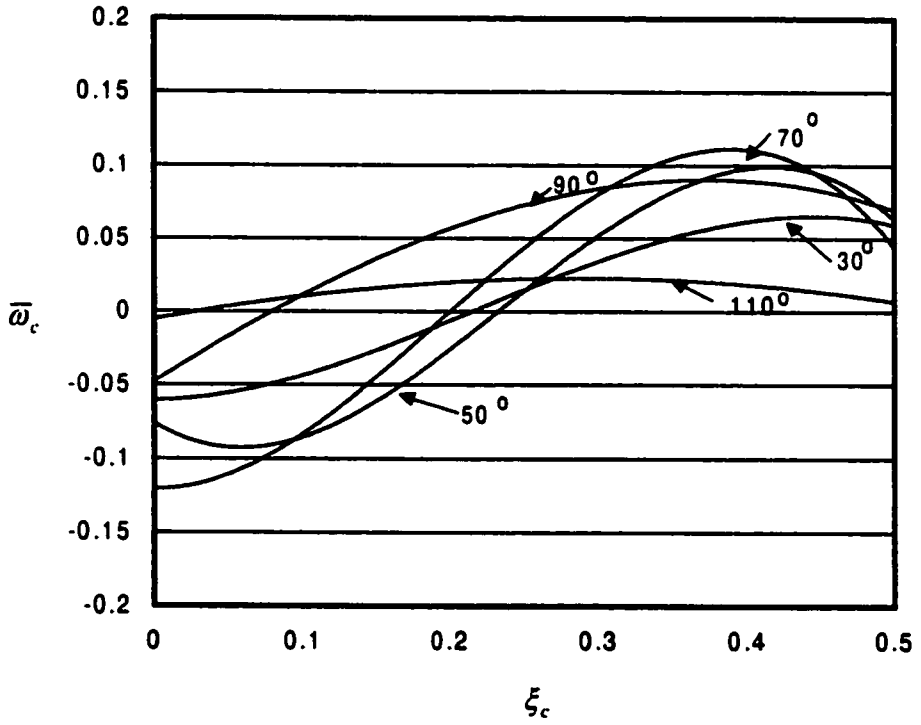

Figure 5.16: Variation of $\overline{\omega}_c$ with respect to ξ_c for all channels

As mentioned earlier in this thesis the flow in the 50°-channel can be considered an ingoing flow and the flow in the 90°-channel can be considered outgoing. One of the contributions of this thesis is thus to establish new boundaries for the existence of ingoing and outgoing flow as illustrated in Fig. 5.17.

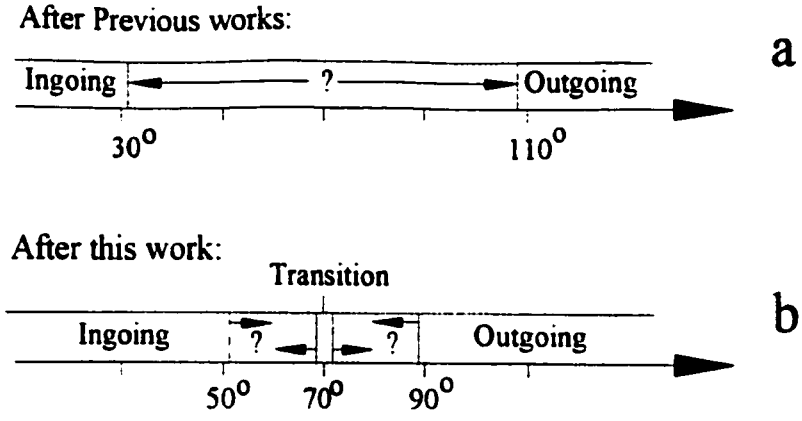

Figure 5.17: Defined ranges of flow

ii.) Consider now the plot of measured $|\overline{\omega}_{c\max}|$ versus θ_0 in Fig. 5.18. Both the present experiment and those of Silva 1995 are represented. The dashed line in this Figure is the line of best fit, which is the following third order polynomial function

$$|\overline{\omega}_{c\max}| = -1\times10^{-7}\theta_0^3 - 3\times10^{-5}\theta_0^2 + .005\theta_0 - 0.0694 . \qquad (5.6)$$

The solid line in Fig. 5.18 is the curve determined by Banerjee 2000 by means of a numerical study (no experimental measurements). The computed values reported by Banerjee 2000 for the 90°-, 70°- and 50°-channels are consistently lower than those measured in this thesis.

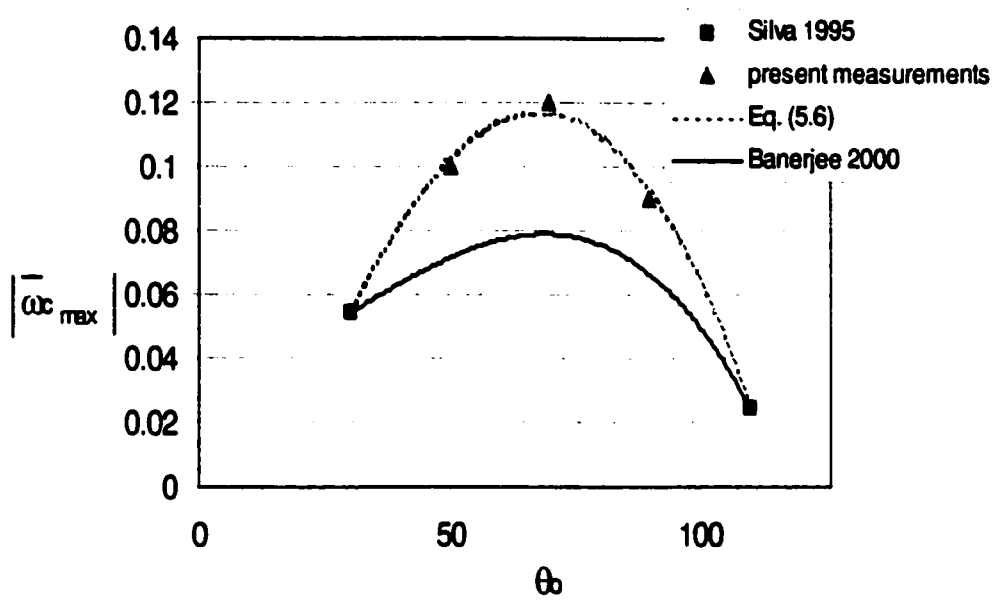

Figure 5.18: Variation of measured $|\overline{\omega}_{c\max}|$ with θ_0

iii.) From past observations and measurements it has been found that the velocity of expansion $(d\theta_0/dt)$ for a meandering channel varies with θ_0 (Yalin 1992, Kondratiev et. al. 1982, etc.). A normalized plot of this relationship ($(d\theta_0/dt)$vs. θ_0) is shown in Fig. 5.19. Note that the maximum velocity of expansion corresponds with $\theta_0 = 70°$. Note that the maximum $|\overline{\omega}_{c\max}|$-value in Fig. 5.18 is also at $\theta_0 = 70°$. Further, the curve (C) in Fig. 5.19 has the same trend as the curves in Fig. 5.18. It has therefore been suggested by Yalin and Silva 2001 that, in fact,

$$\frac{d\theta_0}{dt} = \varphi\left(|\overline{\omega}_{c_{max}}|\right). \tag{5.7}$$

This suggestion is supported by the similarities found between the two graphs (Figs. 5.18 and 5.19).

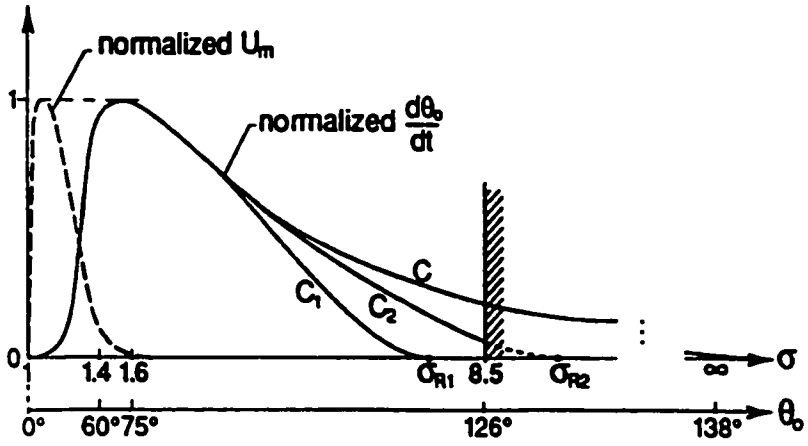

Figure 5.19: Variation of $(d\theta_0 / dt)$ with θ_0 (from Yalin 1992)

6.0 CONCLUSIONS AND RECOMMENDATIONS FOR FUTURE WORK

6.1 Conclusions

From the present experiments the following conclusions can be drawn with respect to the objectives outlined in Chapter 1:

1. From the measurements conducted in each of the three channels it was determined that in the 90°-channel the flow was outgoing, in the 50°-channel the flow was ingoing, and in the 70°-channel the flow was in transition between the two (ingoing and outgoing) flow types.

2. As previously mentioned, from the work of Silva 1995 it is only possible to say that for channels having $\theta_0 <\approx 30°$ the flow is ingoing, and for channels where $\theta_0 >\approx 110°$ the flow is outgoing (see Fig. 5.17a). However, no conditions between these values were known. The present work has extended these aforementioned limits, showing that ingoing flow is present in channels where $\theta_0 <\approx 50°$, and outgoing flow is present in channel where $\theta_0 >\approx 90°$; when $\theta_0 \approx 70°$ the flow is in a transition region (see Fig. 5.17b).

3. The $|\overline{\omega}_{c_{max}}|$ versus θ_0 curve derived from the present experiment (Fig. 5.18) appears to be similar to that of the velocity of expansion for a naturally meandering channel (see Section 5.6). This supports the hypothesis of Yalin and Silva 2001, that $|\overline{\omega}_{c_{max}}|$ is a function of θ_0.

6.2 Suggestions for Future Work

As previously mentioned, the present work has enabled a better definition of the boundaries between ingoing and outgoing flows; therefore, new ranges for θ_0 associated with outgoing and ingoing flow have been established. As well the presence of a marked

transition region between these flows has been identified; however, as follows from Fig. 5.17b the flow pattern for all θ_0-values has not yet been defined. It is, therefore, recommended that further physical modelling be conducted in the range $50° < \theta_0 < 90°$. Such work would also aid in defining the limits of the transition region, thereby completing Fig. 5.17b.

It is further recommend that physical modelling of channels in the range $50° < \theta_0 < 90°$ be conducted for the purpose of defining their equilibrium bed topography. Such work would be in further support of the observations of previous researchers, in that the equilibrium bed topography is "locked" within the initial flow and it is, therefore, distinct for a given channel.

The relationship between $|\overline{\omega}_{c\max}|$ and $(d\theta_o / dt)$ suggested in Section 5.6(iii) should be further explored. An investigation should be conducted into whether there exists a direct relationship between $|\overline{\omega}_{c\max}|$ and $(d\theta_0 / dt)$, or if the similarities between their respective relationships with θ_0 are coincidental.

In the present thesis, the flow patterns are linked only to θ_0; however, the flow patterns must be, to some extent, also a function of the width-to-depth ratio of the stream, as well as its relative roughness. The dependency of the flow pattern on these variables should be the object of future works.

References

1. Ackert, S.F.: *A study of different methods for the determination of regime channel geometry with applications to streams in southwestern Ontario.* M.A.Sc. Thesis, Dept. of Civil and Environmental Engineering, University of Windsor, Windsor, Ontario, Canada 2000.

2. Almquist, C.W., Holley, E.R.: *Transverse mixing in meandering channels with rectangular and naturally varying cross-sections.* Rept. CRWR 205, The Texas University of Texas at Austin, Sept. 1985.

3. Banerjee, D.: *Initiation of bed deformation in meandering channels: a theoretical and numerical study.* M.A.Sc. Thesis, Dept. of Civil and Environmental Engineering, University of Windsor, Windsor, Ontario, Canada 2000.

4. Chang, H.H.: *Fluvial processes in river engineering.* John Wiley and Sons, 1988.

5. Chin, D.A. : *Water resources engineering.* Prentice Hall, N.J. 2000.

6. Choudhary, U.K., Narasimhan, S.: *Flow in 180° open channel rigid boundary bends.* J. Hydr. Div., ASCE, Vol. 103, No. HY6, June 1977.

7. De Vriend H.J., Koch, F.G.: *Flow of water in a curved open channel.* Delft Hydraulics Laboratory/Delft University of Technology, TOW-Report R657-VIIM141SIII, 1978.

8. Dietrich, W.E., Whiting, P.J.: *Boundary shear stress and sediment transport in river meanders of sand and gravel.* Ikeda and G. Parker eds., Am. Geophys. Union, Water Resources Monograph, 12, 1989.

9. Einstein, H.A., Harder, J.A.: *Velocity distribution and boundary layer at channel bends.* Trans. Am. Geophysical Union, Vol. 35, 1954.

10. Engelund, F.: *Flow and bed topography in channel bends.* J. Hydr. Div., ASCE, Vol. 100, No. HY11, Nov. 1974

11. Francis, J.R.D., Asfari, A.F.: *Velocity distributions in wide, curved open channel flows.* J. Hydr. Res., Vol. 9, 1971.

12. Ghanmi, A.: *Modeling of flows between two consecutive reverse curves.* J. Hydr. Res., Vol. 37, No. 1, 1999.

13. Graf, W.H.: *Hydraulics of sediment transport.* McGraw-Hill Book Company, N.Y. 1971.

14. Guymer, I.: *Longitudinal dispersion in sinuous channel with changes in shape*. J. Hydr. Engrg., Vol. 124, No.1, January 1998.

15. Hasegawa, K.: *A Study of flows and bed topographies in meandering channels.* (In Japanese) Proc. JSCE, No. 338, Oct. 1983.

16. Henderson, F.M.: *Open channel flow*. McMillan Publ. Co. Inc., New York, 1966.

17. Hooke, R.L.: *Distribution of sediment transport and shear stress in a meander bend*. Rept. 30, Uppsala Univ. Naturgeografiska Inst., 58, 1974.

18. Ikeda, S., Nishimura, T.: *Flow and bed profile in meandering sand-silt rivers*. J. Hydr. Engrg., Vol. 112, No. 7, July 1986.

19. Ippen, A.T., Drinker, P.A.: *Boundary shear stress in curved trapezoidal channels*. J. Hydr. Div., ASCE, Vol. 88, No. HY5, Sept. 1962.

20. Jackson, R.J.: *Velocity-bed-form texture patterns of meander bends in the lower Wabash River of Illinois and Indiana*. Geol. Soc. Am. Bull., Vol. 86, Nov. 1975.

21. Julien, P.Y., Kawai, S.: *Point bar deposits in narrow sharp bends*. J. Hydr. Res., Vol. 34, No. 2, 1996.

22. Kamphuis, J.W.: *Determination of sand roughness for fixed beds*. J. Hydr. Res., Vol. 12, No. 2, 1974.

23. Khalil, M.B.: *On preserving the sand patterns in river models*. J. Hydr. Res., Vol. 10, No. 3, 1972.

24. Kikkawa, H., Ikeda, S., Kitagawa, A.: *Flow and bed topography in curved open channels*. J. Hydr. Div., ASCE, Vol. 102, No. HY9, Sept. 1976.

25. Kondratiev, N., Popov, I., Snishchenko, B.: *Foundations of hydromorphological theory of fluvial processes.* (In Russian) Gidrometeoizdat, Leningrad, 1982

26. Krishnappan, B.G., Lau, Y.L.: *Transverse dispersion in meandering channels.* Scientific Series No. 75, Canada Centre for Inland Waters, Burlington, Ontario, Canada 1977.

27. Leliavsky, S.: *An introduction to fluvial hydraulics*. Constable, London 1955.

28. Leopold L.B., Langbein, W.B.: *River meanders*. Sci. Am. 214, 1966.

29. Makaveyvev, N.I.: *River bed and erosion in its basic.* Press of the Academy of Sciences of the USSR, Moscow, 1975.

30. Matthes, G.H.: *Basic aspects of stream meanders*. Amer. Geophys. Union, 1941.

31. Nelson, J.M., Smith, J.D.: *Evolution and stability of erodible channel beds.* in *River Meandering*, S. Ikeda and G. Parker eds., American Geophysical Union, Water Resources Monograph, 12, 1989a.

32. Nelson, J.M., Smith, J.D.: *Flow in meandering channels with natural topography* in *River Meandering*, S. Ikeda and G. Parker eds., American Geophysical Union, Water Resources Monograph, 12, 1989b.

33. Odgaard, A.J., Bergs, Mary A.: *Flow Processes in a curved alluvial channel.* Water Resour. Res. Vol. 24, No. 1, January 1988.

34. Odgaard, A.J.: *Flow and bed topography in alluvial channel bend.* J. Hydr. Engrg., Vol. 110, No. 4, April 1984.

35. Parker, G., Edmund A.: *On the time development of meander bends.* J. Fluid Mechanics, Vol. 162, Jan. 1986.

36. Rozovskii, J.L.: *Flow of water in bends of open channels.* The Academy of Sciences of the Ukrainian USSR, 1957, Translated from Russian by the Israel Program for Scientific Translations, Jerusalem, 1961.

37. Shiono, K., Muto, Y., Knight, D.W., Hyde, A.F.L.: *Energy losses due to secondary flow and turbulence in meandering channels with overbank flows.* J. Hydr. Res., Vol. 37, No. 5, 1999.

38. Shimizu, Y., Itakura, T.: *Calculation of bed variation in alluvial channels.* J. Hydr. Engrg., ASCE, Vol. 115, No. 3, 1989.

39. Silva, A.M.F.: *Friction factor of meandering flows.* J. Hydr. Engrg., Vol. 125, No. 7, July 1999.

40. Silva, A.M.F., Yalin, M.S.: *Laboratory measurements in sine-generated meandering channels.* Int. J. Sediment Res., Vol. 12, No. 2, Aug. 1997.

41. Silva, A.M.F.: *Turbulent flow in sine-generated meandering channels.* Ph.D. Thesis, Dept. Civil Engrg., Queens University, Ontario, Canada, 1995.

42. Silva, A.M.F.: *Alternate bars and related alluvial processes.* M.Sc. Thesis, Dept. of Civil Engrg., Queen's Univ., Kingston, Canada, 1991.

43. Smith, J.D., McLean, S.R.: *A model for flow in meandering streams.* Water Resour. Res., Vol. 20, No. 9, 1984.

44. Steffler, P.M.: *Turbulent flow in a curved rectangular channel.* Ph.D. Thesis, University of Alberta, Alberta, Canada, 1984.

45. Struiksma, N., Olesen, K.W., Flokstra, C., De Vriend, H.J.: *Bed deformation in curved alluvial channels.* J. Hydr. Res., Vol. 23, No. 1, 1985.

46. Struiksma, N., Talmon, A.M., Van Mierlo, M.C.L.M.: *Laboratory measurements of the direction of sediment transport on transverse alluvial-bed slopes.* J. Hydr. Res., Vol. 33, No. 4, 1995.

47. Termini, D.: *Evoluzione di un canale meandriforme a fondo inizialmente piano: studio teorico-sperimentale del fondo e le caratteristiche iniziali della corrente.* Ph.D. Thesis, Dept. Hydraulic Engrg. and Environmental Applications, University of Palermo, Italy, 1996.

48. Von Schelling, H.: *Most frequent random walks.* Gen. Elec. Co., Rept. 64 GL92, Schenectady, N.T., 1964.

49. Von Schelling, H.: *Most frequent particle paths in a plane.* Am. Geophysical Union Trans., Vol. 32, 1951.

50. Whiting, P.J. Dietrich, W.E.: *Experimental studies of bed topography and flow patterns in large-amplitude meanders. 1. Observations.* Water Resour. Res., Vol. 29, No. 11, Nov. 1993(a).

51. Whiting, P.J. Dietrich, W.E.: *Experimental studies of bed topography and flow patterns in large-amplitude meanders. 1. Mechanisms.* Water Resour. Res., Vol. 29, No. 11, Nov. 1993(b).

52. Whiting, P.J. Dietrich, W.E.: *Experimental constraints on bar migration through bends: implications for meander wavelength.* Water Resour. Res., Vol. 29, No. 4, April 1993(c).

53. Yalin, M.S., Silva, A.M.F.: *Fluvial Processes.* IAHR Monograph, The Netherlands, 2001

54. Yalin, M.S.: *River Mechanics.* Pergamon Press, Oxford 1992.

55. Ye, J., McCorquodale J.A.: *Simulation of curved open channel flows by 3D hydrodynamic Model.* J. Hydr. Engrg., Vol. 124, No. 7, July 1998.

56. Yen , C.L., Yen, B.C.: *Water surface configuration in channel bends.* J. Hydr. Div., ASCE, Vol. 97, No. HY2, Feb 1971.

57. Zhi-Qiang D., Singh, V.P.: *Mechanism and conditions for change in channel pattern.* J. Hydr. Res., Vol.37, No.4, 1999.

58. Zimmerman, C.: *Roughness effect on the flow direction in channel beds.* J. Hydr. Div., ASCE, Vol. 97, No. HY2, Sept. 1971.

Appendix A

90°-channel: Raw data

Local Velocity Measurements at hm/2

Section												
1-1	n/B	-0.475	-0.443	-0.418	-0.393	-0.343	-0.293	-0.243	-0.193	-0.143	-0.093	-0.043
	u (cm/s)	26.560	26.560	25.990	25.650	24.600	24.110	23.890	23.440	23.100	22.190	21.120
	n/B	0.008	0.058	0.108	0.158	0.208	0.258	0.308	0.333	0.358	0.383	0.408
	u (cm/s)	19.750	18.210	17.060	15.690	14.140	12.500	11.740	10.520	8.370	7.920	7.920
	n/B	0.433	0.458									
	u (cm/s)	7.920	7.920									
2-1	n/B	-0.475	-0.440	-0.415	-0.390	-0.340	-0.290	-0.240	-0.190	-0.140	-0.090	-0.040
	u (cm/s)	28.070	28.943	28.834	27.727	26.368	25.587	24.689	23.962	22.699	21.563	19.971
	n/B	0.010	0.060	0.110	0.160	0.210	0.260	0.310	0.335	0.360	0.385	0.410
	u (cm/s)	18.750	17.388	15.989	15.459	14.100	12.395	11.202	10.190	6.925	6.643	6.644
	n/B	0.435										
	u (cm/s)	6.626										
3-1	n/B	-0.475	-0.450	-0.425	-0.400	-0.375	-0.325	-0.275	-0.225	-0.175	-0.125	-0.075
	u (cm/s)	23.465	27.404	29.290	29.530	28.737	27.132	25.214	24.226	23.535	22.718	21.223
	n/B	-0.025	0.025	0.075	0.125	0.175	0.225	0.250	0.275	0.300	0.325	0.350
	u (cm/s)	19.831	18.399	16.991	15.055	15.191	13.805	10.947	10.239	8.939	9.041	8.533
	n/B	0.375	0.405									
	u (cm/s)	8.562	8.483									

4-1	n/B	-0.475	-0.450	-0.425	-0.400	-0.375	-0.325	-0.275	-0.225	-0.175	-0.125	-0.075
	u (cm/s)	20.391	20.377	21.741	23.640	25.452	26.640	25.641	24.330	23.488	22.931	22.143
	n/B	-0.025	0.025	0.075	0.125	0.175	0.225	0.250	0.275	0.300	0.325	0.350
	u (cm/s)	20.950	19.437	16.947	15.060	14.350	13.270	11.706	12.139	11.561	10.971	10.409
	n/B	0.375	0.400									
	u (cm/s)	10.310	10.310									
5-1	n/B	-0.475	-0.443	-0.418	-0.393	-0.368	-0.318	-0.268	-0.218	-0.168	-0.118	-0.068
	u (cm/s)	18.790	20.355	21.001	21.469	21.904	22.386	23.385	23.994	24.178	24.093	23.956
	n/B	-0.018	0.033	0.083	0.133	0.183	0.233	0.283	0.308	0.333	0.358	0.383
	u (cm/s)	23.426	22.390	19.750	19.000	18.593	15.675	14.043	12.719	10.625	9.034	8.999
	n/B	0.408										
	u (cm/s)	4.162										
6-1	n/B	-0.475	-0.450	-0.425	-0.400	-0.375	-0.350	-0.300	-0.250	-0.200	-0.150	-0.100
	u (cm/s)	7.215	13.262	14.408	14.957	15.308	15.967	17.869	19.348	20.138	20.690	21.038
	n/B	-0.050	0.000	0.050	0.100	0.150	0.200	0.250	0.275	0.300	0.325	0.350
	u (cm/s)	21.240	21.398	22.182	22.468	22.436	21.834	20.822	19.707	18.842	17.788	16.793
	n/B	0.375	0.400	0.425	0.450							
	u (cm/s)	15.265	13.968	13.001	13.026							
7-1	n/B	-0.475	-0.450	-0.425	-0.400	-0.375	-0.350	-0.300	-0.250	-0.200	-0.150	-0.100
	u (cm/s)	7.257	7.683	7.409	9.378	13.353	14.403	15.954	16.792	17.479	18.475	19.364
	n/B	-0.050	0.000	0.050	0.100	0.150	0.200	0.250	0.300	0.325	0.350	0.375
	u (cm/s)	20.243	20.914	21.522	21.819	22.370	22.936	23.490	23.052	22.725	21.868	21.127
	n/B	0.400	0.425	0.450								
	u (cm/s)	20.054	18.930	18.375								

8-1	n/B	-0.475	-0.443	-0.418	-0.393	-0.368	-0.318	-0.268	-0.218	-0.168	-0.118	-0.068
	u (cm/s)	11.340	12.233	13.072	13.555	13.862	15.027	16.169	17.057	17.974	18.482	19.343
	n/B	-0.018	0.033	0.083	0.133	0.183	0.233	0.283	0.308	0.333	0.358	0.383
	u (cm/s)	19.839	20.336	21.082	21.350	21.856	22.243	22.523	22.514	22.414	21.976	21.108
	n/B	0.408	0.433									
	u (cm/s)	20.719	19.586									
1-2	n/B	-0.4375	-0.4125	-0.3875	-0.3625	-0.3375	-0.3125	-0.2875	-0.2375	-0.1875	-0.1375	-0.0875
	u (cm/s)	6.317	6.318	6.320	6.308	6.853	9.436	10.895	11.809	13.780	15.632	17.286
	n/B	-0.0375	0.0125	0.0625	0.1125	0.1625	0.2125	0.2625	0.3125	0.3625	0.3875	0.4125
	u (cm/s)	18.665	20.513	22.148	23.442	24.527	24.932	25.474	25.742	26.331	27.586	28.000
	n/B	0.4375	0.475									
	u (cm/s)	28.685	28.681									
2-2	n/B	-0.4075	-0.3825	-0.3575	-0.3325	-0.3075	-0.2825	-0.2325	-0.1825	-0.1325	-0.0825	-0.0325
	u (cm/s)	10.046	10.478	10.763	11.370	12.367	13.838	14.566	15.485	16.678	17.488	18.298
	n/B	0.0175	0.0675	0.1175	0.1675	0.2175	0.2675	0.3175	0.3675	0.3925	0.4175	0.443
	u (cm/s)	19.238	20.159	20.911	22.043	22.474	23.553289	24.971439	26.258279	26.834069	27.195689	26.807
	n/B	0.475										
	u (cm/s)	24.753182										
3-2	n/B	-0.425	-0.4	-0.375	-0.35	-0.325	-0.3	-0.275	-0.225	-0.175	-0.125	-0.075
	u (cm/s)	10.808	11.256	11.933	12.283	12.903	13.289	13.911	14.988	15.755	16.353	16.896
	n/B	-0.025	0.025	0.075	0.125	0.175	0.225	0.275	0.325	0.375	0.4	0.425
	u (cm/s)	17.753	18.763	19.607	20.573	21.648	22.392	23.569	25.088	25.747	26.319	26.028
	n/B	0.45	0.475									
	u (cm/s)	25.639	25.182									

4-2	n/B	-0.44	-0.415	-0.39	-0.365	-0.34	-0.315	-0.29	-0.24	-0.19	-0.14	-0.09
	u (cm/s)	10.105	10.149	10.478	11.313	12.254	13.068	14.149	15.138	15.789	16.586	17.531
	n/B	-0.04	0.01	0.06	0.11	0.16	0.21	0.26	0.31	0.36	0.385	0.41
	u (cm/s)	18.050	18.939	20.004	20.753	21.993	22.586	23.689	24.614	26.110	26.049	25.518
	n/B	0.435	0.475									
	u (cm/s)	24.648	20.447									
5-2	n/B	-0.4	-0.375	-0.35	-0.325	-0.3	-0.275	-0.225	-0.175	-0.125	-0.075	-0.025
	u (cm/s)	13.232	13.701	14.175	14.845	15.567	16.183	17.798	19.551	20.868	21.411	21.877
	n/B	0.025	0.075	0.125	0.175	0.225	0.275	0.325	0.375	0.4	0.425	0.45
	u (cm/s)	22.226	22.389	22.673	22.742	21.886	20.709	19.318	17.233	16.541	15.977	15.792
	n/B	0.475										
	u (cm/s)	15.221										
6-2	n/B	-0.405	-0.375	-0.35	-0.325	-0.3	-0.275	-0.225	-0.175	-0.125	-0.075	-0.025
	u (cm/s)	17.039	18.348	19.286	20.444	21.668	22.350	22.726	22.349	21.824	21.726	21.247
	n/B	0.025	0.075	0.125	0.175	0.225	0.275	0.325	0.375	0.4	0.425	0.45
	u (cm/s)	20.785	20.480	20.046	19.292	18.669	17.475	16.167	14.855	13.997	12.989	11.371
	n/B	0.475										
	u (cm/s)	9.661										
7-2	n/B	-0.415	-0.4	-0.375	-0.35	-0.325	-0.3	-0.275	-0.225	-0.175	-0.125	-0.075
	u (cm/s)	21.096	21.283	22.086	22.600	23.315	23.212	23.132	22.606	21.857	21.367	20.576
	n/B	-0.025	0.025	0.075	0.125	0.175	0.225	0.275	0.325	0.375	0.4	0.425
	u (cm/s)	20.364	19.563	19.071	18.505	17.975	17.037	16.483	15.356	14.149	13.825	13.072
	n/B	0.45	0.475									
	u (cm/s)	11.990	11.723									

8-2	**n/B**	-0.4375	-0.4125	-0.3875	-0.3625	-0.3375	-0.3125	-0.2875	-0.2375	-0.1875	-0.1375	-0.0875
	u (cm/s)	22.406	23.508	24.043	23.485	23.052	22.586	22.356	21.543	20.495	20.318	19.980
	n/B	-0.0375	0.0125	0.0625	0.1125	0.1625	0.2125	0.2625	0.3125	0.3625	0.3875	0.4125
	u (cm/s)	19.637	19.269	18.852	18.265	17.575	16.955	16.456	15.325	14.407	13.725	13.167
	n/B	0.4375	0.475									
	u (cm/s)	12.647	12.199									
1-3	**n/B**	-0.475	-0.450	-0.425	-0.400	-0.375	-0.325	-0.275	-0.225	-0.175	-0.125	-0.075
	u (cm/s)	27.172	27.439	27.366	26.285	25.118	23.688	22.805	22.041	21.465	20.491	19.903
	n/B	-0.025	0.025	0.075	0.125	0.175	0.225	0.275	0.300	0.325	0.350	0.375
	u (cm/s)	18.710	18.332	17.440	16.639	15.745	15.162	14.294	13.822	13.039	12.468	11.921
	n/B	0.400	0.425									
	u (cm/s)	11.068	10.728									
2-3	**n/B**	-0.475	-0.450	-0.425	-0.400	-0.375	-0.325	-0.275	-0.225	-0.175	-0.125	-0.075
	u (cm/s)	27.647	28.326	28.769	28.458	27.299	25.712	24.219	22.639	22.227	21.101	20.365
	n/B	-0.025	0.025	0.075	0.125	0.175	0.225	0.275	0.300	0.325	0.350	0.375
	u (cm/s)	19.166	18.122	16.884	15.890	14.892	14.240	13.229	12.481	12.578	12.124	11.537
	n/B	0.400	0.425									
	u (cm/s)	11.205	10.596									
3-3	**n/B**	-0.475	-0.438	-0.413	-0.388	-0.363	-0.313	-0.263	-0.213	-0.163	-0.113	-0.063
	u (cm/s)	21.337	24.570	25.853	26.649	26.730	26.134	24.173	22.512	21.703	21.092	20.020
	n/B	-0.013	0.038	0.088	0.138	0.188	0.238	0.288	0.313	0.338	0.363	0.388
	u (cm/s)	18.931	17.885	17.035	16.223	15.049	14.283	13.279	12.967	12.615	12.127	11.674
	n/B	0.413	0.438	0.450								
	u (cm/s)	11.162	10.453	9.874								

4-3	n/B	-0.475	-0.443	-0.418	-0.393	-0.368	-0.318	-0.268	-0.218	-0.168	-0.118	-0.068
	u (cm/s)	18.925	21.320	22.521	23.713	24.342	24.457	23.948	22.763	21.568	21.108	20.265
	n/B	-0.018	0.033	0.083	0.133	0.183	0.233	0.283	0.308	0.333	0.358	0.383
	u (cm/s)	19.543	18.737	17.667	17.019	16.196	15.262	14.813	14.198	13.921	13.732	13.427
	n/B	0.408	0.420									
	u (cm/s)	12.811	12.000									
5-3	n/B	-0.475	-0.438	-0.413	-0.388	-0.363	-0.313	-0.263	-0.213	-0.163	-0.113	-0.063
	u (cm/s)	10.263	10.012	12.434	14.760	15.791	17.661	18.790	19.691	20.092	20.918	20.677
	n/B	-0.013	0.038	0.088	0.138	0.188	0.238	0.288	0.313	0.338	0.363	0.388
	u (cm/s)	19.962	19.006	17.470	16.306	15.597	14.494	13.094	12.265	11.275	10.817	10.701
	n/B	0.413	0.438									
	u (cm/s)	10.040	9.849									
6-3	n/B	-0.475	-0.450	-0.425	-0.400	-0.375	-0.350	-0.300	-0.250	-0.200	-0.150	-0.100
	u (cm/s)	11.377	12.439	13.289	14.835	15.380	16.092	17.997	18.812	19.301	19.881	20.494
	n/B	-0.050	0.000	0.050	0.100	0.150	0.200	0.250	0.275	0.300	0.325	0.350
	u (cm/s)	20.986	20.972	21.524	21.654	21.954	22.015	21.289	20.562	19.853	19.095	17.784
	n/B	0.375	0.400	0.425								
	u (cm/s)	17.168	16.589	15.849								
7-3	n/B	-0.475	-0.445	-0.420	-0.395	-0.370	-0.320	-0.270	-0.220	-0.170	-0.120	-0.070
	u (cm/s)	7.758	8.494	9.671	10.579	11.741	12.742	14.452	15.930	16.884	17.774	18.585
	n/B	-0.020	0.030	0.080	0.130	0.180	0.230	0.280	0.330	0.380	0.405	0.430
	u (cm/s)	19.472	19.916	20.633	21.064	21.803	22.474	23.176	23.453	23.677	23.969	23.947
	n/B	0.455	0.480									
	u (cm/s)	23.849	23.164									

8-3	**n/B**	-0.475	-0.458	-0.433	-0.408	-0.383	-0.358	-0.308	-0.258	-0.208	-0.158	-0.108
	u (cm/s)	8.923	9.592	10.662	11.488	12.544	13.454	15.009	16.353	17.220	18.029	18.767
	n/B	-0.058	-0.008	0.043	0.093	0.143	0.193	0.243	0.268	0.293	0.318	0.343
	u (cm/s)	19.573	19.976	20.628	21.020	21.692	22.302	22.940	23.192	23.395	23.661	23.641
	n/B	0.368	0.393									
	u (cm/s)	23.552	22.929									
1-4	**n/B**	-0.475	-0.440	-0.415	-0.390	-0.365	-0.315	-0.265	-0.215	-0.165	-0.115	-0.065
	u (cm/s)	26.084	26.783	26.213	25.587	24.925	23.777	23.244	22.240	22.276	21.392	20.532
	n/B	-0.015	0.035	0.085	0.135	0.185	0.235	0.285	0.310	0.335	0.360	0.385
	u (cm/s)	19.793	18.975	18.167	17.332	16.566	15.426	14.398	13.422	12.862	12.346	11.873

Flow Depth h (cm)

Section

1-1	**n/B**	-0.475	-0.400	-0.325	-0.250	-0.175	-0.100	-0.025	0.050	0.125	0.200	0.275	0.350	0.425	0.488
	h (cm)	3.038	3.036	3.038	3.035	3.044	3.039	3.050	3.046	3.046	3.056	3.061	3.074	3.079	3.094
2-1	**n/B**	-0.475	-0.400	-0.325	-0.250	-0.175	-0.100	-0.025	0.050	0.125	0.200	0.275	0.350	0.425	0.488
	h (cm)	2.987	2.994	2.999	3.003	3.024	3.038	3.050	3.064	3.074	3.086	3.095	3.101	3.116	3.125
3-1	**n/B**	-0.475	-0.413	-0.338	-0.263	-0.188	-0.113	-0.038	0.038	0.113	0.188	0.263	0.338	0.413	0.488
	h (cm)	2.930	2.948	2.971	2.996	3.014	3.035	3.050	3.068	3.086	3.098	3.110	3.128	3.138	3.148
4-1	**n/B**	-0.475	-0.400	-0.325	-0.250	-0.175	-0.100	-0.025	0.050	0.125	0.200	0.275	0.350	0.425	0.500
	h (cm)	2.944	2.967	2.974	2.993	3.011	3.031	3.050	3.064	3.076	3.083	3.130	3.123	3.139	3.145
5-1	**n/B**	-0.475	-0.400	-0.325	-0.250	-0.175	-0.100	-0.025	0.050	0.125	0.200	0.275	0.350	0.425	0.488
	h (cm)	2.848	2.871	2.914	2.947	2.972	3.008	3.050	3.075	3.092	3.109	3.142	3.172	3.188	3.178
6-1	**n/B**	-0.475	-0.405	-0.330	-0.255	-0.180	-0.105	-0.030	0.045	0.120	0.195	0.270	0.345	0.420	0.490
	h (cm)	2.959	2.969	2.978	2.993	3.012	3.027	3.050	3.071	3.088	3.088	3.109	3.131	3.150	3.163
7-1	**n/B**	-0.475	-0.420	-0.345	-0.270	-0.195	-0.120	-0.045	0.030	0.105	0.180	0.255	0.330	0.405	
	h (cm)	2.970	2.974	2.984	2.992	3.011	3.042	3.050	3.058	3.070	3.086	3.103	3.119	3.136	0.000
8-1	**n/B**	-0.475	-0.405	-0.330	-0.255	-0.180	-0.105	-0.030	0.045	0.120	0.195	0.270	0.345	0.420	0.470
	h (cm)	3.022	3.030	3.042	3.042	3.045	3.050	3.050	3.048	3.052	3.057	3.069	3.077	3.085	3.091
1-2	**n/B**	-0.463	-0.438	-0.375	-0.300	-0.225	-0.150	-0.075	0.000	0.075	0.150	0.225	0.300	0.375	0.450
	h (cm)	3.058	3.060	3.061	3.053	3.064	3.068	3.060	3.050	3.055	3.050	3.048	3.067	3.065	3.048
2-2	**n/B**	-0.488	-0.420	-0.345	-0.270	-0.195	-0.120	-0.045	0.030	0.105	0.180	0.255	0.330	0.405	0.475
	h (cm)	3.131	3.116	3.104	3.102	3.090	3.077	3.057	3.050	3.057	3.033	3.017	3.011	3.002	2.976

3-2	n/B	-0.480	-0.405	-0.330	-0.255	-0.180	-0.105	-0.030	0.045	0.120	0.195	0.270	0.345	0.420	0.475
	h (cm)	3.111	3.107	3.124	3.111	3.098	3.081	3.076	3.050	3.030	3.011	2.996	2.981	2.965	2.953
4-2	n/B	-0.480	-0.405	-0.330	-0.255	-0.180	-0.105	-0.030	0.045	0.120	0.195	0.270	0.345	0.420	0.475
	h (cm)	3.111	3.107	3.124	3.111	3.098	3.081	3.076	3.050	3.030	3.011	2.996	2.981	2.965	2.953
5-2	n/B	-0.488	-0.413	-0.338	-0.263	-0.188	-0.113	-0.038	0.038	0.113	0.188	0.263	0.338	0.413	0.475
	h (cm)	3.188	3.206	3.186	3.152	3.122	3.103	3.077	3.050	2.997	2.953	2.927	2.910	2.914	2.914
6-2	n/B	-0.460	-0.425	-0.350	-0.275	-0.200	-0.125	-0.050	0.025	0.100	0.175	0.250	0.325	0.400	0.475
	h (cm)	3.127	3.113	3.112	3.102	3.090	3.078	3.056	3.050	3.045	3.024	3.006	2.980	2.964	2.927
7-2	n/B	-0.475	-0.415	-0.340	-0.265	-0.190	-0.115	-0.040	0.035	0.110	0.185	0.260	0.335	0.410	0.475
	h (cm)	3.149	3.137	3.127	3.114	3.094	3.082	3.066	3.050	3.040	3.018	3.000	2.983	2.971	2.955
8-2	n/B	-0.485	-0.423	-0.348	-0.273	-0.198	-0.123	-0.048	0.028	0.103	0.178	0.253	0.328	0.403	0.475
	h (cm)	3.072	3.069	3.065	3.061	3.056	3.055	3.050	3.050	3.041	3.035	3.026	3.029	3.025	2.965
1-3	n/B	-0.475	-0.420	-0.345	-0.270	-0.195	-0.120	-0.045	0.030	0.105	0.180	0.255	0.330	0.405	0.480
	h (cm)	3.026	3.028	3.034	3.039	3.043	3.047	3.050	3.053	3.056	3.058	3.055	3.060	3.063	3.065
2-3	n/B	-0.475	-0.413	-0.338	-0.263	-0.188	-0.113	-0.038	0.038	0.113	0.188	0.263	0.338	0.413	0.488
	h (cm)	2.959	2.963	2.981	3.003	3.019	3.037	3.050	3.062	3.082	3.096	3.114	3.120	3.128	3.140
3-3	n/B	-0.475	-0.400	-0.325	-0.250	-0.175	-0.100	-0.025	0.050	0.125	0.200	0.275	0.350	0.425	0.488
	h (cm)	2.946	2.957	2.975	2.999	3.022	3.035	3.050	3.064	3.077	3.087	3.100	3.117	3.126	3.127
4-3	n/B	-0.475	-0.400	-0.325	-0.250	-0.175	-0.100	-0.025	0.050	0.125	0.200	0.275	0.350	0.425	0.488
	h (cm)	2.953	2.955	2.961	2.990	3.015	3.031	3.050	3.051	3.059	3.082	3.101	3.119	3.137	3.153
5-3	n/B	-0.475	-0.400	-0.325	-0.250	-0.175	-0.100	-0.025	0.050	0.125	0.200	0.275	0.350	0.425	0.488
	h (cm)	2.917	2.934	2.955	2.991	3.007	3.034	3.050	3.066	3.099	3.156	3.169	3.185	3.199	3.201

6-3	**n/B**	-0.475	-0.400	-0.325	-0.250	-0.175	-0.100	-0.025	0.050	0.125	0.200	0.275	0.350	0.425	0.488
	h (cm)	2.912	2.949	2.962	2.987	3.004	3.025	3.050	3.070	3.092	3.116	3.123	3.160	3.159	3.161
7-3	**n/B**	-0.475	-0.400	-0.325	-0.250	-0.175	-0.100	-0.025	0.050	0.125	0.200	0.275	0.350	0.425	0.488
	h (cm)	2.958	2.962	2.975	2.994	3.008	3.029	3.050	3.068	3.091	3.105	3.125	3.145	3.165	3.165
8-3	**n/B**	-0.475	-0.400	-0.325	-0.250	-0.175	-0.100	-0.025	0.050	0.125	0.200	0.275	0.350	0.425	0.488
	h (cm)	3.018	3.017	3.019	3.021	3.044	3.041	3.050	3.064	3.064	3.067	3.078	3.077	3.075	3.075

90°-channel: Vertically averaged deviation angle

Section	$\overline{\omega}_c$	Section	$\overline{\omega}_c$	Section	$\overline{\omega}_c$
1-1	0.025	1-2	0.073	1-3	-.076
2-1	0.023	2-2	0.024	2-3	-.082
3-1	0.057	3-2	-0.012	3-3	0.045
4-1	0.086	4-2	-.031	4-3	0.110
5-1	0.049	5-2	-.069	5-3	0.058
6-1	0.105	6-2	-.104	6-3	0.105
7-1	0.083	7-2	-.084	7-3	0.055
8-1	0.091	8-2	-.089	8-3	0.092

Appendix B

70°-channel: Raw data

Longitudinal Velocity Measurements at hm/2

Section												
1-1	n/B	-0.475	-0.443	-0.418	-0.393	-0.343	-0.293	-0.243	-0.193	-0.143	-0.093	-0.043
	u (cm/s)	18.913	19.403	20.033	20.140	20.059	19.369	18.961	18.796	18.768	18.462	18.251
	n/B	0.008	0.058	0.108	0.158	0.208	0.258	0.308	0.333	0.358	0.383	0.408
	u (cm/s)	18.116	17.151	16.496	15.137	13.581	11.496	9.748	7.065	6.300	5.300	4.344
	n/B	0.433	0.458									
	u (cm/s)	3.747	3.673									
2-1	n/B	-0.475	-0.440	-0.415	-0.390	-0.340	-0.290	-0.240	-0.190	-0.140	-0.090	-0.040
	u (cm/s)	21.845	22.350	22.646	22.172	21.689	20.952	19.875	18.733	17.617	16.522	15.293
	n/B	0.010	0.060	0.110	0.160	0.210	0.260	0.310	0.335	0.360	0.385	0.410
	u (cm/s)	14.248	13.169	12.054	10.667	9.673	8.050	6.804	5.432	4.567	3.691	3.161
	n/B	0.435										
	u (cm/s)	3.115										
3-1	n/B	-0.475	-0.450	-0.425	-0.400	-0.375	-0.325	-0.275	-0.225	-0.175	-0.125	-0.075
	u (cm/s)	20.959	22.409	23.249	23.186	22.967	21.976	20.433	19.739	19.154	18.286	17.068
	n/B	-0.025	0.025	0.075	0.125	0.175	0.225	0.250	0.275	0.300	0.325	0.350
	u (cm/s)	15.948	14.544	13.367	11.871	10.154	8.771	7.089	5.075	4.141	1.722	1.807
	n/B	0.375	0.405									
	u (cm/s)	1.529	1.483									

4-1	n/B	-0.475	-0.450	-0.425	-0.400	-0.375	-0.325	-0.275	-0.225	-0.175	-0.125	-0.075
	u (cm/s)	18.524	21.378	22.796	23.496	23.279	21.999	20.712	19.471	18.748	17.827	16.536
	n/B	-0.025	0.025	0.075	0.125	0.175	0.225	0.250	0.275	0.300	0.325	0.350
	u (cm/s)	15.224	13.861	12.908	11.763	9.478	8.238	6.643	5.387	4.741	4.128	1.757
	n/B	0.375	0.400									
	u (cm/s)	2.887	-0.906									
5-1	n/B	-0.475	-0.443	-0.418	-0.393	-0.368	-0.318	-0.268	-0.218	-0.168	-0.118	-0.068
	u (cm/s)	12.285	14.230	17.328	18.973	20.617	22.221	21.940	21.068	19.707	19.058	17.860
	n/B	-0.018	0.033	0.083	0.133	0.183	0.233	0.283	0.308	0.333	0.358	0.383
	u (cm/s)	17.313	16.508	15.318	13.165	10.927	9.269	7.538	6.120	5.509	4.743	3.483
	n/B	0.408										
	u (cm/s)	3.465										
6-1	n/B	-0.475	-0.450	-0.425	-0.400	-0.375	-0.350	-0.300	-0.250	-0.200	-0.150	-0.100
	u (cm/s)	8.930	9.684	10.825	11.586	12.397	13.762	16.032	17.328	18.996	19.826	20.310
	n/B	-0.050	0.000	0.050	0.100	0.150	0.200	0.250	0.275	0.300	0.325	0.350
	u (cm/s)	19.562	19.080	18.435	17.762	15.909	14.360	12.707	11.114	10.259	9.013	8.119
	n/B	0.375	0.400	0.425	0.450							
	u (cm/s)	7.043	4.206	4.206	4.206							
7-1	n/B	-0.475	-0.450	-0.425	-0.400	-0.375	-0.350	-0.300	-0.250	-0.200	-0.150	-0.100
	u (cm/s)	6.519	7.435	8.263	9.264	10.177	11.944	13.093	14.107	15.460	16.070	17.107
	n/B	-0.050	0.000	0.050	0.100	0.150	0.200	0.250	0.300	0.325	0.350	0.375
	u (cm/s)	17.702	18.177	18.841	19.300	19.760	19.177	17.813	15.889	14.819	13.983	13.335
	n/B	0.400	0.425	0.450								
	u (cm/s)	12.438	3.730	3.730								

8-1	**n/B**	-0.475	-0.443	-0.418	-0.393	-0.368	-0.318	-0.268	-0.218	-0.168	-0.118	-0.068
	u (cm/s)	4.993	5.015	5.784	4.976	8.373	10.154	11.513	12.659	13.834	14.765	15.631
	n/B	-0.018	0.033	0.083	0.133	0.183	0.233	0.283	0.308	0.333	0.358	0.383
	u (cm/s)	16.541	17.259	18.157	19.001	19.789	20.332	20.770	19.430	18.929	18.145	17.392
	n/B	0.408	0.433									
	u (cm/s)	17.033	2.890									
1-2	**n/B**	-0.438	-0.413	-0.388	-0.363	-0.338	-0.313	-0.288	-0.238	-0.188	-0.138	-0.088
	u (cm/s)	1.052	3.139	3.251	3.310	4.618	6.042	9.248	10.790	12.742	14.254	15.504
	n/B	-0.038	0.013	0.063	0.113	0.163	0.213	0.263	0.313	0.363	0.388	0.413
	u (cm/s)	16.412	17.108	17.982	18.716	18.911	19.548	19.717	19.695	18.302	17.375	16.602
	n/B	0.438	0.475									
	u (cm/s)	16.654	16.610									
2-2	**n/B**	-0.408	-0.383	-0.358	-0.333	-0.308	-0.283	-0.233	-0.183	-0.133	-0.083	-0.033
	u (cm/s)	3.944	3.990	4.520	5.396	6.261	7.633	8.879	10.502	11.496	12.883	13.998
	n/B	0.018	0.068	0.118	0.168	0.218	0.268	0.318	0.368	0.393	0.418	0.443
	u (cm/s)	15.077	16.122	17.351	18.446	19.562	20.704	21.781	22.518	23.001	23.475	23.179
	n/B	0.475										
	u (cm/s)	22.674										
3-2	**n/B**	-0.425	-0.400	-0.375	-0.350	-0.325	-0.300	-0.275	-0.225	-0.175	-0.125	-0.075
	u (cm/s)	-0.322	2.419	2.956	3.517	4.535	5.640	7.046	8.869	10.022	11.812	12.788
	n/B	-0.025	0.025	0.075	0.125	0.175	0.225	0.275	0.325	0.375	0.400	0.425
	u (cm/s)	14.259	15.467	16.772	18.188	19.445	20.829	22.454	23.824	25.187	25.675	26.097
	n/B	0.450	0.475	-0.450								
	u (cm/s)	25.913	25.483	-0.322								

4-2	n/B	-0.440	-0.415	-0.390	-0.365	-0.340	-0.315	-0.290	-0.240	-0.190	-0.140	-0.090
	u (cm/s)	-1.050	5.695	5.731	6.418	7.053	8.005	9.095	10.166	10.979	11.965	12.796
	n/B	-0.040	0.010	0.060	0.110	0.160	0.210	0.260	0.310	0.360	0.385	0.410
	u (cm/s)	14.082	15.222	16.618	17.568	18.138	19.764	21.244	22.008	22.815	23.364	23.456
	n/B	0.435	0.475									
	u (cm/s)	23.265	21.697									
5-2	n/B	-0.400	-0.375	-0.350	-0.325	-0.300	-0.275	-0.225	-0.175	-0.125	-0.075	-0.025
	u (cm/s)	6.316	6.665	7.168	8.302	9.430	10.916	11.687	12.423	13.934	14.676	15.762
	n/B	0.025	0.075	0.125	0.175	0.225	0.275	0.325	0.375	0.400	0.425	0.450
	u (cm/s)	15.762	17.682	18.559	19.236	20.385	20.984	21.210	20.226	19.543	17.795	15.826
	n/B	0.475										
	u (cm/s)	12.262										
6-2	n/B	-0.405	-0.375	-0.350	-0.325	-0.300	-0.275	-0.225	-0.175	-0.125	-0.075	-0.025
	u (cm/s)	10.199	10.596	11.141	11.796	12.570	14.246	15.394	15.288	15.862	16.500	17.056
	n/B	0.025	0.075	0.125	0.175	0.225	0.275	0.325	0.375	0.400	0.425	0.450
	u (cm/s)	17.473	17.202	17.622	17.580	16.876	15.497	14.159	12.336	11.419	10.172	8.625
	n/B	0.475										
	u (cm/s)	6.902										
7-2	n/B	-0.415	-0.400	-0.375	-0.350	-0.325	-0.300	-0.275	-0.225	-0.175	-0.125	-0.075
	u (cm/s)	2.430	14.154	14.187	15.307	15.947	16.715	17.868	17.887	19.261	18.681	18.504
	n/B	-0.025	0.025	0.075	0.125	0.175	0.225	0.275	0.325	0.375	0.400	0.425
	u (cm/s)	19.360	18.486	17.790	16.882	15.632	14.120	12.168	10.626	7.420	5.996	4.688
	n/B	0.450	0.475									
	u (cm/s)	4.629	4.517									

8-2	**n/B**	-0.438	-0.413	-0.388	-0.363	-0.338	-0.313	-0.288	-0.238	-0.188	-0.138	-0.088
	u (cm/s)	0.850	19.652	20.082	20.604	21.152	21.371	21.062	20.458	19.851	19.112	18.509
	n/B	-0.038	0.013	0.063	0.113	0.163	0.213	0.263	0.313	0.363	0.388	0.413
	u (cm/s)	17.651	17.084	17.072	16.038	14.399	12.536	10.332	8.025	4.851	3.700	3.219
	n/B	0.438	0.475									
	u (cm/s)	2.962	2.929									
1-3	**n/B**	-0.475	-0.450	-0.425	-0.400	-0.375	-0.325	-0.275	-0.225	-0.175	-0.125	-0.075
	u (cm/s)	20.663	20.744	21.169	21.600	21.874	21.082	20.162	19.000	18.126	18.627	17.607
	n/B	-0.025	0.025	0.075	0.125	0.175	0.225	0.275	0.300	0.325	0.350	0.375
	u (cm/s)	16.887	15.686	14.472	13.069	11.365	9.687	8.031	6.019	4.902	3.874	2.471
	n/B	0.400	0.425									
	u (cm/s)	1.661	1.456									
2-3	**n/B**	-0.475	-0.450	-0.425	-0.400	-0.375	-0.325	-0.275	-0.225	-0.175	-0.125	-0.075
	u (cm/s)	23.663	24.050	24.216	23.837	23.397	21.688	20.937	19.475	18.229	17.098	15.824
	n/B	-0.025	0.025	0.075	0.125	0.175	0.225	0.275	0.300	0.325	0.350	0.375
	u (cm/s)	16.228	15.020	13.549	12.573	10.783	9.630	7.807	6.401	5.296	4.278	3.717
	n/B	0.400	0.425	0.438								
	u (cm/s)	3.180	0.439	0.439								
3-3	**n/B**	-0.475	-0.438	-0.413	-0.388	-0.363	-0.313	-0.263	-0.213	-0.163	-0.113	-0.063
	u (cm/s)	25.068	26.754	27.016	26.950	26.428	25.047	23.136	21.370	19.571	18.473	16.886
	n/B	-0.013	0.038	0.088	0.138	0.188	0.238	0.288	0.313	0.338	0.363	0.388
	u (cm/s)	15.835	14.529	13.713	12.141	10.978	9.399	7.981	6.310	5.887	4.718	4.347
	n/B	0.413	0.438	0.450								
	u (cm/s)	4.101	1.297	1.297								

4-3	n/B	-0.475	-0.443	-0.418	-0.393	-0.368	-0.318	-0.268	-0.218	-0.168	-0.118	-0.068
	u (cm/s)	20.519	22.625	24.336	23.698	24.004	23.338	22.111	21.058	19.148	17.460	16.106
	n/B	-0.018	0.033	0.083	0.133	0.183	0.233	0.283	0.308	0.333	0.358	0.383
	u (cm/s)	14.894	13.902	12.784	11.477	9.411	7.648	6.247	4.555	4.222	3.860	3.056
	n/B	0.408	0.420									
	u (cm/s)	3.222	0.418									
5-3	n/B	-0.475	-0.438	-0.413	-0.388	-0.363	-0.313	-0.263	-0.213	-0.163	-0.113	-0.063
	u (cm/s)	14.495	15.365	18.026	19.988	21.141	22.955	22.422	22.421	21.392	19.688	18.404
	n/B	-0.013	0.038	0.088	0.138	0.188	0.238	0.288	0.313	0.338	0.363	0.388
	u (cm/s)	18.059	16.804	15.691	14.709	12.792	10.264	8.664	7.231	6.143	5.552	4.948
	n/B	0.413	0.438									
	u (cm/s)	4.386	1.085									
6-3	n/B	-0.475	-0.450	-0.425	-0.400	-0.375	-0.350	-0.300	-0.250	-0.200	-0.150	-0.100
	u (cm/s)	11.208	12.347	13.126	13.875	14.710	16.277	17.861	18.641	19.099	18.872	18.322
	n/B	-0.050	0.000	0.050	0.100	0.150	0.200	0.250	0.275	0.300	0.325	0.350
	u (cm/s)	18.021	18.504	18.093	17.022	14.941	13.320	11.302	9.751	8.889	8.323	7.875
	n/B	0.375	0.400	0.425								
	u (cm/s)	7.279	3.121	3.121								
7-3	n/B	-0.475	-0.445	-0.420	-0.395	-0.370	-0.320	-0.270	-0.220	-0.170	-0.120	-0.070
	u (cm/s)	9.930	10.969	11.967	12.804	13.430	14.522	15.420	16.608	17.180	17.993	18.312
	n/B	-0.020	0.030	0.080	0.130	0.180	0.230	0.280	0.330	0.380	0.405	0.430
	u (cm/s)	18.628	18.712	19.268	19.413	18.679	17.197	15.218	13.452	12.284	11.596	11.090
	n/B	0.455	0.480	0.500								
	u (cm/s)	10.304	3.419	3.419								

8-3	**n/B**	-0.475	-0.458	-0.433	-0.408	-0.383	-0.358	-0.308	-0.258	-0.208	-0.158	-0.108
	u (cm/s)	7.323	8.159	9.039	9.759	10.440	11.368	12.467	13.193	14.559	15.288	15.954
	n/B	-0.058	-0.008	0.043	0.093	0.143	0.193	0.243	0.268	0.293	0.318	0.343
	u (cm/s)	16.537	17.035	17.483	18.170	19.183	18.672	22.117	22.434	22.209	21.647	21.110
	n/B	0.368	0.393	0.418								
	u (cm/s)	20.669	1.363	1.363								
1-4	**n/B**	-0.475	-0.440	-0.415	-0.390	-0.365	-0.315	-0.265	-0.215	-0.165	-0.115	-0.065
	u (cm/s)	16.887	17.327	17.643	17.390	17.849	18.458	18.769	18.243	17.557	16.842	16.121
	n/B	-0.015	0.035	0.085	0.135	0.185	0.235	0.285	0.310	0.335	0.360	0.385
	u (cm/s)	15.141	14.394	13.611	12.838	12.267	11.407	10.780	9.180	8.598	7.828	7.066

Flow Depth h (cm)

Section															
1-1	**n/B**	-0.475	-0.400	-0.325	-0.250	-0.175	-0.100	-0.025	0.050	0.125	0.200	0.275	0.350	0.425	0.488
	h (cm)	3.062	3.065	3.068	3.071	3.074	3.077	3.079	3.080	3.082	3.083	3.083	3.083	3.084	3.085
2-1	**n/B**	-0.475	-0.400	-0.325	-0.250	-0.175	-0.100	-0.025	0.050	0.125	0.200	0.275	0.350	0.425	0.488
	h (cm)	3.008	3.017	3.018	3.030	3.047	3.064	3.073	3.080	3.088	3.095	3.101	3.107	3.113	3.118
3-1	**n/B**	-0.475	-0.400	-0.325	-0.250	-0.175	-0.100	-0.025	0.050	0.125	0.200	0.275	0.350	0.425	0.488
	h (cm)	2.939	2.961	2.985	3.007	3.027	3.047	3.061	3.080	3.090	3.096	3.112	3.123	3.134	3.134
4-1	**n/B**	-0.475	-0.400	-0.325	-0.250	-0.175	-0.100	-0.025	0.050	0.125	0.200	0.275	0.350	0.425	0.500
	h (cm)	2.900	2.929	2.961	2.991	3.019	3.043	3.062	3.080	3.093	3.108	3.113	3.123	3.129	3.155
5-1	**n/B**	-0.475	-0.400	-0.325	-0.250	-0.175	-0.100	-0.025	0.050	0.125	0.200	0.275	0.350	0.425	0.488
	h (cm)	2.940	2.952	2.973	2.986	3.019	3.050	3.064	3.080	3.083	3.103	3.117	3.131	3.143	3.151
6-1	**n/B**	-0.475	-0.400	-0.325	-0.250	-0.175	-0.100	-0.025	0.050	0.125	0.200	0.275	0.350	0.425	0.488
	h (cm)	2.946	2.977	2.991	3.004	3.021	3.038	3.059	3.080	3.090	3.108	3.119	3.130	3.159	3.144
7-1	**n/B**	-0.475	-0.400	-0.325	-0.250	-0.175	-0.100	-0.025	0.050	0.125	0.200	0.275	0.350	0.425	0.488
	h (cm)	3.008	3.023	3.033	3.040	3.048	3.058	3.069	3.080	3.087	3.098	3.106	3.112	3.141	3.156
8-1	**n/B**	-0.475	-0.408	-0.333	-0.258	-0.183	-0.108	-0.033	0.043	0.118	0.193	0.268	0.343	0.418	0.493
	h (cm)	3.052	3.060	3.064	3.066	3.071	3.075	3.080	3.088	3.095	3.101	3.105	3.110	3.113	3.116
1-2	**n/B**	-0.488	-0.425	-0.350	-0.275	-0.200	-0.125	-0.050	0.025	0.100	0.175	0.250	0.325	0.400	0.475
	h (cm)	3.094	3.091	3.092	3.089	3.086	3.083	3.080	3.078	3.075	3.072	3.069	3.067	3.060	3.065
2-2	**n/B**	-0.488	-0.425	-0.350	-0.275	-0.200	-0.125	-0.050	0.025	0.100	0.175	0.250	0.325	0.400	0.475
	h (cm)	3.100	3.102	3.100	3.098	3.092	3.088	3.080	3.073	3.068	3.063	3.056	3.045	3.049	3.049

3-2	n/B	-0.488	-0.425	-0.350	-0.275	-0.200	-0.125	-0.050	0.025	0.100	0.175	0.250	0.325	0.400	0.475
	h (cm)	3.129	3.129	3.119	3.109	3.109	3.100	3.080	3.061	3.055	3.042	3.027	2.996	2.955	2.906
4-2	n/B	-0.483	-0.425	-0.350	-0.275	-0.200	-0.125	-0.050	0.025	0.100	0.175	0.250	0.325	0.400	0.475
	h (cm)	3.176	3.176	3.127	3.107	3.096	3.086	3.080	3.071	3.062	3.048	3.001	2.978	2.965	2.955
5-2	n/B	-0.488	-0.413	-0.338	-0.263	-0.188	-0.113	-0.038	0.038	0.113	0.188	0.263	0.338	0.413	0.475
	h (cm)	3.164	3.154	3.144	3.120	3.108	3.095	3.085	3.080	3.057	3.032	2.998	2.985	2.950	2.930
6-2	n/B	-0.488	-0.425	-0.350	-0.275	-0.200	-0.125	-0.050	0.025	0.100	0.175	0.250	0.325	0.400	0.475
	h (cm)	3.160	3.170	3.154	3.073	3.108	3.093	3.080	3.065	3.046	3.028	3.011	2.983	2.935	2.951
7-2	n/B	-0.488	-0.425	-0.350	-0.275	-0.200	-0.125	-0.050	0.025	0.100	0.175	0.250	0.325	0.400	0.475
	h (cm)	3.120	3.113	3.101	3.096	3.091	3.088	3.080	3.076	3.068	3.062	3.049	3.041	3.038	2.979
8-2	n/B	-0.488	-0.425	-0.350	-0.275	-0.200	-0.125	-0.050	0.025	0.100	0.175	0.250	0.325	0.400	0.475
	h (cm)	3.105	3.100	3.095	3.083	3.081	3.079	3.080	3.077	3.073	3.069	3.067	3.067	3.068	3.067
1-3	n/B	-0.475	-0.400	-0.325	-0.250	-0.175	-0.100	-0.025	0.050	0.125	0.200	0.275	0.350	0.425	0.493
	h (cm)	3.039	3.047	3.054	3.061	3.067	3.072	3.076	3.080	3.083	3.086	3.089	3.091	3.092	3.095
2-3	n/B	-0.475	-0.400	-0.325	-0.250	-0.175	-0.100	-0.025	0.050	0.125	0.200	0.275	0.350	0.425	0.488
	h (cm)	3.028	3.035	3.043	3.050	3.058	3.065	3.073	3.080	3.088	3.095	3.103	3.110	3.118	3.124
3-3	n/B	-0.475	-0.400	-0.325	-0.250	-0.175	-0.100	-0.025	0.050	0.125	0.200	0.275	0.350	0.425	0.488
	h (cm)	2.972	2.985	3.003	3.027	3.044	3.058	3.067	3.080	3.093	3.100	3.112	3.120	3.132	3.132
4-3	n/B	-0.475	-0.400	-0.325	-0.250	-0.175	-0.100	-0.025	0.050	0.125	0.200	0.275	0.350	0.425	0.488
	h (cm)	2.888	2.935	2.972	3.007	3.030	3.053	3.067	3.080	3.089	3.098	3.108	3.120	3.126	3.139
5-3	n/B	-0.475	-0.400	-0.325	-0.250	-0.175	-0.100	-0.025	0.050	0.125	0.200	0.275	0.350	0.425	0.488
	h (cm)	2.925	2.940	2.964	2.986	3.014	3.034	3.054	3.080	3.096	3.109	3.124	3.139	3.148	3.156

6-3	**n/B**	-0.475	-0.400	-0.325	-0.250	-0.175	-0.100	-0.025	0.050	0.125	0.200	0.275	0.350	0.425	0.488
	h (cm)	2.958	2.983	2.992	3.003	3.019	3.035	3.065	3.080	3.095	3.115	3.128	3.143	3.153	3.163
7-3	**n/B**	-0.475	-0.413	-0.338	-0.263	-0.188	-0.113	-0.038	0.038	0.113	0.188	0.263	0.338	0.413	0.488
	h (cm)	3.014	3.018	3.029	3.040	3.054	3.068	3.080	3.097	3.113	3.122	3.132	3.135	3.150	3.153
8-3	**n/B**	-0.475	-0.400	-0.325	-0.250	-0.175	-0.100	-0.025	0.050	0.125	0.200	0.275	0.350	0.425	0.475
	h (cm)	3.053	3.054	3.058	3.062	3.065	3.072	3.075	3.080	3.085	3.090	3.101	3.105	3.092	3.108
1-4	**n/B**	-0.475	-0.400	-0.325	-0.250	-0.175	-0.100	-0.025	0.050	0.125	0.200	0.275	0.350	0.425	0.488
	h (cm)	3.054	3.063	3.066	3.068	3.071	3.073	3.076	3.080	3.084	3.086	3.088	3.090	3.091	3.093

70°-channel: Vertically averaged deviation angle

Section	$\overline{\omega}_c$	Section	$\overline{\omega}_c$	Section	$\overline{\omega}_c$
1-1	-0.163	1-2	0.090	1-3	-0.091
2-1	-0.082	2-2	0.127	2-3	-0.132
3-1	-0.058	3-2	0.050	3-3	-0.110
4-1	-0.038	4-2	0.080	4-3	-0.080
5-1	0.003	5-2	0.019	5-3	0.039
6-1	0.098	6-2	-0.092	6-3	0.087
7-1	0.105	7-2	-0.112	7-3	0.108
8-1	0.096	8-2	-0.091	8-3	0.083

Appendix C

50°-channel: Raw data

Longitudinal Velocity Measurements at $l_m/2$

Section												
1-1	n/B	-0.475	-0.443	-0.418	-0.393	-0.343	-0.293	-0.243	-0.193	-0.143	-0.093	-0.043
	u (cm/s)	22.593	25.152	24.982	26.982	27.567	28.508	27.755	26.418	23.787	24.014	23.303
	n/B	0.008	0.058	0.108	0.158	0.203	0.258	0.308	0.333	0.358	0.383	0.408
	u (cm/s)	23.382	23.098	23.178	23.103	17.598	16.260	13.773	11.474	9.948	8.987	7.085
	n/B	0.433	0.458									
	u (cm/s)	8.709	9.024									
2-1	n/B	-0.475	-0.440	-0.415	-0.390	-0.340	-0.290	-0.240	-0.190	-0.140	-0.090	-0.040
	u (cm/s)	33.505	34.369	34.509	34.303	34.303	30.112	29.231	28.939	28.394	26.815	26.815
	n/B	0.010	0.060	0.110	0.160	0.210	0.260	0.310	0.335	0.360	0.385	0.410
	u (cm/s)	23.865	23.865	20.980	19.684	18.012	16.084	14.287	11.645	9.609	7.928	6.002
	n/B	0.435										
	u (cm/s)	3.976										
3-1	n/B	-0.475	-0.450	-0.425	-0.400	-0.375	-0.325	-0.275	-0.225	-0.175	-0.125	-0.075
	u (cm/s)	29.758	29.749	29.406	29.005	28.240	28.821	27.818	27.170	25.488	23.671	23.292
	n/B	-0.025	0.025	0.075	0.125	0.175	0.225	0.250	0.275	0.300	0.325	0.350
	u (cm/s)	22.472	20.798	20.244	19.561	18.230	16.603	14.804	12.950	11.136	10.752	9.842
	n/B	0.375										
	u (cm/s)	9.842										

4-1	n/B	-0.475	-0.450	-0.425	-0.400	-0.375	-0.325	-0.275	-0.225	-0.175	-0.125	-0.075
	u (cm/s)	27.960	29.227	30.818	30.818	30.326	30.326	28.591	27.184	25.763	25.201	24.294
	n/B	-0.025	0.025	0.075	0.125	0.175	0.225	0.250	0.275	0.300	0.325	0.350
	u (cm/s)	23.579	23.579	22.342	20.240	18.717	17.684	15.699	13.721	11.791	10.795	9.877
	n/B	0.375										
	u (cm/s)	9.152										
5-1	n/B	-0.475	-0.443	-0.418	-0.393	-0.368	-0.318	-0.268	-0.218	-0.168	-0.118	-0.068
	u (cm/s)	15.299	19.876	24.119	28.800	30.791	32.019	30.953	28.675	26.368	25.526	24.753
	n/B	-0.018	0.033	0.083	0.133	0.183	0.233	0.283	0.308	0.333	0.358	0.383
	u (cm/s)	23.971	22.971	22.177	21.110	17.410	13.376	11.077	10.910	8.088	8.284	7.733
	n/B	0.408										
	u (cm/s)	7.566										
6-1	n/B	-0.475	-0.450	-0.425	-0.400	-0.375	-0.350	-0.300	-0.250	-0.200	-0.150	-0.100
	u (cm/s)	1.630	4.803	9.208	14.160	22.703	28.285	29.208	28.420	28.775	27.499	26.893
	n/B	-0.050	0.000	0.050	0.100	0.150	0.200	0.250	0.275	0.300	0.325	0.350
	u (cm/s)	26.531	24.583	23.969	23.361	22.462	21.100	18.285	17.012	15.839	14.253	12.340
	n/B	0.375										
	u (cm/s)	11.768										
7-1	n/B	-0.475	-0.450	-0.425	-0.400	-0.375	-0.350	-0.300	-0.250	-0.200	-0.150	-0.100
	u (cm/s)	7.143	7.143	10.280	12.679	16.889	20.775	23.177	25.040	25.831	25.963	26.137
	n/B	-0.050	0.000	0.050	0.100	0.150	0.200	0.250	0.300	0.325	0.350	0.375
	u (cm/s)	25.950	25.553	25.554	24.885	24.912	24.912	23.707	16.676	16.596	15.415	15.007
	n/B	0.400										
	u (cm/s)	14.206										

8-1	**n/B**	-0.475	-0.443	-0.418	-0.393	-0.368	-0.318	-0.268	-0.218	-0.168	-0.118	-0.068
	u (cm/s)	5.932	8.888	10.668	12.849	16.855	19.457	22.194	23.986	25.209	26.093	26.844
	n/B	-0.018	0.033	0.083	0.133	0.183	0.233	0.283	0.308	0.333	0.358	0.383
	u (cm/s)	26.989	26.790	26.703	27.003	26.648	24.906	25.419	25.500	24.635	23.307	21.959
	n/B	0.408										
	u (cm/s)	22.047										
1-2	**n/B**	-0.413	-0.388	-0.363	-0.338	-0.313	-0.288	-0.238	-0.188	-0.138	-0.088	-0.038
	u (cm/s)	13.595	10.910	11.871	12.436	14.923	16.469	20.439	21.535	22.426	23.069	23.803
	n/B	0.013	0.063	0.113	0.163	0.213	0.263	0.313	0.363	0.388	0.413	0.438
	u (cm/s)	23.803	24.452	25.964	28.357	30.814	28.131	26.606	27.170	24.871	23.533	19.897
	n/B	0.475										
	u (cm/s)	16.601										
2-2	**n/B**	-0.408	-0.383	-0.358	-0.333	-0.308	-0.283	-0.233	-0.183	-0.133	-0.083	-0.033
	u (cm/s)	2.900	4.925	6.851	8.532	10.568	13.210	15.007	16.935	18.607	19.903	22.788
	n/B	0.018	0.068	0.118	0.168	0.218	0.268	0.318	0.368	0.393	0.418	0.443
	u (cm/s)	22.788	25.738	25.738	27.317	27.863	28.154	29.035	33.227	33.227	33.432	33.292
	n/B	0.475										
	u (cm/s)	32.428										
3-2	**n/B**	-0.400	-0.375	-0.350	-0.325	-0.300	-0.275	-0.225	-0.175	-0.125	-0.075	-0.025
	u (cm/s)	2.943	2.943	5.292	6.829	8.322	10.380	13.585	16.872	16.872	18.637	20.436
	n/B	0.025	0.075	0.125	0.175	0.225	0.275	0.325	0.375	0.400	0.425	0.450
	u (cm/s)	22.440	23.890	25.354	27.004	29.306	30.148	31.126	31.902	35.448	33.628	33.440
	n/B	0.475										
	u (cm/s)	32.625										

4-2	n/B	-0.415	-0.390	-0.365	-0.340	-0.315	-0.290	-0.240	-0.190	-0.140	-0.090	-0.040
	u (cm/s)	3.405	3.424	3.811	5.440	6.611	9.696	12.471	15.680	18.534	20.618	22.130
	n/B	0.010	0.060	0.110	0.160	0.210	0.260	0.310	0.360	0.385	0.410	0.435
	u (cm/s)	23.592	24.671	26.002	28.172	29.565	30.092	31.146	33.985	35.870	35.410	33.951
	n/B	0.475	-0.440									
	u (cm/s)	31.835	1.352									
5-2	n/B	-0.400	-0.375	-0.350	-0.325	-0.300	-0.275	-0.225	-0.175	-0.125	-0.075	-0.025
	u (cm/s)	3.934	3.934	3.745	4.584	5.294	7.963	10.515	13.691	16.538	21.447	25.282
	n/B	0.025	0.075	0.125	0.175	0.225	0.275	0.325	0.375	0.400	0.425	0.450
	u (cm/s)	25.772	26.990	28.152	29.373	31.301	34.923	34.923	34.972	30.349	30.349	26.719
	n/B	0.475										
	u (cm/s)	22.668										
6-2	n/B	-0.405	-0.375	-0.350	-0.325	-0.300	-0.275	-0.225	-0.175	-0.125	-0.075	-0.025
	u (cm/s)	5.511	5.695	7.195	8.600	9.722	13.046	15.841	18.930	23.522	27.023	26.670
	n/B	0.025	0.075	0.125	0.175	0.225	0.275	0.325	0.375	0.400	0.425	0.450
	u (cm/s)	27.024	28.581	28.581	29.625	30.315	30.498	29.265	25.130	19.778	17.472	13.797
	n/B	0.475										
	u (cm/s)	11.857										
7-2	n/B	-0.400	-0.375	-0.350	-0.325	-0.300	-0.275	-0.225	-0.175	-0.125	-0.075	-0.025
	u (cm/s)	9.993	9.993	10.678	11.739	14.055	16.234	26.189	26.233	27.314	28.026	27.994
	n/B	0.025	0.075	0.125	0.175	0.225	0.275	0.325	0.375	0.400	0.425	0.450
	u (cm/s)	28.248	28.199	28.134	27.669	26.471	22.165	22.165	19.846	16.172	14.671	13.261
	n/B	0.475	-0.415									
	u (cm/s)	11.226	1.729									

8-2	n/B	-0.413	-0.388	-0.363	-0.338	-0.313	-0.288	-0.238	-0.188	-0.138	-0.088	-0.038
	u (cm/s)	17.077	17.008	17.916	18.899	20.736	23.974	26.587	28.982	28.954	28.355	27.676
	n/B	0.013	0.063	0.113	0.163	0.213	0.263	0.313	0.363	0.388	0.413	0.438
	u (cm/s)	26.784	25.811	24.604	23.142	21.668	20.162	18.340	16.370	13.778	12.346	10.050
	n/B	0.475										
	u (cm/s)	10.050										
1-3	n/B	-0.475	-0.450	-0.425	-0.400	-0.375	-0.325	-0.275	-0.225	-0.175	-0.125	-0.075
	u (cm/s)	22.178	24.131	24.933	26.515	29.214	30.856	30.100	29.163	29.163	26.740	25.654
	n/B	-0.025	0.025	0.075	0.125	0.175	0.225	0.275	0.300	0.325	0.350	0.375
	u (cm/s)	25.654	22.555	21.464	21.464	17.470	15.617	14.897	10.476	8.993	7.391	5.898
	n/B	0.400	0.425									
	u (cm/s)	5.238	1.740									
2-3	n/B	-0.475	-0.450	-0.425	-0.400	-0.375	-0.325	-0.275	-0.225	-0.175	-0.125	-0.075
	u (cm/s)	9.253	30.786	31.245	31.422	32.810	32.400	31.334	31.334	27.374	26.421	26.424
	n/B	-0.025	0.025	0.075	0.125	0.175	0.225	0.275	0.300	0.325	0.350	0.375
	u (cm/s)	26.424	21.636	20.219	20.219	15.410	14.056	14.056	8.242	7.146	7.146	4.702
	n/B	0.400	0.425	0.438								
	u (cm/s)	4.697	1.998	1.998								
3-3	n/B	-0.475	-0.438	-0.413	-0.388	-0.363	-0.313	-0.263	-0.213	-0.163	-0.113	-0.063
	u (cm/s)	4.230	31.673	32.184	32.176	32.176	32.176	32.176	30.619	27.818	26.000	23.596
	n/B	-0.013	0.038	0.088	0.138	0.188	0.238	0.288	0.313	0.338	0.363	0.388
	u (cm/s)	20.607	19.395	17.828	15.884	13.982	9.850	7.753	5.256	4.351	3.252	3.082
	n/B	0.413	0.438	0.450								
	u (cm/s)	3.082	1.005	1.005								

4-3	n/B	-0.475	-0.443	-0.418	-0.393	-0.368	-0.318	-0.268	-0.218	-0.168	-0.118	-0.068
	u (cm/s)	30.848	32.436	33.013	33.472	34.059	33.822	32.512	30.335	28.621	26.360	24.446
	n/B	-0.018	0.033	0.083	0.133	0.183	0.233	0.283	0.308	0.333	0.358	0.383
	u (cm/s)	22.439	20.326	18.612	16.390	14.571	12.437	9.910	8.092	6.415	5.601	5.032
	n/B	0.408	0.420									
	u (cm/s)	4.911	2.844									
5-3	n/B	-0.475	-0.438	-0.413	-0.388	-0.363	-0.313	-0.263	-0.213	-0.163	-0.113	-0.063
	u (cm/s)	18.008	21.618	25.903	30.572	32.232	33.255	33.880	32.649	30.894	29.357	27.647
	n/B	-0.013	0.038	0.088	0.138	0.188	0.238	0.288	0.313	0.338	0.363	0.388
	u (cm/s)	24.631	22.046	18.537	17.031	15.058	12.624	9.966	8.107	6.938	6.124	5.985
	n/B	0.413	0.438									
	u (cm/s)	5.971	3.908									
6-3	n/B	-0.475	-0.450	-0.425	-0.400	-0.375	-0.350	-0.300	-0.250	-0.200	-0.150	-0.100
	u (cm/s)	8.566	8.686	11.015	15.045	21.262	26.466	31.118	32.249	33.013	32.369	31.432
	n/B	-0.050	0.000	0.050	0.100	0.150	0.200	0.250	0.275	0.300	0.325	0.350
	u (cm/s)	29.965	27.092	23.629	20.779	19.218	16.575	14.188	11.420	9.925	10.466	8.459
	n/B	0.375	0.400	0.425								
	u (cm/s)	8.262	6.190	6.190								
7-3	n/B	-0.475	-0.445	-0.420	-0.395	-0.370	-0.320	-0.270	-0.220	-0.170	-0.120	-0.070
	u (cm/s)	9.707	9.865	9.865	10.956	14.399	18.292	22.182	24.803	27.891	30.197	29.300
	n/B	-0.020	0.030	0.080	0.130	0.180	0.230	0.280	0.330	0.380	0.405	0.430
	u (cm/s)	29.993	29.780	29.346	25.728	23.365	21.106	18.740	16.228	15.490	14.777	13.725
	n/B	0.455	0.480	0.500								
	u (cm/s)	12.610	7.646	7.646								

8-3	**n/B**	-0.475	-0.458	-0.433	-0.408	-0.383	-0.358	-0.308	-0.258	-0.208	-0.158	-0.108
	u (cm/s)	8.449	8.441	8.441	8.453	10.528	14.208	17.808	20.479	22.448	24.201	25.286
	n/B	-0.058	-0.008	0.043	0.093	0.143	0.193	0.243	0.268	0.293	0.318	0.343
	u (cm/s)	26.964	28.462	29.975	30.417	28.980	28.980	26.013	22.826	21.822	21.078	19.631
	n/B	0.368	0.393	0.418								
	u (cm/s)	18.723	6.384	6.384								
1-4	**n/B**	-0.475	-0.440	-0.415	-0.390	-0.365	-0.315	-0.265	-0.215	-0.165	-0.115	-0.065
	u (cm/s)	23.890	24.203	25.397	26.032	27.644	29.042	30.523	30.948	29.799	27.983	25.973
	n/B	-0.015	0.035	0.085	0.135	0.185	0.235	0.285	0.310	0.335	0.360	0.385
	u (cm/s)	24.357	22.874	21.425	19.594	17.578	15.140	11.633	8.830	8.010	7.445	7.489

Flow Depth h (cm)

Section															
1-1	n/B	-0.488	-0.413	-0.338	-0.263	-0.188	-0.113	-0.038	0.038	0.113	0.188	0.263	0.338	0.413	0.488
	h (cm)	31.769	31.769	31.565	31.442	31.478	31.454	31.400	31.363	31.331	31.502	31.529	31.547	31.553	31.581
2-1	n/B	-0.488	-0.413	-0.338	-0.263	-0.188	-0.113	-0.038	0.038	0.113	0.188	0.263	0.338	0.413	0.488
	h (cm)	30.573	30.713	30.888	31.026	31.134	31.272	31.400	31.513	31.609	31.760	31.832	31.975	32.031	31.862
3-1	n/B	-0.488	-0.413	-0.338	-0.263	-0.188	-0.113	-0.038	0.038	0.113	0.188	0.263	0.338	0.413	0.488
	h (cm)	30.042	30.191	30.485	30.829	31.000	31.198	31.400	31.565	31.773	31.900	32.092	32.157	32.228	32.300
4-1	n/B	-0.488	-0.413	-0.338	-0.263	-0.188	-0.113	-0.038	0.038	0.113	0.188	0.263	0.338	0.413	0.488
	h (cm)	29.613	29.755	30.048	30.449	30.797	31.118	31.400	31.694	31.931	32.139	32.362	32.526	32.678	32.794
5-1	n/B	-0.488	-0.413	-0.338	-0.263	-0.188	-0.113	-0.038	0.038	0.113	0.188	0.263	0.338	0.413	0.488
	h (cm)	29.698	29.724	29.942	30.429	30.715	31.116	31.400	31.691	31.983	32.228	32.383	32.675	32.836	33.001
6-1	n/B	-0.488	-0.413	-0.338	-0.263	-0.188	-0.113	-0.038	0.038	0.113	0.188	0.263	0.338	0.413	0.488
	h (cm)	30.121	30.083	30.283	30.478	30.830	31.132	31.400	31.632	31.901	32.170	32.230	32.313	32.498	32.374
7-1	n/B	-0.488	-0.413	-0.338	-0.263	-0.188	-0.113	-0.038	0.038	0.113	0.188	0.263	0.338	0.413	0.488
	h (cm)	30.281	30.381	30.482	30.692	30.898	31.174	31.400	31.622	31.748	32.220	32.459	32.713	32.796	32.856
8-1	n/B	-0.488	-0.413	-0.338	-0.188	-0.113	-0.038	0.038	0.113	0.188	0.263	0.338	0.413	0.488	
	h (cm)	30.807	30.717	30.989	31.330	31.354	31.400	31.525	31.698	31.878	32.077	32.298	32.460	32.499	
1-2	n/B	-0.338	-0.263	-0.188	0.038	-0.113	-0.038	0.113	0.188	0.263	0.338	0.488	0.413	-0.413	-0.488
	h (cm)	31.461	31.443	31.407	31.400	31.405	31.406	31.410	31.423	31.460	31.466	31.528	31.473	31.479	31.513
2-2	n/B	-0.338	-0.263	-0.188	0.038	-0.113	-0.038	0.113	0.188	0.263	0.338	0.488	0.413	-0.413	-0.488
	h (cm)	31.635	31.606	31.428	31.400	31.447	31.422	31.400	31.403	31.315	31.118	30.797	30.843	31.736	31.847

3-2	n/B	-0.338	-0.263	-0.188	0.038	-0.113	-0.038	0.113	0.188	0.263	0.338	0.488	0.413	-0.413	-0.488
	h (cm)	32.057	31.867	31.728	31.400	31.565	31.543	31.120	30.715	30.352	29.966	29.727	29.944	32.300	32.429
4-2	n/B	-0.338	-0.263	-0.188	0.038	-0.113	-0.038	0.113	0.188	0.263	0.338	0.488	0.413	-0.413	-0.488
	h (cm)	32.330	32.190	31.795	31.400	31.667	31.699	31.251	31.048	30.649	30.033	29.230	29.076	32.836	32.619
5-2	n/B	-0.338	-0.263	-0.188	0.038	-0.113	-0.038	0.113	0.188	0.263	0.338	0.488	0.413	-0.413	-0.488
	h (cm)	32.635	32.224	32.125	31.400	31.835	31.908	31.089	30.729	30.169	29.661	29.235	29.330	32.835	32.972
6-2	n/B	-0.338	-0.263	-0.188	0.038	-0.113	-0.038	0.113	0.188	0.263	0.338	0.488	0.413	-0.413	-0.488
	h (cm)	32.192	32.123	32.025	31.400	32.048	31.778	31.227	30.897	30.540	30.408	30.504	30.450	32.192	32.542
7-2	n/B	-0.413	-0.263	-0.188	0.038	-0.113	-0.038	0.113	0.188	0.263	0.338	0.488	0.413	-0.488	
	h (cm)	32.560	32.096	32.071	31.400	31.939	31.670	31.178	31.119	31.119	30.710	30.508	30.661	32.521	
8-2	n/B	-0.413	-0.338	-0.263	-0.038	-0.188	-0.113	0.038	0.113	0.188	0.263	0.413	0.338		
	h (cm)	32.185	32.008	31.904	31.576	31.560	31.411	31.400	31.343	31.270	31.087	30.875	30.875		
1-3	n/B	-0.488	-0.413	-0.338	-0.263	-0.188	-0.113	-0.038	0.038	0.113	0.188	0.263	0.338	0.413	0.488
	h (cm)	31.417	31.432	31.442	31.436	31.414	31.402	31.400	31.414	31.376	31.431	31.404	31.325	31.316	31.328
2-3	n/B	-0.488	-0.413	-0.338	-0.263	-0.188	-0.113	-0.038	0.038	0.113	0.188	0.263	0.338	0.413	0.488
	h (cm)	30.583	30.717	30.843	30.843	31.165	31.323	31.400	31.563	31.684	31.738	31.814	31.893	31.799	31.826
3-3	n/B	0.488	0.413	0.338	0.263	0.188	0.113	0.038	-0.038	-0.113	-0.188	-0.263	-0.338	-0.413	-0.488
	h (cm)	-29.730	-29.873	-30.302	-30.794	-31.025	-31.211	-31.400	-31.617	-31.742	-31.827	-32.000	-32.145	-32.190	-32.178
4-3	n/B	-0.488	-0.413	-0.338	-0.263	-0.188	-0.113	-0.038	0.038	0.113	0.188	0.263	0.338	0.413	0.488
	h (cm)	29.670	29.615	29.986	30.412	30.781	31.113	31.400	31.727	31.936	32.170	32.371	32.504	32.614	32.723
5-3	n/B	-0.488	-0.413	-0.338	-0.263	-0.188	-0.113	-0.038	0.038	0.113	0.188	0.263	0.338		
	h (cm)	29.502	30.045	30.199	30.436	30.775	31.096	31.400	31.650	31.943	32.186	32.509	32.369		

6-3	**n/B**	-0.488	-0.413	-0.338	-0.263	-0.188	-0.113	-0.038	0.038	0.113	0.188	0.263	0.338	0.413	0.488
	h (cm)	30.274	30.432	30.510	30.714	30.797	31.126	31.400	31.890	32.378	32.528	32.540	32.649	32.769	32.831
7-3	**n/B**	-0.488	-0.413	-0.338	-0.263	-0.188	-0.113	-0.038	0.038	0.113	0.188	0.263	0.338	0.413	0.488
	h (cm)	30.761	30.760	30.873	30.970	31.166	31.344	31.400	31.400	31.930	32.234	32.354	32.476	32.526	32.539
8-3	**n/B**	-0.488	-0.413	-0.338	-0.263	-0.188	-0.113	-0.038	0.038	0.113	0.188	0.263	0.338	0.413	0.488
	h (cm)	30.755	30.755	30.970	30.993	31.140	31.249	31.400	31.547	31.630	31.881	32.079	32.339	32.347	32.344
1-4	**n/B**	-0.488	-0.413	-0.338	-0.263	-0.188	-0.113	-0.038	0.038	0.113	0.188	0.263	0.338	0.413	0.488
	h (cm)	31.438	31.518	31.510	31.475	31.450	31.401	31.400	31.400	31.385	31.361	31.361	31.361	31.305	31.302

50°-channel: Vertically averaged deviation angle

Section	ω_c	Section	ω_c	Section	ω_c
1-1	-0.082	1-2	0.077	1-3	-0.073
2-1	-0.084	2-2	0.087	2-3	-0.096
3-1	-0.068	3-2	0.082	3-3	-0.079
4-1	-0.031	4-2	0.037	4-3	-0.033
5-1	-0.009	5-2	0.008	5-3	-0.008
6-1	0.086	6-2	-0.091	6-3	0.088
7-1	0.095	7-2	-0.088	7-3	0.092
8-1	0.082	8-2	-0.085	8-3	0.077

Appendix D

Deviation Angle Profiles for all Channels

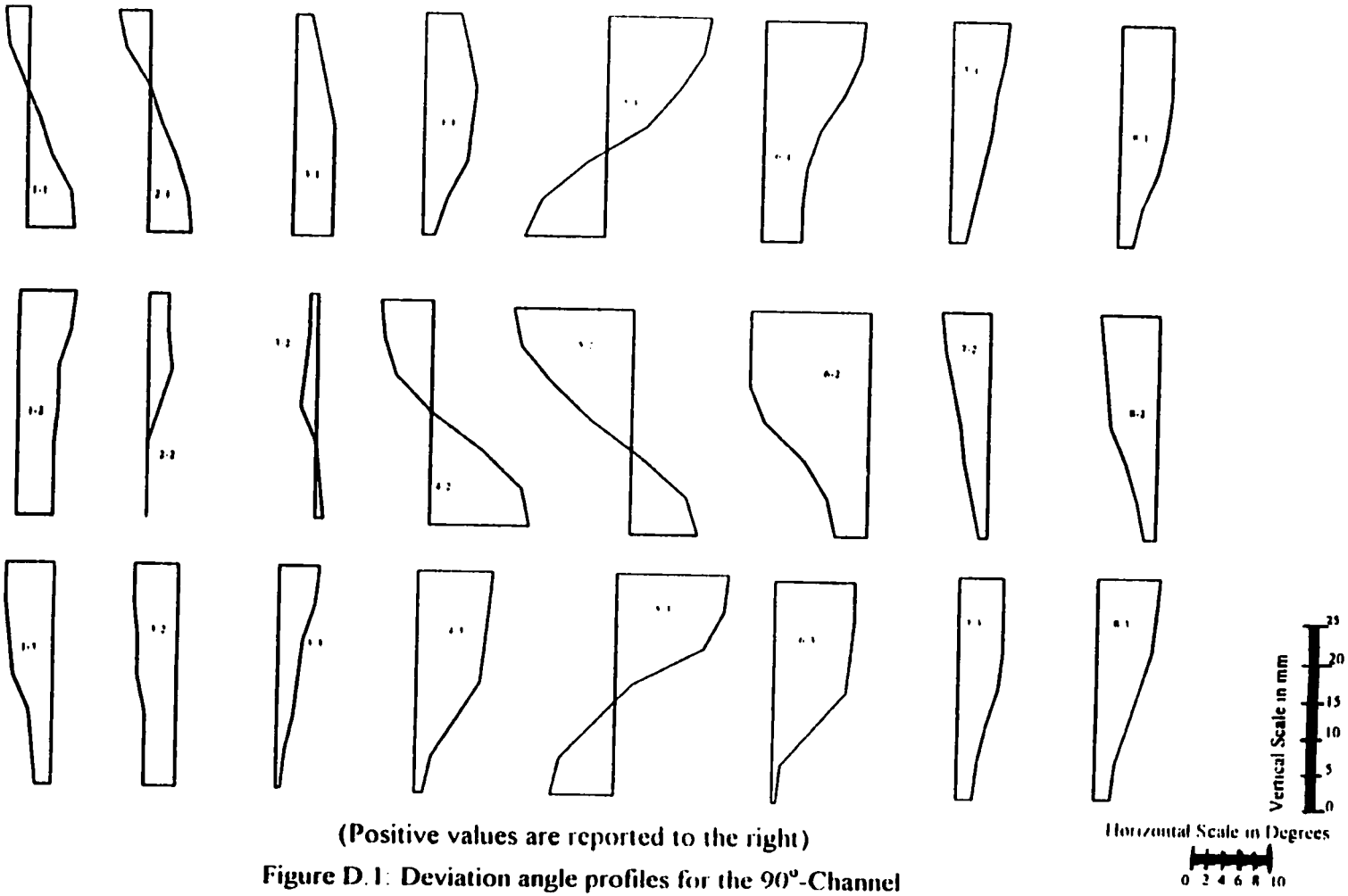

(Positive values are reported to the right)

Figure D.1: Deviation angle profiles for the 90°-Channel

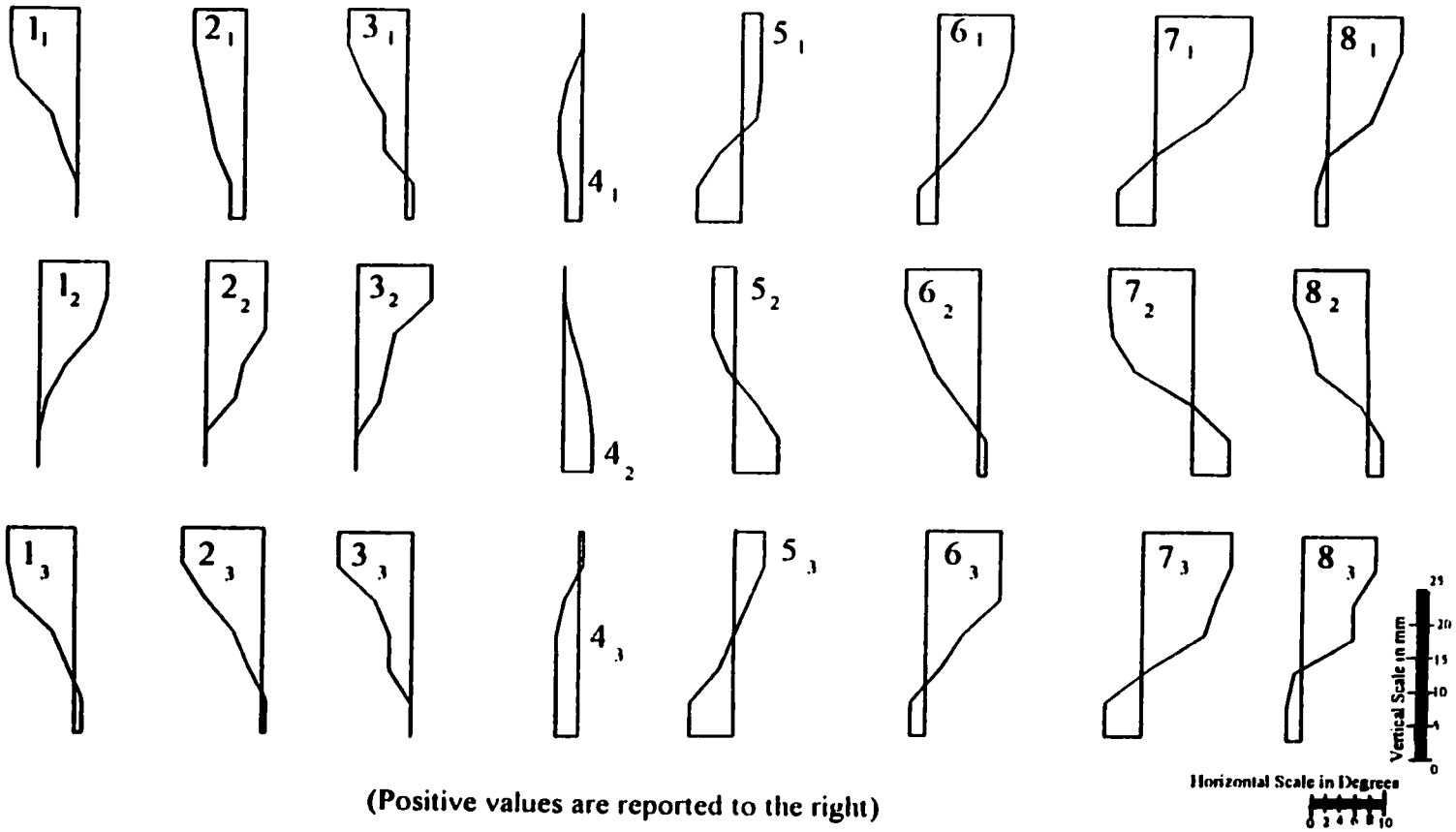

(Positive values are reported to the right)

Figure D 2. Deviation angle profiles for the 50"-Channel

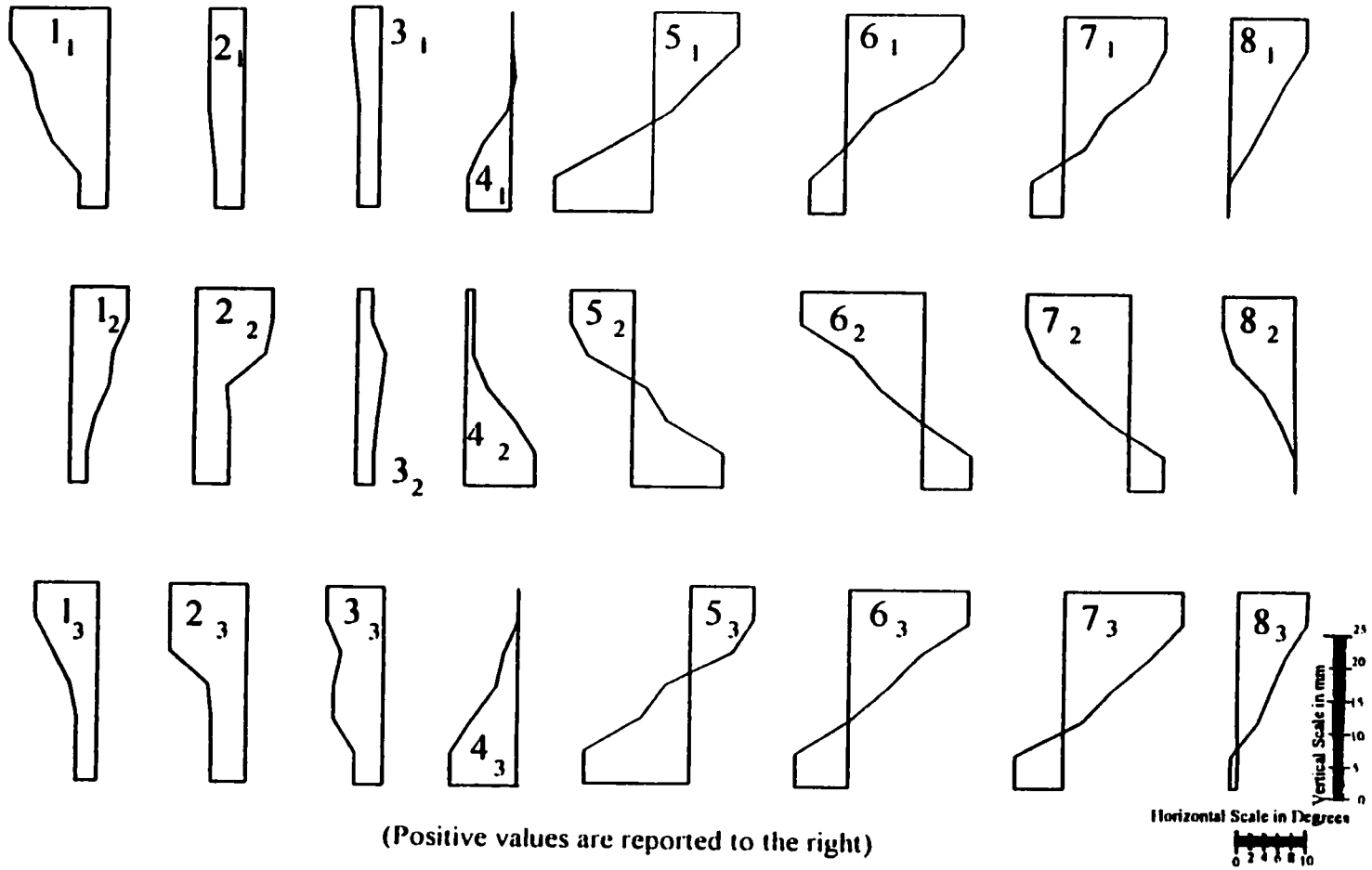

Figure D 3. Deviation angle profiles for the 70"-Channel

Appendix E

Pictures of Channel Assembly

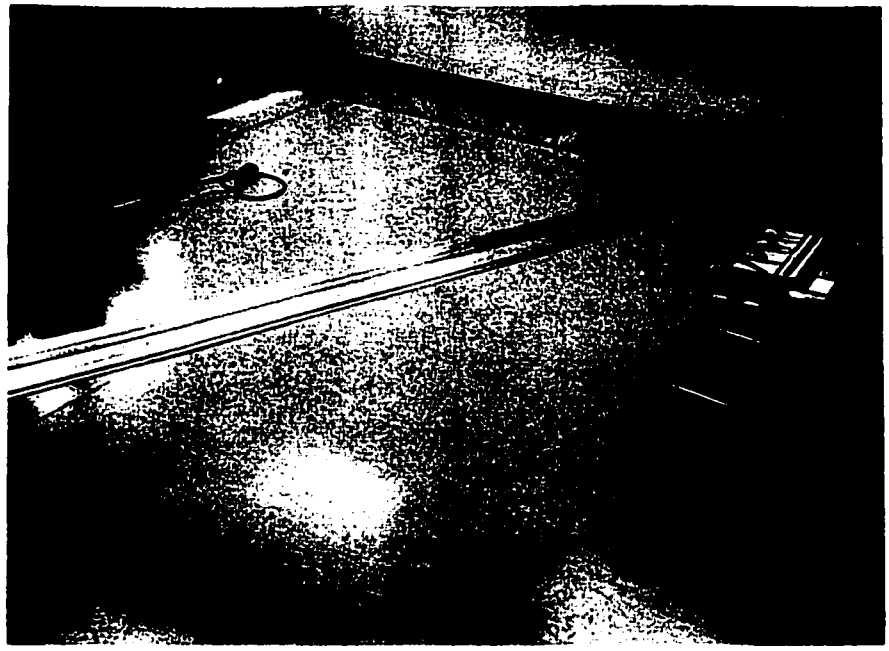

Figure E.1: Outline of first channel on the floor prior to frame installation

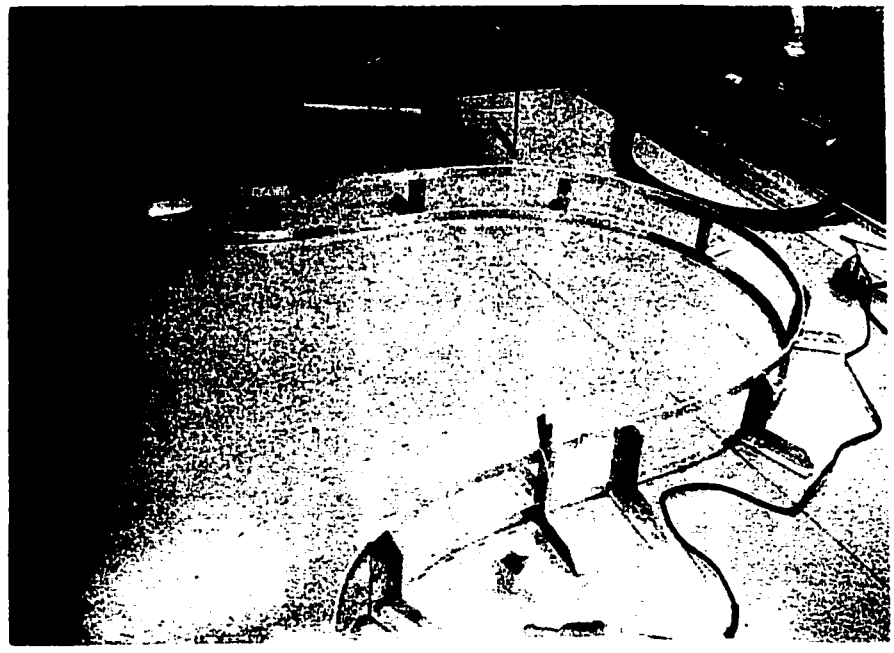

Figure E.2: Installation of first wall of channel

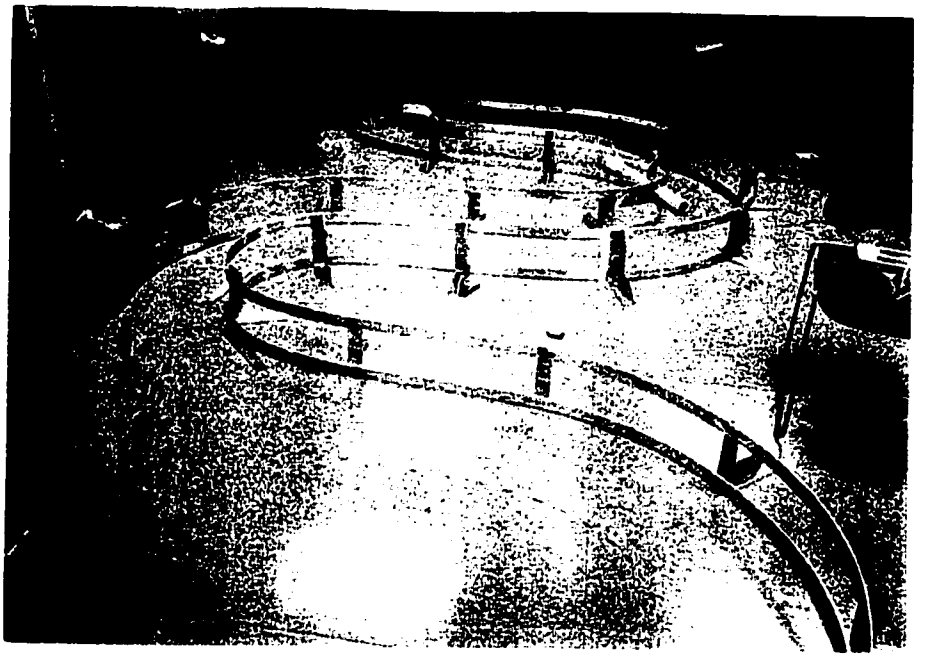

Figure E.3: Installation of the second wall. First wall completed

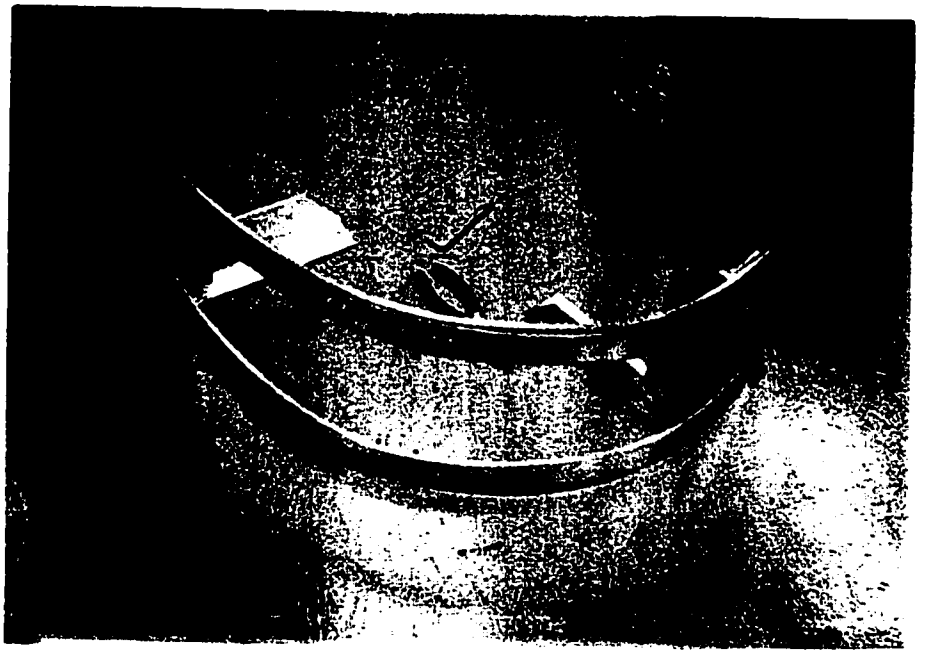

Figure E.4: Installation of Plexiglas walls. This picture shows a joint in the Plexiglas wall

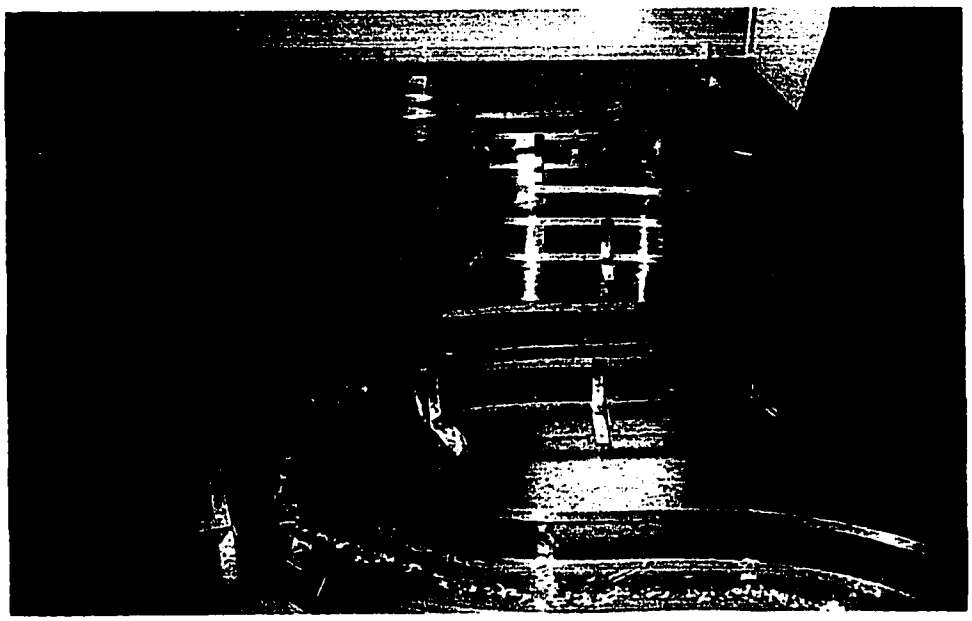

Figure E.5: Flow test of 90°-channel after wall installation

Figure E.6: Compaction of Base layer of Channel bed

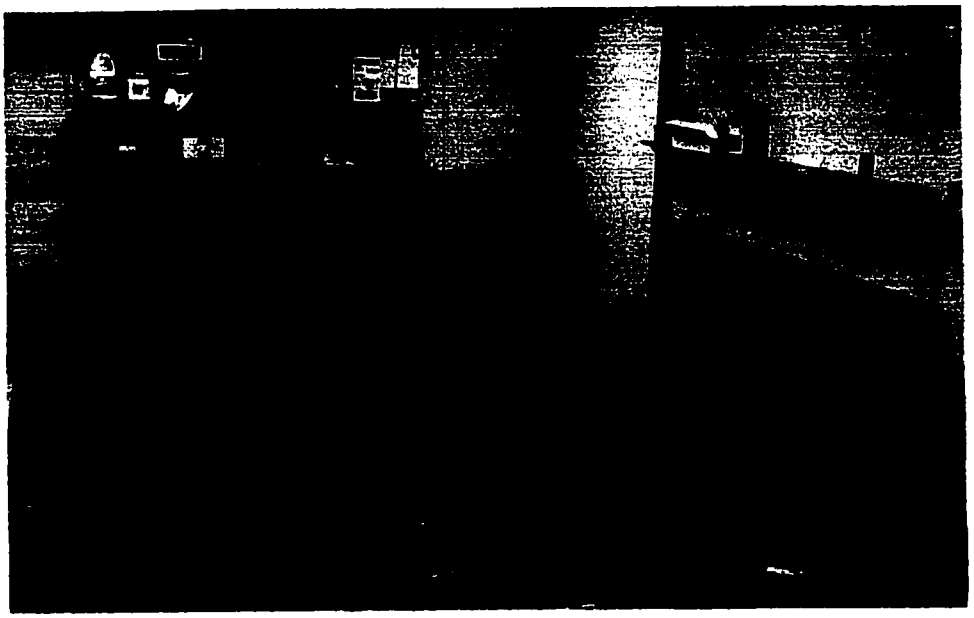

Figure E.7: 90°-channel prior to final leveling of bed. The bed's layer is Compacted

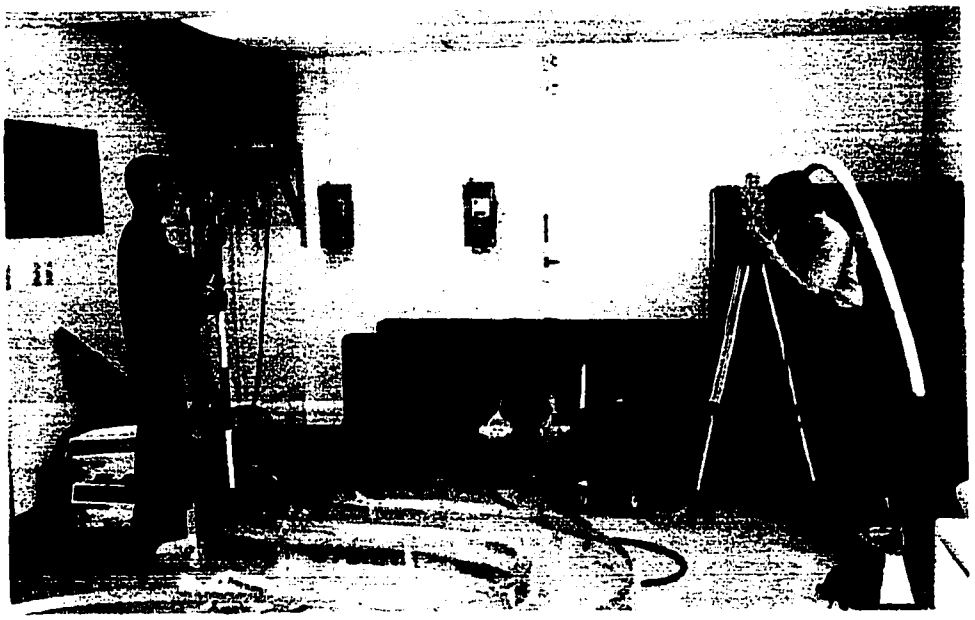

Figure E.8: Leveling of bed to achieve desired slope

Figure E.9: Application of varnish to bed for purposes of immobilization

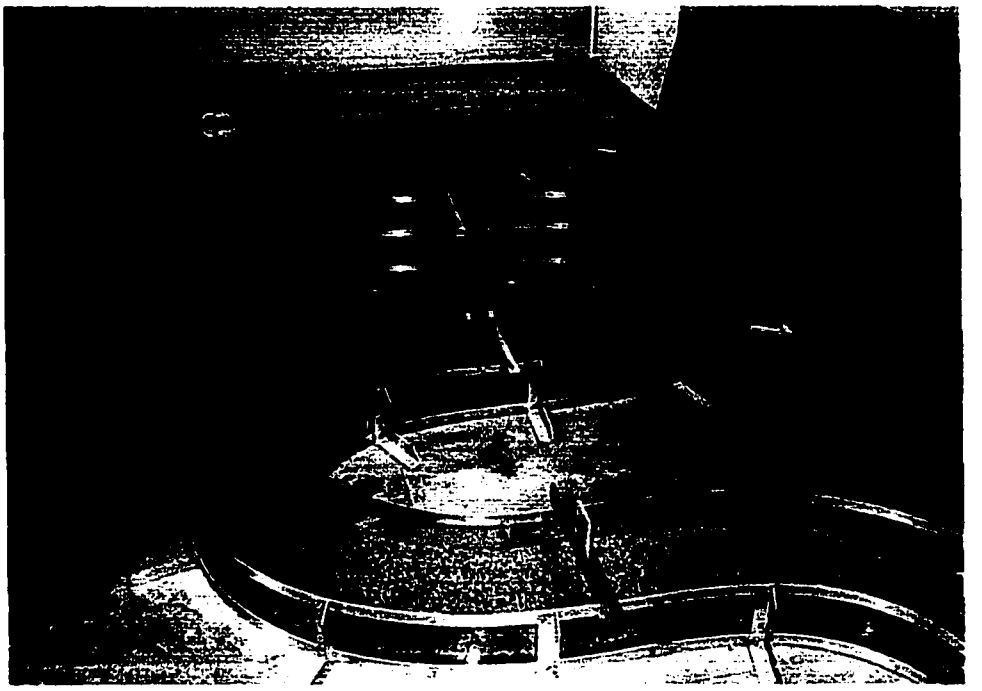

Figure E.10: 90°-channel after varnish was applied to bed

Appendix F

Pictures of Testing

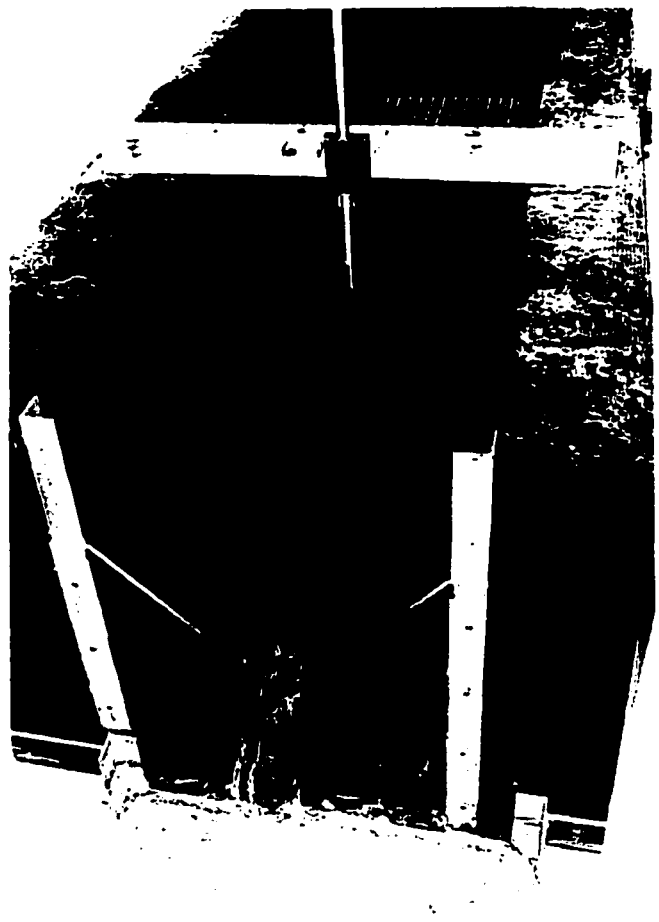

Figure F.1:
V-notch weir at the downstream end of Head Tank

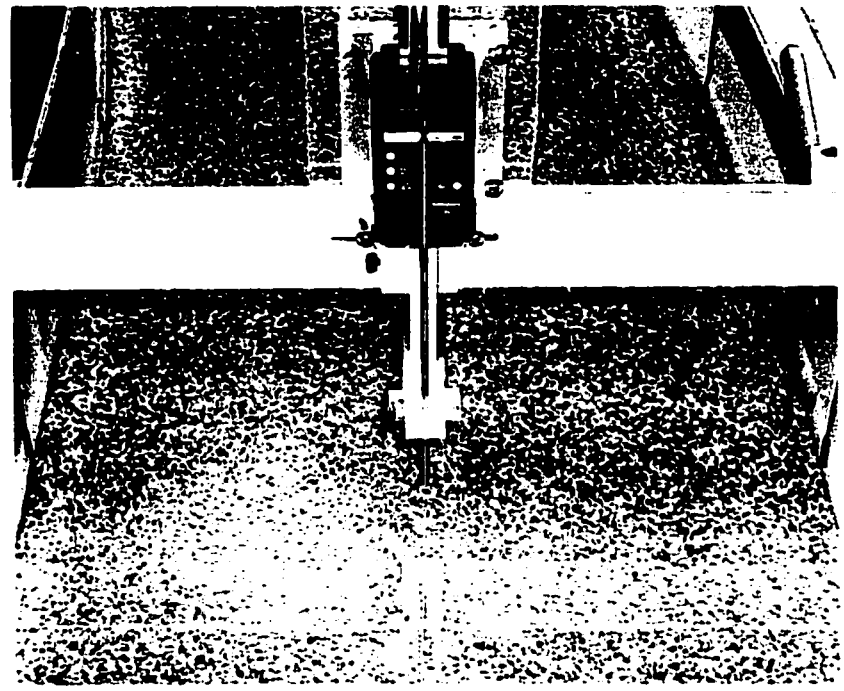

Figure F.2:
One of 4 height gauges located at the crossovers of the Channel

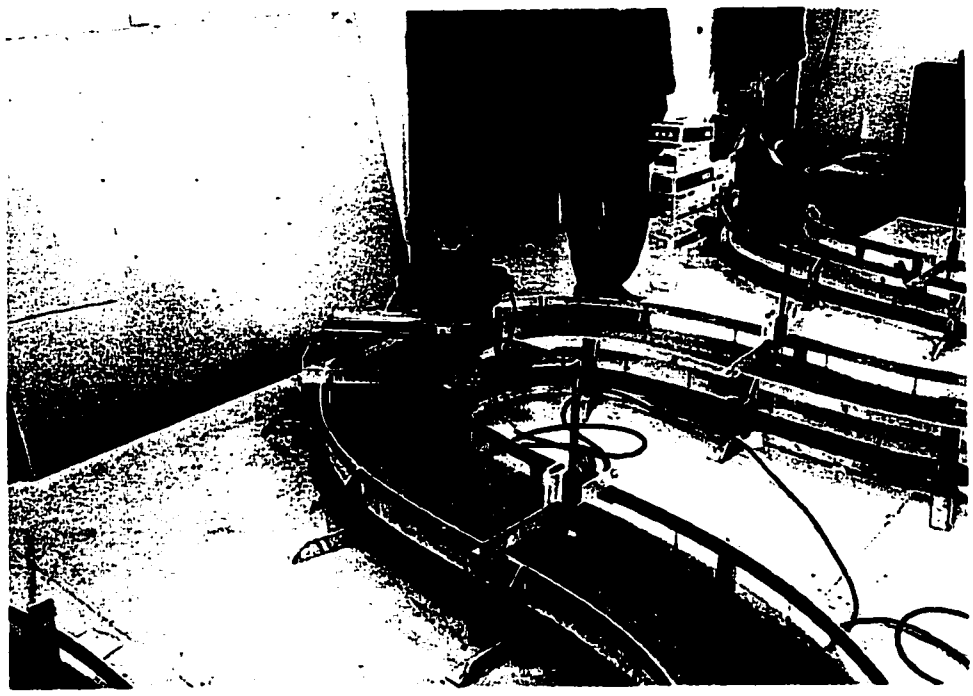

Figure F.3: Recording of the free surface height using the Wavo
(picture showing 90°-channel, recording at section 6_2)

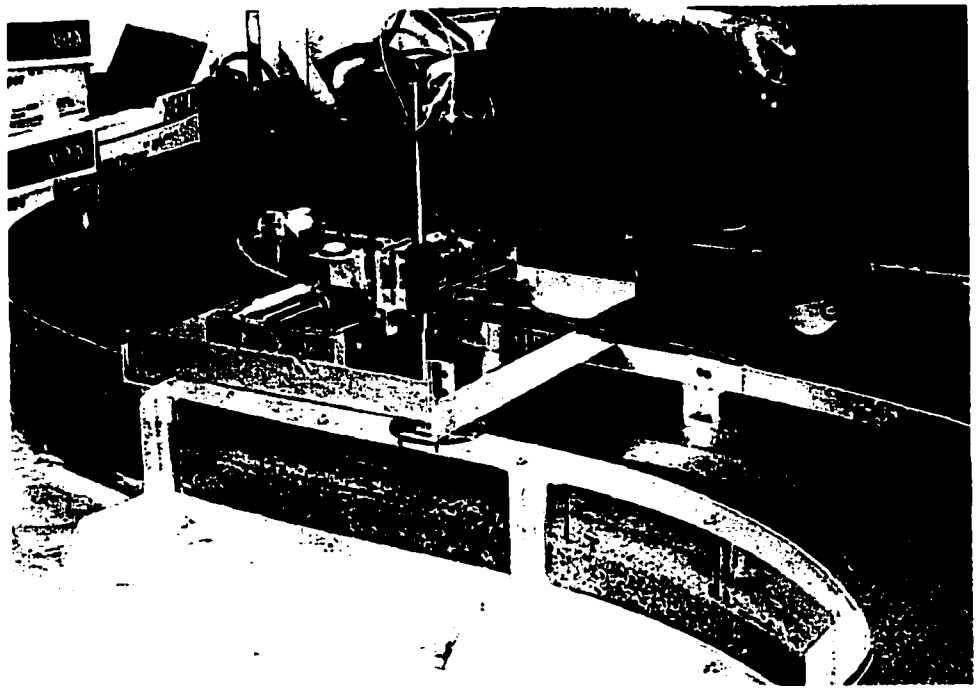

Figure F.4: Recording of the longitudinal velocity profile
(picture showing 90°-channel, recording at section 1_1)

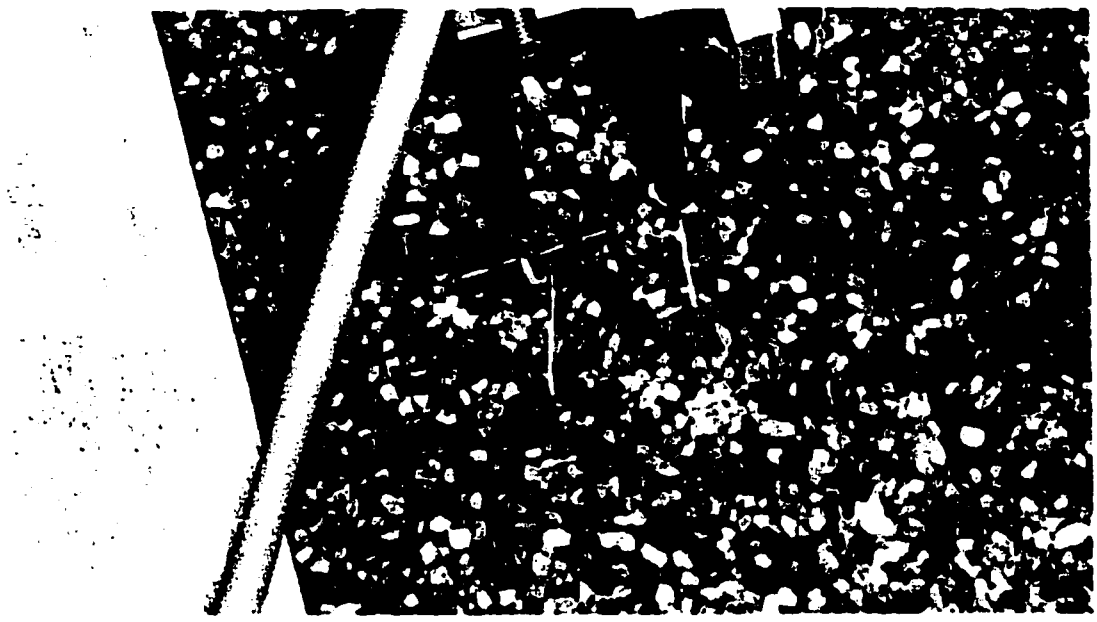

Figure F.5: Probe measuring velocity at $h_w/2$

Figure F.6: Data acquisition system and Equipment controls
(picture taken during testing of the 90°-channel)

VITA

William D. Tape, B.A.Sc., E.I.T.

Education

1999- Present:	University of Windsor Preparation of Master's Thesis
1995-1999	University of Windsor B.A.Sc. in Civil Engineering (Granted in October 1999)

Awards

- Natural Sciences and Engineering Research Council Graduate Scholarship (2000 – Present)
- University of Windsor Tuition Scholarship (1999 – Present)
- Ontario Graduate Scholarship for Science and Technology (1999 – 2000)

Experience

1999 – Present	Research and Teaching Assistant, Civil and Environmental Engineering, University of Windsor
Fall 2000	Sessional Instructor, Civil and Environmental Engineering, University of Windsor
Fall 1998	Field Inspector, City of Windsor, Traffic Engineering Department, Windsor, ON
1997-1998	Co-op Student, Windsor Utilities Commission, Water Engineering Department, Windsor, ON
Summer 1996	Computer Operator, Town of LaSalle, Environmental Services Department, LaSalle, ON
1996 – 1996	Assistant, Casino Windsor (Woodcliff Construction Consultants) Construction Project Management Office, Windsor, ON

Memberships

- Professional Engineers Ontario (E.I.T.)

- International Association of Hydraulic Engineering and Research (Member)
- Canadian Society for Civil Engineering (Member)

Publications

[1] A.M.F. da Silva, M.S. Yalin, T.H. El-Tahawy, W.D. Tape: *Patterns of Flow in Meandering Channels of Varying Sinuosity.* XXIX IAHR Congress Conference, Beijing, China, 2001 (Submitted).

[2] A.M.F. da Silva, W.D. Tape, T.H. El-Tahawy: *Mechanics of Turbulent Flow in Meandering Channels of Varying Sinuosity: an Experimental Study.* CSCE Conference, British Columbia, 2001 (Submitted).

[3] W.D. Tape, T.H. El-Tahawy, A.M.F. da Silva: *Experimental Investigation of Turbulent Flow in Meandering Channels.* Abstract, CSCE Conference, London, 2000.

[4] W.D. Tape, A.M.F. da Silva: *Experimental Investigation of Turbulent Boundary Layer Growth in Open Channel Flow.* Abstract, CSCE Conference, London, 2000.